Functional Analysis of Autism Genes in Zebrafish

Investigation of the Autism Related 16p11.2 Deletion

Inaugural-Dissertation
to obtain the academic degree
Doctor rerum naturalium (Dr. rer. nat.)

submitted to the Department of Biology, Chemistry and Pharmacy
of Freie Universität Berlin

by
Udo Georgi
from Berlin
2014

This doctoral research project was conducted between October 2009 and January 2014 at the Max Planck Institute for Molecular Genetics, department of Vertebrate Genomics under the supervision of Prof. Dr. Hans Lehrach

1st Reviewer: Prof. Dr. Hans Lehrach
Department of Vertebrate Genomics
Max Planck Institute for Molecular Genetics

2nd Reviewer: Prof. Dr. Rupert Mutzel
Institute for Biology - Microbiology
Freie Universität Berlin

Date of defence: 12.05.2014

Acknowledgments

I would like to thank Prof. Dr. Hans Lehrach for the opportunity he gave me to carry out this work at the department of Vertebrate Genomics at the Max Planck Institute for Molecular Genetics in Berlin. Additionally, I would like to gratefully acknowledge Prof. Dr. Rupert Mutzel of the Freie Universität Berlin for supporting me as my second supervisor.

I would like to especially thank my group leaders Dr. Georgia Panopoulou and Dr. Albert Poustka for their guidance and support throughout the last years. Furthermore, I would like to thank all former members of the Evolution & Development group. Especially, Magdalena Ciurkiewicz who constructed most of the vectors for the *in situ* hybridizations during her Diplom thesis.

Also I want to thank all my colleagues at the Max Planck Institute for Molecular Genetics for the inspiring and supporting working atmosphere which acted as a tonic of motivation. Especially I want to emphasize the excellent support of the people maintaining the zebrafish facility at the Max Planck Institute and in particular Dr. Ludger Hartmann and Ulf Schroeder. Without their expertise it would not have been possible to have a constant embryo supply which was vital for this project.

Finally, I would particularly like to thank some people, who supported this work with inspiring discussions, comments and corrections: Steve Michel, Anita Neumann, Christina Neumann, Oliver Herrmann and Anne Steininger.

Contents

List of figures

List of tables

List of abbreviations

aa	amino acid
aCGH	array based comparative genomic hybridization
AP	alkaline phosphatase
ASD	autism spectrum disorder
BCIP	5-Bromo-4-chloro-3-indolyl phosphate p-toluidine salt
CA	caudal arorter
Ce	cerebellum
CGH	comparative genomic hybridization
CH	caudal hindbrain
chr	Chromosome
CNV	copy number variation
CV	caudal vein
DA	dorsal aorta
Di	diencephalon
DIG	digoxigenein
DNA	deoxyribonucleic acid
Es	esophagus
Hi	hindbrain
HTA	head trunk angel
IHPF	*in situ* hybridization on paraffin section
ISV	intersegmental vessels
Kb	kilobase
Me	mesencephalon
My	myelencephalon
NGS	next generation sequencing
NBT	nitro blue tetrazolium
OVL	otic vesicle length
ORF	open reading frame
p50	small subunit of the DNA polymerase delta
Pf	pectoral fins
PME	progressive myoclonic epilepsy
PCNA	proliferating cell nuclear antigene protein
pol δ	DNA polymerase delta
PCV	posterior cardinal vein
RNA	ribonucleic acid
RT	room temperature
SC	spinal cord
SCMO	standard control morpholino
SNV	single nucleotide polymorphism
SM	somitic muscle
Tc	tectum
Te	telencephalon
WGD	whole-genome duplication
WMISH	whole mount *in situ* hybridization

Abstract

Autism refers to a large number of neurological disorders known as autism spectrum disorders (ASD). ASD patients display difficulties in social interactions and a large variety of accompanying symptoms which manifest the complex genetic background underlying this disease. To date, over 2000 copy number variations (CNVs) and 300 genes potentially linked to ASD have been identified via array-based comparative genomic hybridization. However, the physiological function of these genes and their relation to ASD is mostly unknown. This thesis examines the potential of zebrafish as being, a suitable model to functionally analyze such large number of potential neuronal disease genes and their relevance for ASD.

For this thesis the most frequently reported ASD related CNV, located in the human 16p11.2 chromosomal region, was chosen for analyses. This 500 kb long CNV encompasses 27 genes of which 22 orthologs and 6 paralogs exist in the zebrafish genome. This thesis concentrated on only those zebrafish orthologs which are organized in syntenic clusters in both zebrafish and human genomes as this conservation of genomic organization indicates strong evolutionary pressure acting to preserve functionally important gene interaction and regulation. Specifically, I analyzed the zebrafish orthologs organized in two syntenic clusters on chromosome 3 consisting of the genes *kctd13*, *sez6l2*, *asphd1* and *ppp4ca (and ppp4cb)*, *mapk3*, *gdpd3*, *ypel3*.

As a result of this thesis, it was identified that all the analyzed genes are active in the brain during development. The analysis by morpholino knockdown of: I) *kctd13* and *sez6l2* revealed a possible connection to ASD by induction of head size changes, II) the *ppp4c* genes resulted in heart and blood vessel deformations, which is in line with the heart malformations present in some 16p11.2 CNV carriers. III) *mapk3* induced notochord, heart, and head deformations which are possibly related to the neuro-cardio-facial-cutaneous syndrome. IV) *ypel3* and *gdpd3a* resulted in embryo mortality indicating their essential role during development.

In conclusion, this thesis establishes the possible involvement of *kctd13* and *sez6l2* in ASD and more importantly serves as a case study that demonstrates the potential of zebrafish as the preferred model system for identifying and analyzing the molecular pathways involved in neurological disorders with complex genetic background such as ASD.

Zusammenfassung

Autismus und weitere neurologische Erkrankungen werden heute zu den Autismus-Spektrum-Störungen (ASS) zusammengefasst. Patienten mit dieser Störung zeigen übereinstimmend Schwierigkeiten in sozialen Interaktionen, variieren jedoch stark in der Ausprägung und den Begleiterscheinungen, was sich ebenfalls in einem komplexen genetischem Hintergrund wiederspiegelt. Bisher wurden mittels der microarray-basierten vergleichenden genomischen Hybridisierung rund 2000 Kopienzahl-variationen und 300 Gene als potentielle Ursachen von ASS identifizierte, deren Funktion und Beziehung zu ASS unbekannt sind. Ziel dieser Arbeit ist es die Eignung des Zebrabärblings zur funktionellen Analyse großer Mengen potentieller neuronaler Krankheitsgenen und deren Zusammenhang mit ASS zu testen.

Ausgangspunkt dieser Arbeit ist die bei ASS Patienten am häufigsten gefundene Kopienzahlvariation in der chromosomalen Region 16p11.2. Diese rund 500 kb große Region beinhaltet 27 Gene, von denen 22 Orthologe und 6 Paraloge im Zebrabärblings-genom nachgewiesen sind. Um eine hohe Vergleichbarkeit zwischen Mensch und Zebrabärbling zu ermöglichen wurden die Gene zweier syntenischer Cluster für funktionelle Untersuchungen ausgewählt welche aus *kctd13*, *sez6l2*, *asphd1* und *ppp4ca* (und *ppp4cb*), *mapk3*, *gdpd3* sowie *ypel3* bestehen.

Die Ergebnisse dieser Arbeit zeigen, dass alle untersuchten Gene im Gehirn der Zebrabärblinge aktiv sind. Daher wurden sie in Morpholino knockdown Experimenten auf ihre Funktion untersucht, wobei: I) *kctd13* und *sez6l2* eine Veränderung der Kopfgröße erzeugten, welche möglicherweise im Zusammenhang mit ASS steht, II) die *ppp4c* Gene Veränderungen der Herz- und Blutgefässentwicklung ergaben, welche eine mögliche Verbindung mit Herzerkrankungen einiger der 16p11.2 Deletionsträger darstellt, III) *mapk3* induzierte Veränderungen an der Chorda dorsalis, dem Herzen und dem Kopf, was im möglichen Zusammenhang mit dem Neuro-Cardio-Fazio-Cutanem Syndrom steht, IV) *ypel3* und *gdpd3a* zum Absterben der Embryonen führten, was auf eine essentielle Rolle während der Embryonalentwicklung hindeutet.

Die gefundene Verbindung von *kctd13* und *sez6l2* mit ASS, sowie die Hinweise auf Zusammenhänge zu Erkrankungen und Embryonalentwicklung der anderen Gene zeigt deutlich das Potential des Zebrabärbling-Modells zur Analyse von molekularen Ursachen im Zusammenhang mit komplexen genetischen neuronalen Erkrankungen.

1. Introduction

1.1 Short introduction into autism spectrum disorders

Autism is a neural developmental disorder belonging to the autism spectrum disorders (ASD) which also includes the Asperger syndrome, childhood disintegrative disorder and pervasive developmental disorder not otherwise specified (PDD-NOS). The estimated prevalence of ASD ranges from 1.0 - 2.6 % among the world-wide population. This places ASD the most common neurological disorders (Fombonne 2010, Boyle, Boulet *et al*. 2011, Kim, Leventhal *et al*. 2011, MMWR 2012). ASD is characterized by three diagnostic core domains: impaired social interaction, communication difficulties and stereotypical behavior (Box 1). A guideline serving psychiatrists to identify problems in the core domains of ASD is the Diagnostic and Statistical Manual of Mental Disorders (DSM-V), of which the fifth revision is available since 2013 (American Psychiatric Association 2013). The DSM allows psychiatrists to classify patients according to their diagnostic features and provides suggestions for therapies and medications. Since problems in the ASD core domains appear early in the development, the DSM enables to diagnose most children already before the age of

Box 1 Summary of the ASD diagnostic core factors of the DSM-V (American Psychiatric Association 2013)

Impairment in social interaction

- difficulties in use of nonverbal behaviors such as eye-to-eye gaze, facial expression, body postures, and gestures to regulate social interaction
- disabilities to form age appropriate peer relationships
- failure to share interests, enjoyment or achievements with other people

Impairment in communication

- delay or lack of language
- impairment in the ability to initiate a conversation with others
- stereotypical and repetitive use of language

Stereotypical and restrictive repetitive pattern of behavior

- fixed to specific routines or rituals
- repetitive movements and gestures
- persistent preoccupation with objects

three (American Psychiatric Association 2013).

Besides behavioral, social and communication problems almost no clinical phenotype coincides with ASD. Only in some rare cases ASD patients exhibit microcephaly or macrocephaly. It is speculated that the reasons for the macrocephaly is based on an enlargement of the ventricles (MMWR 2012). However, the reason for this co-occurrence remains unknown (Courchesne, Karns *et al*. 2001, Lainhart, Bigler *et al*. 2006).

Unfortunately, there is no cure for autism, but there are ways to minimize the autism core features to improve the quality of life. This is achieved by educational interventions and medical management (Seida, Ospina *et al.* 2009). Furthermore, certain drugs can be used to treat illnesses which occur simultaneously, like sleep dysfunction, coexisting challenging behaviors or psychiatric conditions like seizures. The most efficient way to improve life quality of an affected person and their social environment is the educational intervention. With consequent training, the children who suffer from ASD can be trained to develop the skills needed to ensure personal responsibility and independence. The educational intervention not only applies to the child. It also includes the family to allow them to better adapt to the needs of ASD patients. (Myers, Johnson *et al.* 2007)

1.1.1 Genetic basis of ASD

Although, Folstein and Rutter already predicted a genetic component of ASD by twin studies in 1977, the molecular causes remained undiscovered. Since the discovery of a genetic background, which was confirmed in later studies, an autosomal recessive mode of inheritance was expected (Steffenburg, Gillberg *et al.* 1989, Bailey, Le Couteur *et al.* 1995, Le Couteur, Bailey *et al.* 1996). This was also supported by pedigree analyses which showed a clustering of autism in family members. However, these analyses could not confirm a Mendelian inheritance. Therefore, a more complex background of an inheritance model is indicated (Jorde, Mason-Brothers *et al*. 1990).

The difficulties in finding an inheritance model for ASD also led to a non-genetic hypothesis. For example epigenetic reasons like the X-chromosomal imprinting, which could explain the 4 : 1 male to female ratio (Skuse 2000, Jones, Skinner *et al.* 2008). Other hypotheses include environmental reasons like prenatal exposure to viruses or

drugs, even though a direct coherence has not been shown (Persico and Bourgeron 2006).

In conclusion, the evidence available let most researchers to believe that ASD has a genetic component. But the question how to identify the autism-causing genes remains unanswered. To identify the genetic component responsible for ASD, researchers used mainly two approaches: linkage analysis and array-based comparative genomic hybridization (aCGH). Reason for choosing those techniques was the complexity of ASD, which required large cohorts to overcome the heterogeneity of the manifestations. Therefore, the relative cheapness of the array-based methods was favored and a large number of CNVs were discovered (Autism Genome Project, Szatmari *et al.* 2007, Shi, Zhang *et al.* 2013). Today, with the enormous reduction in cost, the next generation sequencing replacing the aCGH and first publications are coming up using this technique to analyze ASD affected families (Shi, Zhang *et al*. 2013). However, even the high resolution of whole-genome sequencing will need large cohorts to overcome the complexity of ASD.

1.1.2 16p11.2 - the most frequently found deletion in autism subjects

The main problem in autism is its complex genetic background, which makes the identification of potential disease-causing genes very challenging. Because of its minor cost and its whole-genome attempt most researchers used array based comparative genomic hybridization (aCGH) to identify candidate genes. The idea was to screen hundreds of patients to overcome the complexity of the disease. In the last 10 years the microarray approach was used in several studies, which resulted in 2022 copy number

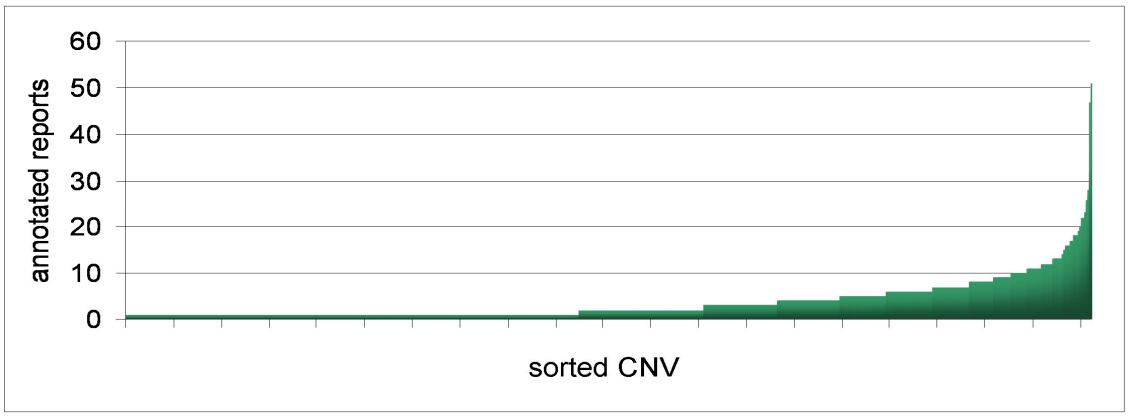

Figure 1 CNV annotation frequency
2022 CNVs form the AutDB database (Basu, Kollu *et al*. 2009)sorted for their annotation frequency. Most CNVs are only reported once (946). With 51 reports the 16p11.2 locus is the most frequently described (updated September 2013).

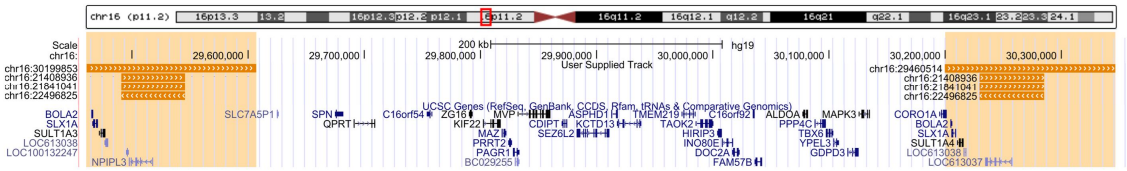

Figure 2 Chromosomal location of the 16p11.2 CNV
Screenshot of the 16p11.2 CNV region from UCSC Genome Browser, human assembly Feb. 2009 (GRCh37/hg19), position chr16: 29,455,038 - 30,361,950. The CNV is flanked by segmental duplications (orange bars, sequence similarity greater than 99 %) (Bailey, Gu *et al*. 2002, Kent, Sugnet *et al*. 2002)

variations (CNVs) from 283 reports lists to date in the autism database AutDB (updated September 2013) (Basu, Kollu *et al*. 2009). Surprisingly, the reported CNVs do not localize to a few hotspots. Instead, they are spread over the whole-genome and most of them are only reported once (47 %; Figure 1). Interestingly, only 24 CNVs are reported 20 times and more, therefore they are supposed to be good candidate regions for further investigations. For this reason the most reported locus 16p11.2 was chosen for further amalyses.

The CNV 16p11.2 is not only the most reported one, but also the most frequently found CNV in ASD subjects. It appears in approximately 1 % of all autism patients. The 16p11.2 CNV was reported for the first time by Kumar, KaraMohamed *et al.* in 2008. They screened 180 autism patients with aCGH and found the 16p11.2 microdeletion in two nonrelated autism patients. Because it was so surprising to find the same deletion in two independent patients, they tested 532 additional patients by quantitative PCR. In this second screen they found another two patients with the 16p11.2 deletion (total 4/712). Importantly, the deletion was not found in one of the 837 control samples. Since then, the 16p11.2 deletion was confirmed in other studies as well. In most patients, the 16p11.2 locus is deleted, nevertheless there are also a few duplications reported in ASD patients (Marshall, Noor *et al.* 2008, Weiss, Shen *et al.* 2008, Levy, Ronemus *et al.* 2011). The 16p11.2 deletion consists of a ~ 500 kb long DNA fragment which is flanked by >99 % identical segmental duplications (147 kb each side) (Kumar, KaraMohamed *et al.* 2008). Within this locus the UCSC Genome Browser lists 27 genes (Figure 2). However, it is unknown if all or only one of these genes is involved in the formation of ASD.

1.1.3 Clinical manifestation of the 16p11.2 CNV

First the 16p11.2 CNV was only associated with autism and schizophrenia (Weiss, Shen *et al*. 2008, Fernandez, Roberts *et al*. 2010, Shen, Chen *et al*. 2011). However, the

increasing number of aCGH analyses with large cohorts of patients presenting mental retardation or congenital anomalies showed, that the 16p11.2 CNV is not exclusively present in autism or schizophrenia patients (Horev, Ellegood *et al*. 2011). The description from different publications of subjects carrying a 16p11.2 deletion or duplication showed phenotypes including mostly developmental delay and problems with learning, speech, language, and behavior (Rosenfeld, Coppinger *et al*. 2010, Schaaf, Goin-Kochel *et al*. 2011). Beside the mostly similar reported phenotypes, two publications mentioned also that the 16p11.2 deletion is cosegregating with obesity (Shinawi, Liu *et al*. 2010, Walters, Jacquemont *et al*. 2010). Further, one of the publications also describes that patients with the 16p11.2 deletion presented macrocephaly, whereas patients with the duplication displayed microcephaly (Shinawi, Liu *et al*. 2010). Interestingly, all publications describe a strong variance in the phenotype of the 16p11.2 deletion carriers. One of the best examples for this is the publication by Shen, Chen *et al*. (2011). They investigated a Chinese family with three members carrying the 16p11.2 deletion. The observed phenotypes ranged from only language delay at an early stage in one brother to neurodevelopmental issues, dysmorphic features and malformations like atrial septal defect, scoliosis, myopia and ptosis in the other one. The conclusion of these results is that most of the dysmorphic features and malformations have to be caused by other events then the 16p11.2 deletion. Most probably they are caused by mutations in the hemizygous 16p11.2 locus. Even though the reason for the large variability remains unknown, all patients with the 16p11.2 locus showed problems in the diagnostic core features of ASD (Shen, Chen *et al*. 2011). This demonstrates that further investigations of the genes inside the 16p11.2 CNV are needed to understand the molecular mechanisms and their relation to ASD.

1.2 Zebrafish, a model for human neuronal diseases

Since its introduction as a new model organism for developmental studies in the 1970s by George Streisinger, the zebrafish *Danio rerio* has become a widely used tool in modern science. The reasons for this success was its availability all over the world, the cheap and easy maintaining of the embryos in fresh water, and the simple breeding. Furthermore, the *ex vivo* fertilization enables the manipulation of embryos. In addition, the embryos are transparent, which allows the optical examination of developmental defects in the living embryo. The embryos develop very quickly, within 3 days post

fertilization (dpf) the embryos hatch and start to swim. After three months the fish are fertile and can be used to produce the next generation.

But what makes this developmental model, which lacks the repertoire of human behaviors, suitable to understand the backgrounds of neuronal diseases. Most importantly, the neuronal development is following the same pattern like all vertebrates (see 1.3.2 Brain development of the zebrafish). Therefore, it is expected that the pattern of the brain development is based on the same molecular mechanism (Tropepe and Sive 2003). Another important reason for using the zebrafish to investigate diseases with a complex genetic background like ASDs is the great clutch size of 100 – 200 eggs and its fast development. This allows the screening of a large number of genes in a short time within an identical genetic background. The technique mostly used in these screens is a gene knockdown with morpholinos (Nasevicius and Ekker 2000). However, the zebrafish model is also suitable to test the overexpression of a gene by mRNA injection (Hyatt and Ekker 1999). The evaluation of a knockdown or overexpression in zebrafish is relatively easy. To uncover changes in the development the visual inspection is mostly sufficient. This can be supported by *in situ* hybridization, GFP labeled proteins or injection of fluorescent dyes into the vascular system or ventricles (Weinstein, Stemple *et al.* 1995, Gutzman and Sive 2009, Kalen, Wallgard *et al.* 2009). In addition to the optical examination of the knockdown embryos, zebrafish also offers the possibility of performing behavioral tests. For example, the choice chamber or conditioned place preference were mutant embryos are tested for a change of their preference for small molecules like morphine. Another method is the visual threshold measurement which tests the response of the mutant embryos to light (Darland and Dowling 2001, Bretaud, Li *et al.* 2007, Gerlai, Chatterjee *et al.* 2009).

An example where zebrafish has already been successfully used as a model for functional analyses of a human neuronal disease is the fragile X syndrome. This disease which is caused by the loss of the *FMR1* (*fragile X mental retardation*) gene is one of the most common forms of inherited mental retardation. In 2006 Tucker, Richards *et al.* showed that the knockdown of the orthologous *fmr1* gene in zebrafish results in abnormal axonal branching which could be rescued by treatment with MPEP [2-methyl-6-(phenylethynyl) pyridine]. MPEP is a known antagonist of the metabotropic glutamate receptor mGluR5 and has been shown to reduce the fmr1 loss induced behavior in mouse (Yan, Rammal *et al*. 2005). Additionally to Tucker, Richards *et al*.

(2006) the results of the *fmr1* knockdown in zebrafish were confirmed by Lin, Chang *et al.* (2006), who obtained similar results with a miRNA knockdown of the *FRM1* orthologous gene.

Another complex neuronal disease studied in zebrafish is schizophrenia, which is described as a debilitating psychiatric illness of which the causes are still unknown. However, it is postulated that in addition to genetic components also environmental factors are involved in the manifestation of schizophrenia (Lewis and Levitt 2002). One of the genes associated with schizophrenia is *DISC1* (*disrupted in schizophrenia 1*) (Chubb, Bradshaw *et al.* 2008). In 2009 Drerup and Wiora *et al.* tested the knockdown of the *DISC1* orthologous gene in zebrafish embryos. The knockdown showed abnormal craniofacial development together with a changed migration pattern of the cranial neural crest cells. This indicates the involvement of the *disc1* gene in the neuronal development.

Another schizophrenia-associated gene investigated in zebrafish is *SHANK3* (*SH3 and multiple ankyrin repeat domains 3*) (Gauthier, Champagne *et al.* 2010). Interestingly, *SHANK3* is not only associated with schizophrenia but also with ASD (Durand, Betancur *et al.* 2007). When the *SHANK3* orthologs were knocked down by morpholinos in zebrafish, embryos presented a reduced head, eye and trunk size and no response to physical stimuli. The presented phenotype of the embryos indicated a neuronal cause. This is supported by *SHANK3*-mutant rates where overexpression of *SHANK3* led to an increase in primary neurite outgrowth from somata (Gauthier, Champagne *et al.* 2010). Thus, the zebrafish ability for a reverse genetic investigation with the morpholino knockdown tool offers the chance to examine a large number of putative neuronal diseases (Tropepe and Sive 2003, Kabashi, Brustein *et al.* 2010, Mathur and Guo 2010).

1.3 Zebrafish, development and tools

As seen above the zebrafish has all features of a great model organism and offers also the ability to investigate human neuronal diseases. In this chapter the fundamentals of the zebrafish model organism are presented.

1.3.1 Brief description of the zebrafish development - from single cell to swimming larvae

This section is based on the very detailed descriptions of zebrafish development by Kimmel, Ballard *et al.* (1995) which is part of "The zebrafish book" (Westerfield 2000). The developmental stages of zebrafish embryo are linked to easy recognizable morphological structures. The zebrafish development starts with fertilization which is immediately followed by the swelling and lifting of the chorion from the yolk ball. During the enlargement of the first cell cytoplasmic movements towards the animal pole become visible. After approximately 20 min the first cell reaches its full size and the first cleavage starts. This repeats every 15 min so that 2.25 hours post fertilization (hpf) 128 cells are formed on top of the yolk ball. This event marks the entrance to the blastula period. At 4 hpf, the ongoing cell deviation has formed a smooth spherical structure on the yolk called blastoderm. The period in which the cells start to spread over the yolk is called epiboly stage (

Figure 3). The epiboly is measured in percent of blastoderm covering the yolk. Once 50 % of the yolk is covered by the blastoderm, the gastrulation starts. At full epiboly nearly 100 % of the yolk is covered with blastoderm. Now the posterior end of the embryo starts to swell which is theref cells start ore named bud stage. Next, in the segmentation period the embryo starts to grow along the anterior- posterior axis. It starts approximately 10 hpf and finishes at 24 hpf. During this time the somites are formed and the tail lifts from the yolk and lengthens. The distinct increase of somites along the anterior- posterior axis is now used to stage the embryos. At the end of the segmentation period 30 to 34 somites are formed. Beside the somites also eyes, ears, notochord and all three main parts of the brain start to form. At this point the embryo is comparable to the classical vertebrate anatomy.

The segmentation period is followed by the pharyngula period (24 – 48 hpf). During this phase the staging of the embryos is based on the position of the primordia, which is moving from the head anterior along the trunk and tail. During its motion the primordium leaves groups of sensory cells behind which form the lateral line.Beside the migration of the primordium also the opening of the head-trunk angle (HTA) and the reduction of the otic vesicle length (OVL) are used for staging embryos during the pharyngula period. The HTA is formed by two imaginary lines one through the middle of eye and ear and the other one along the notochord. Due to the lifting of the head from the yolk the HTA reduces during the hatching period and reaches nearly 0° by the end of the hatching period. Because of its direct association with the growth of the embryo the HTA allows a very quick approximation of the stage. In the same way the OVL is used to estimate the stage of the embryos. The OVL is simply the estimated number of otic vesicles fitting between eye and ear. During the development this distance will decrease because of the straightening of the head. Other important landmarks during the pharyngula period are the beginning of the pigmentation, the development of the cardiovascular system and most prominent the formation of the mouth.

The last stage of the embryonic development is the hatching period (48 – 72 h) which takes place during the entire third day. Therefore, the hatching itself is not useful as a developmental landmark. However, the constant growth of the embryos is not affected by the hatching.

The hatching period is divided into three different stages named after the growth of the pectoral fins. The first one is the long-pec stage (48 h). At this stage the embryos are approximately 3.1 mm long with an HTA = 45° and an OVL = ½. The pectoral fins are twice as long as they are wide. Viewed from the side the yolk ball is the same size as the head of the embryo. However, in the dorsal view the yolk is still wider than the head. During the long-pec stage also the circulatory system of the tail is completed, which is visible by the movement of erythrocytes.

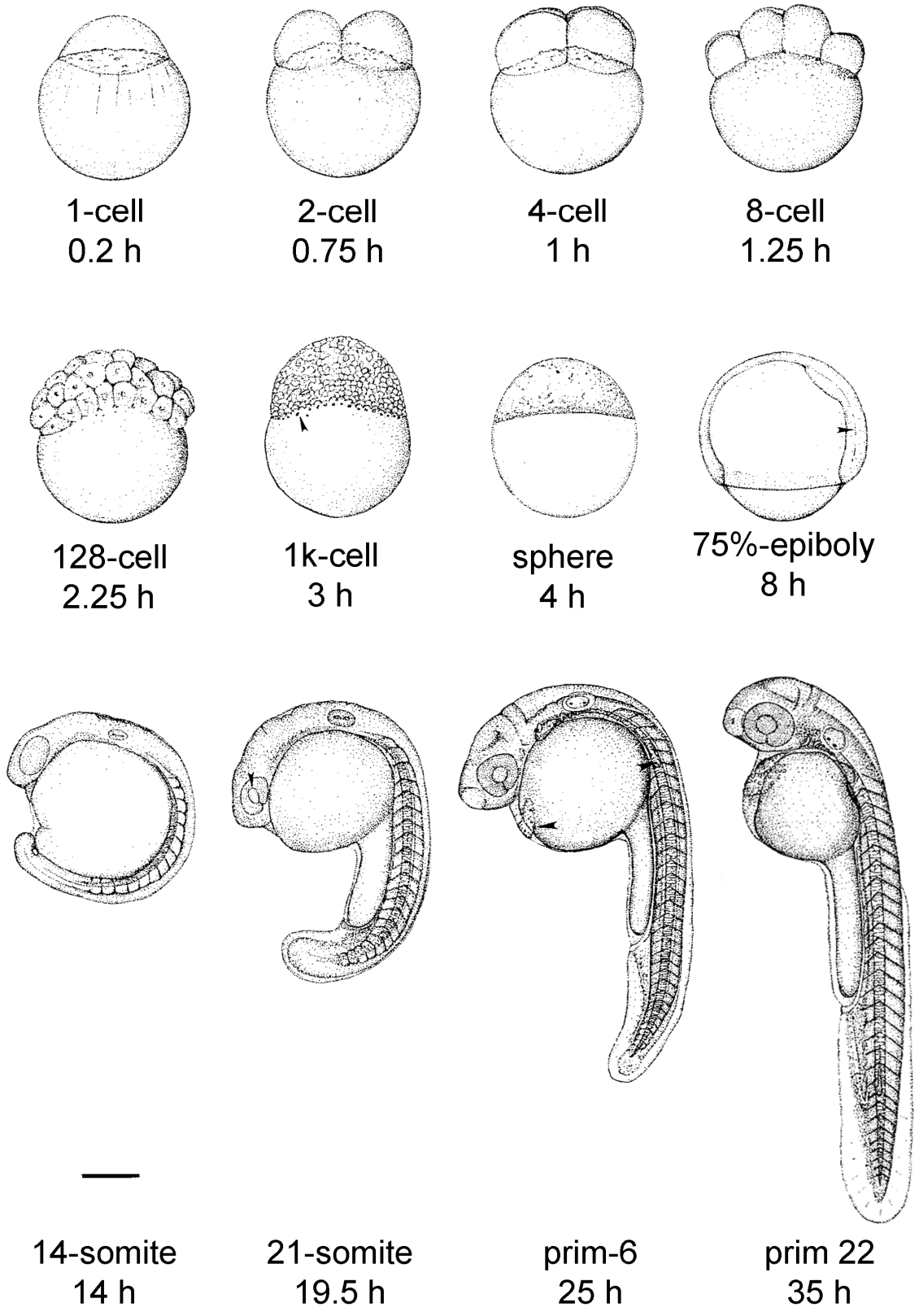

Figure 3 Early zebrafish developmental stages
Drawings of selected embryonic stages from one cell stage to the pharyngula period. Developmental stages before the epiboly are positioned with animal pole up. The later embryos are positioned anterior up, ventral left. Modified figure from Kimmel, Ballard *et al.* (1995). Scale bar 250 µm

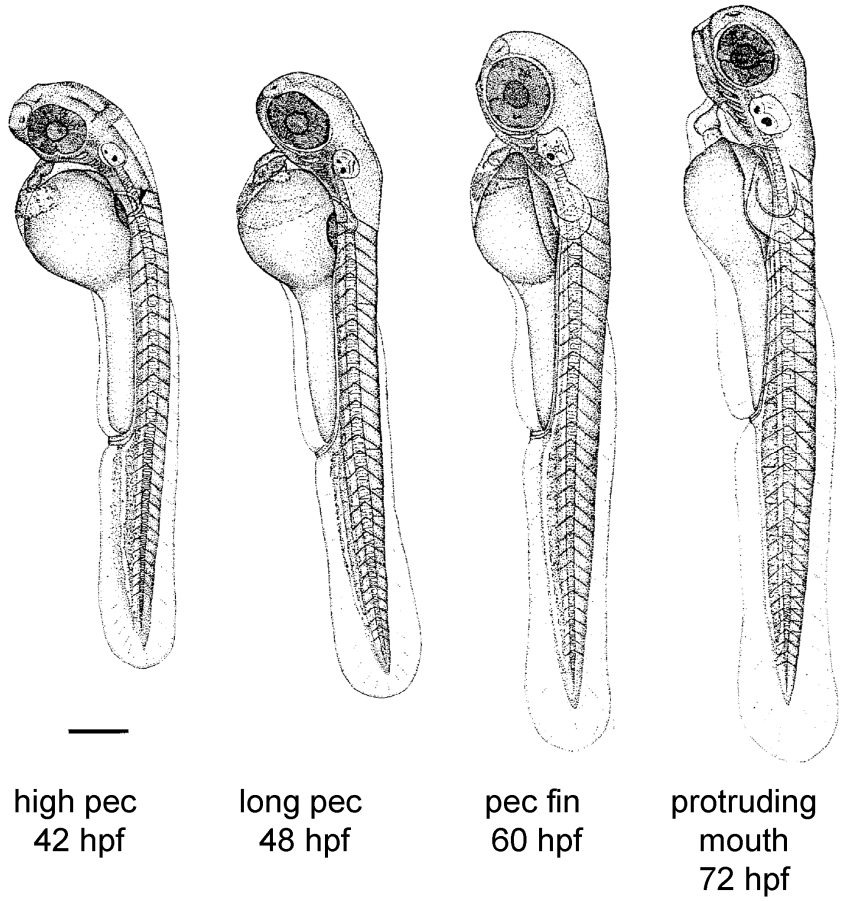

Figure 4 Developmental stages of zebrafish during hatching period
Embryos are positioned anterior up, ventral left. Figure taken from Kimmel, Ballard *et al.* (1995). Scale bar 250 µm

The second stage during hatching period is the pec-fin stage. The embryos are 3.3 mm long and the HTA = 55°. The distal part of the pectoral fin is flat with a blade like form. The end of the fin has reached the middle of the yolk ball. The width of the head measured between the middle of the eye is wider than the yolk. Viewed from the ventral side the forming mouth is visible at the anterior end of the eyes. The pigmentation of the retina is so strong that the lens are slightly visible in the dorso-ventral view. The embryos show a rapid escape response on a stimulus and rest dorsal up after swimming.

The last part of the hatching period is the protruding- mouth stage. The embryos reached a length of 3.5 mm with a HTA = 25°. The wide opened mouth protrudes anteriorly. The pectoral fins reached the length of the yolk ball. Inside the embryo intestines like gut, liver, kidneys and swim bladder start to develop. Further, the embryos start to swim with only small periods of resting. The protruding mouth stage marks the end of the embryonic development and the start of the larval development. At

4 dpf the swim bladder is fully inflated and easily visible within the trunk. Therefore, it can be used as a good staging feature.

The description of the zebrafish embryogenesis presented here is only a short summary based on the very detailed publication of Kimmel, Ballard *et al.* (1995).

1.3.2 Brain development of the zebrafish

The brain development is an evolutionary highly conserved and well examined process. Therefore, the brain-forming progenitor cell, can be traced back already to the shield stage (6 hpf). The gastrulation is followed by the formation of the neural plate (10 hpf). During the next three hours the neural plate is folding towards the midline and transforms into the neural rod (Figure 5). The neural rod is the basis of the brain which starts to differentiate at the segmentation period. During this process 10 segments, called neuromeres, become visible. The first three of them are larger and correspond to the three rostral parts of the brain: the telencephalon and diencephalon, which are forming the forebrain, and the midbrain. The last seven neuromeres are called rhombomeres and form the hindbrain (14 somite stage) (Kimmel 1993, Quesada-Hernandez, Caneparo *et al.* 2010).

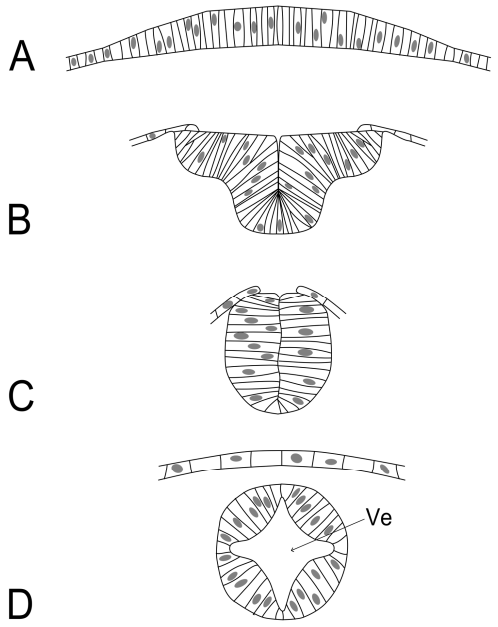

Figure 5 Morphogenesis from plate to tube
A) The neural plate shows a vertical enlargement of the cells (10 hpf). During the morphogenesis the neural plate is folded towards the midline, when folded half the structure is called keel (B, 13 hpf). At the end of the folding the shape is cylindrical and called neuronal rod (C, 16 hpf). At 20 hpf inside the neuronal rod the ventricle starts to swell, the structure is now called neuronal tube. Figure is a redraw from Papan and Camposortega (1994) and Gutzman, Graeden *et al.* (2008)

The next structural change of the brain is based on the swelling of the ventricles inside the neural rod, which therefore is termed neural tube. The ventricles are filled with cerebrospinal fluid (CSF) which provides nutrients, signal molecules, and metabolites for the brain. Therefore, changes in the ventricles can affect the formation of the brain (Sawamoto, Wichterle *et al.* 2006, Gutzman and Sive 2010). After reaching its maximum size at 1 dpf the ventricles

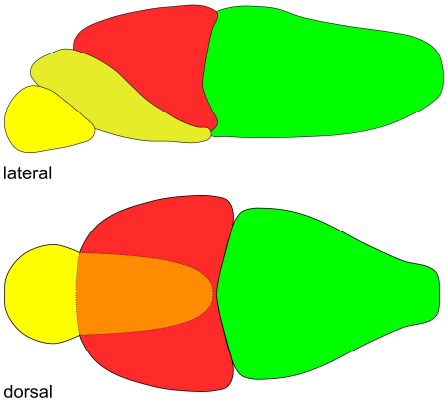

Figure 6 Sketch of a zebrafish brain 3 - 5 dpf
Brain is viewed lateral and dorsal. The forebrain consists of the telencephalon (yellow) and diencephalon (dark yellow). In the dorsal view the diencephalon is hidden by the midbrain (red). The last part of the brain is the hindbrain (green) which is connected to the spinal cord

decrease dramatically (Kramer-Zucker, Olale *et al.* 2005). During the ventricle formation also the formation of motor, sensory and interneurons starts, this process is called the primary neurogenesis (Kimmel, Powell *et al.* 1982, Bernhardt, Chitnis *et al.* 1990, Chitnis and Kuwada 1990). Surprisingly, these primary neurons are only used for a short period. They are completely replaced at the secondary neurogenesis, which takes place at 2 - 3 dpf. On the third day the brain reaches its general shape built by forebrain, midbrain and hindbrain (Figure 6) (Bernhardt, Chitnis *et al.* 1990). Interestingly, the differentiation and the neuronal structuring of the zebrafish brain require the same molecular mechanisms like all other vertebrates. Therefore, it is possible to use zebrafish also as a model for brain development (Tropepe and Sive 2003).

1.3.3 Two of one, whole-genome duplication of the teleost fish

Almost two decades ago whole-genome duplication (WGD) events at the origin of the vertebrate lineage were proposed (Ohno 1970). Meanwhile, the analysis of the human genome and other vertebrates revealed convincing evidence for two WGD in the ancestral vertebrate lineage (Holland, Garcia-Fernandez *et al*. 1994, Gibson and Spring 2000, Hughes, da Silva *et al*. 2001, Panopoulou, Hennig *et al*. 2003, Dehal and Boore 2005). Interestingly, the comparison of the vertebrate and the teleost genome showed an additional copy of syntenic clusters which indicates a third WGD at the base of the teleost fish (Christoffels, Koh *et al*. 2004, Meyer and Van de Peer 2005).

Most of the duplicated genes originating from a WGD are lost during evolution. However, some genes retain a subset of the ancestral gene function (subfunctionalization) while others adopted a complete new function (neofunctionalization) (Christoffels, Koh *et al.* 2004, Hufton, Groth *et al.* 2008). Therefore, the knockdown of a gene present twice in a genome has to be carefully interpreted.

1.3.4 Morpholinos - the smart knockdown tool

One of the most important tools to work with zebrafish are morpholinos, which were first described by Summerton and Weller (1997). They created a synthetic DNA-like structure with a backbone based on a morpholino ring and a phosphorodiamidate group instead of a deoxyribose ring connected by a phosphate group. This synthetic backbone prevents the degradation and enhances the melting temperature in morpholino RNA hybrids. Therefore, morpholinos are highly efficient in a specific target gene knockdown by blocking the translation or splicing of the mRNA.

Morpholinos offer two possible mechanisms to knockdown a gene. The first mechanism blocks the translation, therefore the morpholino sequence is designed complementary to the 5' UTR of the target gene. The binding of the morpholino in this region will prevent the assembly of the ribosome so that the mRNA cannot be translated into a protein. Importantly, the morpholino does not induce the degradation of the mRNA. The mRNA will remain intact until its natural degradation, which releases the morpholino. Therefore, RT-PCR cannot be used to test the success of the knockdown (Summerton and Weller 1997, Nasevicius and Ekker 2000, Bill, Petzold *et al.* 2009).

The second morpholino knockdown mechanism is the altering of the splicing, which leads to a misspliced mRNA. In this case the morpholino is designed complementary to an intron-exon (I-E) or exon-intron (E-I) junction. This will mostly result in an exon skipping during the splicing process (Figure 8, page 15). Only the morpholinos against the first or last exon are likely to cause an intron insertion (E1-I1; I3-E4 Figure 7). In some rare cases the morpholino blocking of a splice site can also lead to cryptic splicing (Draper, Morcos *et al.* 2001). In this case the splicing machinery uses an unpredicted splice site, which in most cases lead to a partial deletion or insertion. All splice blocking morpholinos generate a differently processed mRNA which can be identified by PCR. Simply two primers in the neighboring exons are needed to verify a shift of the amplified PCR product size. Both methods of morpholino induced knockdown show a

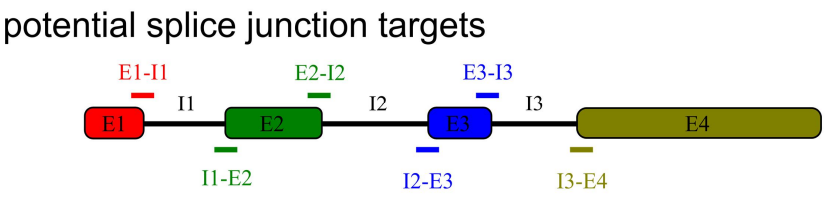

Figure 7 Splice junction targets of morpholinos
Illustration of a mRNA consisting of 4 exons (E) and 3 introns (I). Morpholinos are indicated as bars close to the mRNA at their targeting splice junction.

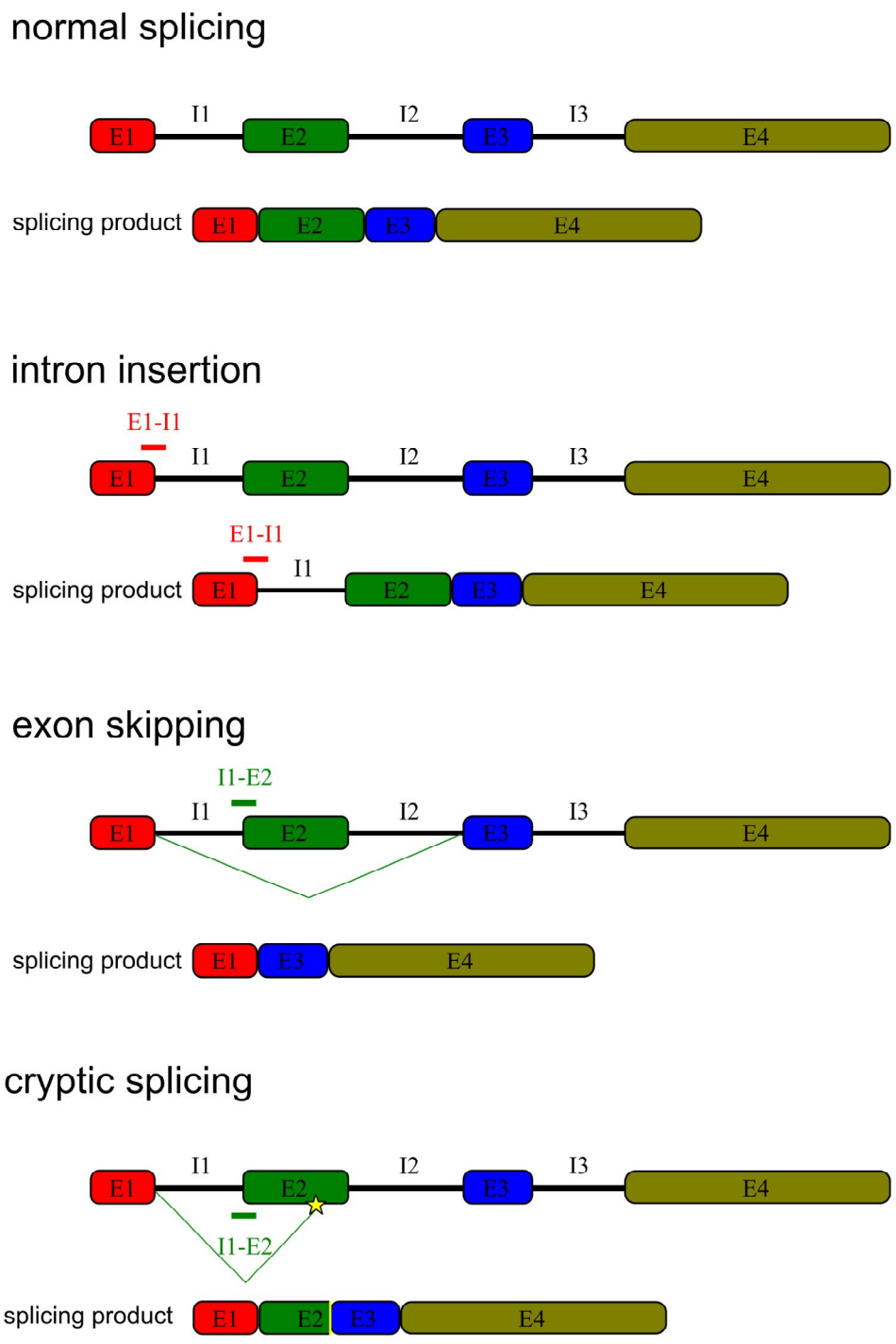

Figure 8 Mechanisms of splice blocking morpholino knockdown
Represented is an mRNA with 4 exons (E) and 3 introns (I) before and after splicing. Morpholinos are indicated by bars above the mRNA at their targeting intron-exon junction.

very high success rate (Summerton and Weller 1997, Bill, Petzold *et al.* 2009, Bedell, Westcot *et al.* 2011).

The challenge when using morpholinos is that they have to be actively delivered into the cell. The easiest way to do this in zebrafish is the injection into the yolk ball.

Because of the superficial cell division the cell does not have a membrane towards the yolk and the morpholino can enter the cell by diffusion. The injection itself does not affect the development of the embryo so that all observed changes are attributable to the morpholino. However, it has to be kept in mind that the morpholino effect will reduce during development. The reason for this is the growing number of cells, which lowers the concentration of morpholinos per cell. Therefore, a morpholino is more likely to generate a knockdown rather than a complete knockout. However, the morpholino injection is the fastest way for reverse genetic investigation and offers the possibility to examine a knockdown in the most important time during the development (Nasevicius and Ekker 2000, Bedell, Westcot *et al.* 2011).

1.4 Information for selected genes of the 16p11.2 locus

Due to the large number of genes within the human 16p11.2 locus only 7 were selected for further investigation in zebrafish. A detailed explanation of the reasons for this selection is given in the result section. For each of the selected human genes, the published information is summarized here.

1.4.1 Aspartate beta-hydroxylase domain containing gene 1

One of the selected genes from the 16p11.2 locus is the aspartate beta-hydroxylase domain containing gene 1 (*asphd1*). Hydroxylation is an important post-transcriptional modification facilitated by a group of enzymes named hydroxylases. The modification processed by these enzymes is the addition of a hydroxyl group to an amino acid (aa). Interestingly, hydroxylation is one of the few known removable post-transcriptional modifications (Gronke, VanDusen *et al*. 1989, Lavaissiere, Jia *et al*. 1996). The importance of hydroxylases can be shown by the well-known disease phenylketonuria, which is caused by mutations in the phenylalanine hydroxylase gene (Blau, van Spronsen *et al*. 2010). However, the function of the *asphd1* gene is completely unknown. Therefore, the results of this thesis can help getting a better understanding of its function.

1.4.2 Glycerophosphodiester phosphodiesterase domain containing gene 3

In the human genome, five glycerophosphodiester phosphodiesterase domain containing (*GDPD1-5*) genes are found. These enzymatic proteins are highly conserved during evolution. They catalyze the hydrolysis of glycerolphosphorlipides to glycerol phosphate and an alcohol (Shi, Liu *et al*. 2008). Surprisingly, there was no publication about the 16p11.2 located *GDPD3* available. However, the importance of these enzymes is shown by the known functions of the other members of the *GDPD* family. For example *GDPD2*, which is expressed during the osteoblast differentiation, is capable of changing the morphology of HEK293T cells from a spread to round phenotype (Corda, Kudo *et al.* 2009). Another member of the *GDPD* family, which was found to be expressed in the brain and spinal cord, is *GDPD5*. It was shown that *GDPD5* is important for the differentiation of motor neurons and is also involved in the outgrowth of Neuro2A cells (Rao and Sockanathan 2005, Yanaka 2007, Yanaka,

Nogusa *et al.* 2007, Lang, Zhang *et al.* 2008). Due to the additional whole-genome duplication in teleosts, the zebrafish genome harbors two *gdpd3* genes. The first is *gdpd3a* which is located on chromosome 3 and the second is *gdpd3b* located on chromosome 12. However, the function of both genes is unknown.

1.4.3 *kctd13* an interaction partner of the DNA polymerase δ

In a yeast two-hybrid screen He, Tan *et al.* (2001) searched for interaction partners for the small subunit (p50) of the DNA polymerase delta (Pol δ). The screen identified an open reading frame (ORF) which was coding for a 36kDa protein named polymerase delta-interacting protein (PDIP1). This protein encoded by the potassium channel tetramerisation domain containing gene 13 (*KCTD13*) is located at 16p11.2. In further pull down experiments He, Tan *et al.* (2001) showed that PDIP1 interacted simultaneously with the p50 subunit of the Pol δ and the proliferating cell nuclear antigene protein (PCNA), which is a known coordinator of DNA replication and cell-cycle progression (Waga and Stillman 1998).

Interestingly, members of the *KCTD* family have already been shown to influence the human neuronal system. One of them is *KCTD7*, which it associated with progressive myoclonic epilepsy (PME) (Van Bogaert, Azizieh *et al.* 2007). Further, experiments in cultured mouse cortical neurons showed that the overexpression of *KCTD7* reduces the excitability of the neurons (Azizieh, Orduz *et al.* 2011). Another interesting finding is the link of the brain-expressed *KCTD15* with obesity (Willer, Speliotes *et al*. 2009).

Because of the association of the KCTD family with neuronal diseases, *KCTD13* became interesting for others as well. In 2012, Golzio, Willer *et al*. published that the overexpression and knockdown of *KCTD13* influences the head size of 4 day old zebrafish embryos. In their study, they tested the overexpression of each gene located in the 16p11.2 CNV. To verify a change in the brain size they measured the head size of 4 day old mRNA injected embryos. They found that only the injection of the *KCTD13* mRNA reduced the head size of the embryos. Further, they tested the morpholino knockdown which resulted in an enlargement of the heads. To verify that the number of cells changed they counted them in slices of the telencephalon, diencephalon and mesencephalon. As seen in the head size measurement, the number of cells was decreased in the *KCTD13* overexpression and increased in the knockdown. Golzio,

Willer *et al.* (2012) found out, that the increase of cells was accompanied by cell deviation (phosphor-histone H3 assay), whereas the overexpression resulted in a higher number of apoptotic cells (TUNEL assay). Yet the molecular reasons for these results remain unknown.

1.4.4 *MAPK3, a* member of the Ras/Raf/ERK1 pathway

The mitogen-activated protein kinases represent an evolutionary strongly conserved family, present in the three eukaryotic kingdoms: Animalia, Plantae and Fungi. Proteins of this family have been shown to be important in various cellular processes such as cell growth, proliferation, differentiation, survival and development. A member of this family is the mitogen-activated protein kinase 3 gene (*MAPK3*), which is located at 16p11.2. This gene consists of eight exons which encode the extracellular signal-regulated kinase 1 (ERK1) protein (Johnson and Lapadat 2002, Krens, He *et al.* 2006).

The ERK1 protein is part of the Ras/Raf/ERK1 pathway which is involved in growth factor signaling, cytokine signaling and cancer pathogenesis (Bentires-Alj, Kontaridis *et al.* 2006). This pathway is associated with the neuro-cardio-facial-cutaneous syndrome (NCFC). Patients with this disease show several strong phenotypic changes like congenital anomalies, mental retardation, macrocephaly, heart defects and a general developmental delay (OMIM 115150) (Roberts, Allanson *et al.* 2006).

From the zebrafish experiments by Krens, He *et al.* (2008), it is known that the knockdown of ERK1 and ERK2 results in a cell migration defect during development. Due to this defect the embryos present a reduced body axis with a small but distinguishable head.

In 2011, the group of Xiaohong Li published a direct connection between the Ras/Raf/ERK1 pathway and autism (Yang, Sheikh *et al.* 2011, Zou, Yu *et al.* 2011). However, the publications based on mice and human brain tissue examinations were retracted in 2013. Therefore, further investigation to identify a link between *MAPK3* and ASD is needed.

1.4.5 *ppp4c* - one gene many functions

At the end of the 1930s, Carl and Gerty Coti found two forms of glycogen phosphorylases. However, it was a long way until the relevance of protein phosphorylation was accepted (Hubbard and Cohen 1993, Cohen 2002). Today three

protein phosphatase families are known: the phosphoprotein phosphatases, the metal-dependent protein phosphatases and the aspartate-based phosphatases. The *PPP4C* gene located at 16p11.2 encodes a phosphoprotein phosphatase 4 catalytic subunit which is involved in a variety of processes. As an example, *PPP4C* is involved in the microtubule organization at centrosomes (Sunkel, Gomes *et al.* 1995, Helps, Brewis *et al.* 1998, Sumiyoshi, Sugimoto *et al.* 2002), in the maturation of spliceosomal snRNPs (Melki 1997, Matera 1999, Gubitz, Mourelatos *et al.* 2002), in the tumor necrosis factor (TNF)-alpha signaling (Zhou, Mihindukulasuriya *et al.* 2002), and in the regulation of histone acetylation (Cohen, Philp *et al.* 2005, Zhang, Ozawa *et al.* 2005). However, the role of *PPP4C* during the embryogenesis remains unknown.

The first publication showing how *ppp4c* is influencing the embryogenesis was written by Kalén, Wallgard *et al.* in 2009. They performed a zebrafish reverse genetic screen on 50 potential angiogenesis genes to test their influence on the heart and blood vessel formation. Surprisingly, three of them were serine/threonine phosphatases including *ppp4c*. Investigating the *ppp4c* knockdown embryos by microangiography revealed, that the circulatory loop in the trunk vascular system was not established at 48 hpf. To confirm their results Kalén, Wallgard *et al.* used two morpholinos per gene. Because of the teleost specific whole-genome duplication, some of the selected genes existed in two copies, in which case they performed double knockdown experiments. Since *PPP4C* has two orthologs in zebrafish, namely *ppp4ca* and *ppp4cb*, it must be concluded that Kalén, Wallgard *et al* performed a double knockdown. However, in their supplement the microangiography is only shown for *ppp4ca* and Kalén, Wallgard *et al.* are not mentioning the second ortholog of *ppp4c*. Most importantly the embryos were not investigated for changes in the nervous system. So it still remains unknown if *ppp4c* is affecting the neuronal development.

During the experiments for this thesis, another *ppp4c* morpholino knockdown in zebrafish was published. Surprisingly, this one was different from the Kalén, Wallgard phenotype. Jia, Dai *et al.* (2012) showed that the *ppp4ca* and *ppp4cb* knockdown resulted in a dorsalization of the embryos. Further, they found that *ppp4c* is required for the ventralizing activity of BMP which is initiated by binding to Smad1/Smad5. For the knockdowns Jia, Dai *et al.* also used two independent morpholinos per gene.

The reason for the difference of the published phenotype by Kalén, Wallgard *et al.*(2009) (problems in trunk vessel formation) and Jia, Dai *et al.* (2012) (ventralization of the embryos) is unclear. Therefore, further investigation of *ppp4ca* and *ppp4cb* is necessary to clarify this difference.

1.4.6 *SEZ6L2*, a gene with many variations in autism patients

The human *seizure related 6 homolog* gene family consists of three genes. The first gene identified was *SEZ-6.* It was found in a study were cortical neurons were treated with the seizure-inducing reagent pentylenetetrazole (Shimizu-Nishikawa, Kajiwara *et al.* 1995). Since that time the two other members *SEZ6L* and *SEZ6L2* have been identified. The *seizure related 6 homolog (mouse)-like 2* (*SEZ6L2*) is located in the 16p11.2 region (Kumar, KaraMohamed *et al.* 2008).

Because of the relatively low resolution of aCGH, Kumar, Marshall *et al.* (2009) sequenced eight genes of the 16p11.2 region in 1106 autism patients to identify smaller variations important for ASD. As a result of the sequencing, they identified 12 sequence variations in the promoter and the coding sequence of *SEZ6L2*. However, they also found three variations in the *SEZ6L2* gene of the control cohort (1161 persons). In 2011, Konyukh and Delorme *et al.* confirmed this study by testing 170 autism patients for variations in the *SEZ6L2* gene. They identified seven previously unknown non-synonymous mutations in ASD patients. However, surprisingly they also found six *SEZ6L2* variations in the control cohort (282 persons). From these results Konyukh, Delorme *et al.* concluded that the high variability in the *SEZ6L2* gene of ASD-unaffected persons reduces its possible impact on ASD (Konyukh, Delorme *et al.* 2011).

Nevertheless, the expression of *SEZ6L2* in the human fetal brain (Kumar, Marshall *et al.* 2009) and the strong homology to the epilepsy and language disorder associated gene *SRPX2* (Roll, Rudolf *et al.* 2006) make *SEZ6L2* still a considerable candidate for being part of the complex genetic background in autism spectrum disorder.

1.4.7 The Yippee like gene 3, potentially regulated by *p53*

The first *YPEL* gene was found in *Drosophila* and named Yippee (Lanz-Mendoza, Bettencourt *et al.* 1996). Meanwhile, the increasing number of sequenced genomes uncovered Yippee like genes in all three eukaryotic kingdoms: Aninmalia, Plantae and Fungi. In 2004, Hosono and coworkers identified more than 100 different Yippee like

genes in 68 species (Hosono, Sasaki *et al*. 2004). By aligning the different Yippee like genes they uncovered a consensus sequence including a zinc finger binding motif. By comparing the human with the zebrafish genome five different *ypel* genes were found. Like all *ypel* genes also the zebrafish ortologs show a strong conservation. The strong conservation during evolution in animals, plants and fungi indicates an important function of *ypel3* (Hosono, Sasaki *et al.* 2004), (Roxstrom-Lindquist and Faye 2001).

The functions of the *ypel3* gene are still not completely understood, but it was found that the human YPEL1-4 proteins localize at the centrosome and nucleolus during the interphase, visible as several dot-like structures. The human YPEL5 protein also localizes at the centrosome and nucleus during interphase, but in contrast to the other four YPEL proteins it localizes additionally at the spindle apparatus (Hosono, Sasaki *et al.* 2004). Other recent studies described *YPEL3* as a downstream target of *TP53* a known tumor suppressor gene, which under DNA damaging conditions, is capable to induce cell cycle arrest or senescence. They presented microarray studies where *YPEL3* reacted the same way like the *TP53* expression level of the knockout or reactivations. Furthermore, it is known that a p53 binding site is located close to the human *YPEL3* promoter. Yet a direct link between p53 and *YPEL3* is not known. However, it can be concluded that its function is upstream of p53 (Kelley, Miller *et al.* 2010, Berberich, Todd *et al.* 2011).

1.5 Aim of the thesis

With an estimated prevalence of 1.0 - 2.6 % among the population, autism spectrum disorder is the most common neurological disorder (Fombonne 2010, Boyle, Boulet *et al*. 2011, Kim, Leventhal *et al*. , MMWR 2012). However, its complex genetic background disguises the molecular cause of the disease. The most commonly used technology to uncover genes directly associated with autism has been microarray-based comparative genomic hybridization (aCGH), which revealed more than 2000 CNVs and 300 genes (AutDB) linked to ASD (Basu, Kollu *et al*. 2009). To be able to functionally analyze all these candidate genes, a model organism that: I) is evolutionary not very distant from humans, II) has got the potential of large scale screening, III) enables to perform the analysis in short time at an affordable price is required. This thesis aims at demonstrating the potential of zebrafish in fulfilling this role through the functional analysis of a zebrafish genomic region which is syntenic to the human 16p11.2 region, the most frequently deleted region in ASD patients.

As a first step, the zebrafish orthologs of the human 16p11.2 region will be identified by phylogenetic analysis based on sequence conservation. Then suitable candidate genes will be selected based on synteny as this indicates a strong functional evolutionary conservation. Subsequently, the spatial and temporal expression of selected genes will be tested in embryos via *in situ* hybridization with the purpose of selecting only neuronal expressed genes for further analyses via morpholino-based knockdown studies. The aim of this thesis is to investigate the potential of zebrafish as a model system for studying the molecular pathways underlying ASD through the study of the zebrafish orthologs of the human 16p11.2 genes

2 Materials

In this chapter all materials used in this thesis are listed.

Table 1 Primer for antisense RNA design

Primer name	Primer sequence 5' – 3'
ASPHD1-F	CACTACAAGAGTATGCCAAGC
ASPHD1-R	AATTCACACTGAGCAGGAGTC
GDPD3-F	ACACTCGACGGATATGTTGTAG
GDPD3-R	ATGTAGTCAGACAGGACAGTC
KCTD13-F	CAAGATTGCTGAAGTCTGCTG
KCTD13-R	GGCTTACATTAGTCATTGAAA
MAPK3-F	TCCATTTGAACACCAGACCTAC
MAPK3-R	TACAAACAGATCGCCGACTTAC
PPP4Ca-F	TGACCTGGACAGACAAATTGAG
PPP4Ca-R	TGGAGCAGACCATACTGTCAAC
PPP4Cb-F	ATGGGTGACATGAGTGATCTG
PPP4Cb-R	TACAGCATACCGTGAGTCTGAG
YPEL3-F	CCTATCTGGACTCCTGTCATC
YPEL3-R	CTACACAATCATAACACATCTGC
SEZ6L2-zf-F	CGGCAGATTCCTCCTCCATC
SEZ6L2-zf-R	ACTTTACAGAAGGGCGGTGG

Table 2 Primer for verification of morpholino splice site effects

Primer name	Primer sequence
P-*kctd13*-e2-F	GAGCGTTTGGACTGTGGTGT
P-*kctd13*-e3-R	GGGACGGGACAGTTCCTTTG
P-*kctd13*-e4-R	TGCAGAGGTTGTCACATTCCTA
P-ypel3-e2-F	ACACCTGGCCAATCACGATG
P-ypel3-e5-R	GCTCAACTCAAAGGCCTGCT
P-ypel3-i3-R	GCCTTTGTGGAGTTAAGCAAG
P-*mapk3*-e1F	TGACCGACTCCTCTTCGACT
P-*mapk3*-e3-R	CCTTGAGGTCACAGGTGGTG
P-*ppp4ca*-e1F	AGGCCTTTTCCCTTTCCCAA
P-*ppp4ca*-e4-R	GTGACAGGAGAATCTACACTCTGA
P-*ppp4cb*-i3-R	TTGGCCACGACCATTCATGT
P-*ppp4cb*-e2-F	CCGCATCTCTGGTGTGAGTG
P-*ppp4cb*-e4-R	GGTCATAAAACTGCCCGTGGA
P-*ppp4cb*-i3-2-R	CTTCTCTATGCAGTGTTTGTGA
P-*gdpd3*-e1F	CGAGCTGCCTGTACTACCTG
P-*gdpd3*-e3R	TCTGTGCCCACTTCAACAGC

Table 3 Morpholino sequences and their target sites
Morpholinos were purchased from Gene Tools LLC

morpholino target gene	target site	morpholino sequence
MO-*kctd13*	5'UTR	CGAACCAGATGCCTCGGCAGACATC
MO-*kctd13*	i2e3	CCAGCCTTCAATACAAATGGACACA
MO-*ypel3*	5'UTR	TTTTGGCCTTGGTCTGCTTCACCAT

morpholino target gene	target site	morpholino sequence
MO-*ypel3*	e3i3	TTGAAAGAAGTCATACTCACACAGA
MO-*gdpd3*	5'UTR	AGTACAGGCAGCTCGCCATATTTCC
MO-*gdpd3*	i2e3	CACCAGAACCTGAGGACAGAGAGCA
MO-*mapk3*	5'UTR	TACTGCCCGATTCCGCCATCGTTTC
MO-*mapk3*	e2i2	TGTGAGTGTTTAAGGATACACATCC
MO-*ppp4ca*	5'UTR	AAGTCGCCCATGATGACACACATGC
MO-*ppp4ca*	e2i2	TGGAGTAAAAGGAGTTACCTTGCTT
MO-*ppp4cb*	5'UTR	GGTCCAGATCACTCATGTCACCCAT
MO-*ppp4cb*	e3i3	TTTGTGAATACTCACCGTGACAGGA
MO-*asphd1*	5'UTR	AAGTCCAGAGACCAGGACATAATGC
MO-*sez6l2*	5'UTR	CATGGTTCAATATGACAGAACAGCC
SCMO		CCTCTTACCTCAGTTACAATTTATA

Table 4 List of used chemicals

Chemical	Company / distributor	Catalog-Nr.
Agarose	Invitrogen	15510-019
Ampicillin	Sigma	A9393
5-Bromo-4-chloro-3-indolyl phosphate p-toluidine salt (BCIP)	Sigma	B8503
Betaine	Sigma	B2629
BigDye-Terminator-Mix	Lifetechnologies	4337458
Bovine serum albumin (BSA)	Roth	8076.1
Bromphenol blue	Merck	1.081.220.025
Calcium chloride	Merck	1.023.821.000
Chloroform	Merck	1.024.312.500
Citric acid	Merck	1.064.481.000
DEPC	Sigma	D5758
Denhardt's Solution	Lifetechnologies	750018
DIG-RNA Labelling Mix	Roche	1277073
DNazol	Invitrogen	10503-027
dNTPs	Pharmacia	27-2035
DTT	Invitrogen	D-1532
EDTA	Sigma	E4378
Ethanol	Merck	1.009.862.500
Ethidium bromide	Sigma	E1510
Formamid	Merck	109.684
Formamid (bioUltra 99,5 %)	Fluka	47671
Glucose	Merck	1.083.422.500
Glycerin	Merck	104.093.100
Heparin	Sigma	H9399
HEPES	Calbiochem	391338
Hydrochloric acid	Merck	1.090.571.000
Hydrogene peroxide	Merck	108597
Isopropyl alcohol	Merck	1.096.342.500
Kanamycin	Sigma	K4000
Lithium chloride	Merck	1.056.790.250
Magnesium chloride	Merck	1.058.331.000
Magnesium sulfate	Merck	1.058.861.000

Chemical	Company / distributor	Catalog-Nr.
Maleic acid	Sigma-Aldrich	M0375-1KG
Methanol	Merck	106009-2500
Methylene blue	Merck	1.159.430.025
Nitro blue tetrazolium (NBT)	Sigma	N6876
Paraformaldehyde (PFA)	Sigma	P6148-500G
PBS - tablets	Geneaxxon	D2002.010
Penicillin	Sigma	P3032
Phenol red	Sigma	P0290-100ML
Paraplast (Paraffin)	Leica	
Potassium chloride	Merck	1.049.361.000
RNA Storage Solution	Ambion	7000
RNasin Ribonuclease Inhibitor	Promega	N2511
Rhodamine B isothiocyanate-Dextran (wt~70.000)	Sigma-Aldrich	R9379
Sodium acetate	Merck	1.062.681.000
Sodium chloride	Merck	1.064.001.000
Sodium phosphate	Merck	1.065.855.000
Tricaine	Sigma	A5040-5G
TRIS	Merck	1.083.820.500
Triton X-100	Sigma	X100-5ML
Triethanolamine	Sigma	T1377
tRNA from yeast	Sigma	R6625
Tween 20	Sigma	P9416
UltraClear clearing reagent		
X-Gal	Sigma	B9146

Table 5 List of used enzymes

Name	Company / distributor	Catalog-Nr.
BstXI	New England Biolabs	R0113S
Eco RI	New England Biolabs	R0101S
Eco RV	New England Biolabs	R0195S
Kpn I	New England Biolabs	R0142S
Not I	New England Biolabs	R0189S
Spe I	New England Biolabs	R0133S
Xba I	New England Biolabs	R0145S
Xho I	New England Biolabs	R0146S
NEB I buffer	New England Biolabs	B7001S
NEB II buffer	New England Biolabs	B7002S
NEB III buffer	New England Biolabs	B7003S
NEB IV buffer	New England Biolabs	B7004S
BSA	New England Biolabs	B9001S
T4 DNA ligase	New England Biolabs	M0202S
T4 DNA ligase buffer	New England Biolabs	B7003S
M-MLV reverse transcriptase / reverse transcriptase buffer	Promega	M531A
RNasin RNase inhibitor	Promega	N2511
Sp6 RNA polymerase	Roche	810274
T7 RNA polymerase / transcription-buffer	Roche	881767

Name	Company / distributor	Catalog-Nr.
Pronase E	Sigma	P69111G
Phire Hot Start II DNA polymerase	Thermo Scientific	F-122S

Table 6 List of used DNA / RNA ladders

Name	Company / distributor	Catalog-Nr.
2-log DNA ladder (0.1-10.0 kb)	New England Biolabs	N3200L
RiboRuler RNA ladder	Fermentas	SM1821

Table 7 List of used Kits

Name	Company / distributor	Catalog-Nr.
QIAprep Spin Miniprep Kit	Qiagen	27106
QIAquick PCR Purification Kit	Qiagen	28106
QIAquickGel Extraction Kit	Qiagen	20021
peqGold Total RNA kit	Peqlab	12-6834-01
TOPO TA cloning Kit dual promoter	Invitrogen	45-0640
Dual Promoter TA cloning Kit	Invitrogen	45-0007
Anti-digoxigenin-antibody	Roche	11093274910

Table 8 List of used devices

Device	Manufacturer
incubator BK700	Heraeus
binocular Leica MZ8	Leica
electrophoreses-chamber	Stratagene
heating block	Eppendorf
magnetic stirrer	Heidolph
micro injector FemtoJet	Eppendorf
micropipette puller P-97	Sutter Instruments
borosilicate glass filament O.D.:1,0 mm I.D.:0.78mm 415-883-0128	Sutter Instruments
microscope LSM510	Zeiss
microscope inverse with micromanipulator	Leica
microtome HM 355 S	Leica
nanodrop	Nanodrop
precision scales	Mettler Toledo
shaker horizontal	New Brunswick Scientific
speed Vac	Savant
thermo cycler	MJ Research Inc.
table centrifuge	Eppendorf
UV-Illuminator	Alpha Innotech
vortexer	Bender & Hobein
NM 355S Automatic Microtome	Thermo scientific
axiovert 200M	Zeiss
AxioCam MR	Zeiss

Table 9 List of standard solutions

Solution	Chemicals for preparation
Agarose gel loading buffer	4 mM TRIS (pH 8.0), 0.2 mM EDTA, 0.25 % bromophenol blue (w/v), 50 % glycerin (v/v)
TAE-buffer 50x 1L	242 g Tris base, 100 ml 0.5 M EDTA, 57.1 ml glacial acetic acid add ddH_2O to 1L
E3 buffer 60x	5 M NaCl, 250 mM KCl, 0.5 M $CaCl_2$, 1 M $MgSO_4$
Preparation of 4 % PFA/PBS	For 50 ml: for 2 g paraformaldehyde add 40 ml DEPC H2O and 2 ml 1 M NaOH. solve at 65°C. Add 1.6 ml 1 M HCl and 4 ml 10x PBS, 7 pH at room temperature (RT) (use pH paper).Add DEPC H2O up to 50 ml. Cool on ice
Hybridization mix (HM+) / HM- without heparin and tRNA (WMISH)	25 ml formamide (in the fridge), 12.5 ml 20x SSC (DEPC stock), 460 µl citric acid (1 M stock solution), 250 µl Tween (20 % stock solution), 250 µl tRNA (50 mg/ml stock solution in -20°C freezer in freezer room), 50 µl heparin (50 mg/ml stock solution in -20°C freezer in freezer room), add DEPC-treated water up to 50 ml
Blocking solution	PBST with 2 mg/ml BSA and 2 % sheep serum
AP buffer	1 ml NaCl (5 M stock solution), 5 ml Tris, pH 9.5 (1 M stock solution), 2.5 ml $MgCl_2$ (1 M stock solution), 5 ml Tween (10 % stock solution), add sterilized water up to 50 ml
PBST	1x PBS +-0,1 % Tween20
Hybridisation buffer	1 ml Tris 1 M pH 7.5, 12ml NaCL 5 M , 200 µl EDTA 0.5 M, 1.25 ml SDS 20 % , 25 ml Dextran Sulfat 40 %, 2 ml Denhardt's , 2ml tRNA (yeast, Gibco 10 mg/ml), 50 ml formamid , Add to 100 ml H2O DEPC , Aliquot 8ml store -20°C
MABT-buffer	100 ml Maleic acid 1 M (pH7.0 ~70g NaOH pellets), 30 ml NaCl 5 M, 0.05 % Tween20, add to 1000 ml H2O bidistilled
ALP-buffer	16 ml NaCl 5 M, 80 ml Tris 1 M pH 9.5, 40 ml Mg_2Cl 1 M, 4 ml Tween20 10 %, add to 800 ml with H_2O bidistilled

3 Methods

3.1 From RNA isolation to a digoxigenin labeled antisense RNA probe

To perform an *in situ* hybridization a digoxigenin (DIG) labeled antisense RNA probe is needed. To obtain this probe, RNA from zebrafish embryos was isolated and transcribed into cDNA. Afterwards, the cDNA served as a template for PCR amplification. The amplified DNA was cloned into a RNA expression vector. This vector was used to generate a DIG labeled antisense RNA probe. After RNA synthesis the probe was used for *in situ* hybridization. The detailed description of the process can be found below.

3.1.1 RNA isolation and cDNA transcription

RNA was isolated from zebrafish embryos at 3 dpf. 10 to 15 embryos were staged using a microscope and transferred into a 1.5 ml reaction tube. Afterwards the embryos were euthanized by snap freezing in liquid nitrogen. At this point the embryos were directly used for RNA isolation or stored at -80°C. For RNA isolation the peqGold Total RNA kit was used following the descriptions of the manufacturer. Lysis of the embryos was supported with 10-15 strokes of a micropestle. RNA quality was assessed on a 1 % agarose gel and the concentration was determined with the Nanodrop measuring system. Subsequently the RNA was stored at -80°C or directly used for cDNA synthesis.

cDNA synthesis was performed with SuperScript II reverse transcriptase following the manual instructions. To obtain a full-length product and especially the 3'UTR, oligo(dT) primers were used. The yielded cDNA was stored in TE buffer at -20°C.

3.1.2 Cloning of DNA fragments

Amplified cDNA was used for the synthesis of the DIG labeled antisense RNA probe. To reduce the probability of non-specific hybridization, the 3'UTR is preferably used for generating DIG labeled antisense probes. Using 3'UTR which represents a less conserved part of genes, to construct labeled probes ensures that there is no false binding of the RNA probe to another member of the gene family. The primers to amplify the probe were designed to obtain DNA fragments between 700 bp and 1500 bp. The PCR was performed according to the manufacturer's instructions (Phire

Hot Start II DNA polymerase/ Thermo Scientific). The correct size of the amplified PCR product was verified by a 1 % agarose gel. To remove primer and nucleotides the PCR product was cleaned using the PCR purification Kit (Qiagen). Next, the PCR fragment was cloned into a dual promoter vector and transformed into *E. coli* TOP10 cells according to the instructions of the manufacturer (TOPO TA cloning Kit dual promoter/ Dual Promoter TA cloning Kit, Invitrogen). The correct insertion of the PCR fragment was verified via colony PCR (M13 primer). Positive colonies were grown in overnight cultures (5 ml LB) and the plasmids were purified (QIAprep Spin Miniprep Kit, Qiagen). Afterwards, the inserts were tested for their orientation with asymmetric digestion and Sanger sequencing.

3.1.3 Synthesis of DIG labeled antisense RNA probe

The dual promoter vectors pCRII-TOPO and pCRII, used in the cloning process, carry an SP6 promoter on the one and a T7 promoter on the other side of the insert. Based on the orientation of the insert, the appropriate polymerase, which creates the required antisense RNA was chosen. Since RNA polymerases do not detect a stop codon a linearized template for the RNA amplification is required. Therefore, a M13 PCR was used to amplify a DNA fragment containing both promoter sites and the insert (standard PCR protocol, Phire Hot Start II DNA polymerase). To obtain a better quality of the RNA probe, the PCR product was purified of primers, nucleotides and polymerases prior to RNA probe synthesis (PCR purification Kit, Qiagen). Afterwards, the purified M13 PCR product was used for the RNA synthesis which was performed according to the protocol of the manufacturer (SP6 Polymerase / T7 Polymerase, Roche). For the synthesis process the DIG-RNA Labeling Mix (Roche) and the RNasin RNase inhibitor (Promega) were used according to the SP6/T7 polymerase manual. The RNA syntheses were followed by lithium ethanol precipitation as described in the SP6/T7 polymerase manual. The RNA was dissolved in 50 µl RNase free water and the fragment size was verified on a 1 % agarose gel. Finally, the RNA concentration was determined using the Nanodrop measuring system and the RNA was stored at -80°C.

3.2 Zebrafish methods

The zebrafish (strain AB) used in this thesis were maintained in the animal facility of the Max Planck Institute for Molecular Genetics. The breeding and handling of the zebrafish were performed according to the guidelines of "The Zebrafish Book" (Westerfield 2000). Further, the experiments were declared and approved by the Landesamt für Gesundheit und Soziales (Anzeigennummer G 0133/13).

3.2.1 Production and keeping of zebrafish embryos

To obtain embryos, 12 zebrafish couples of one fish tank (~30 animals) were set in individual small breeding chambers overnight (12 hrs day/night cycle) at 27°C. The breeding chamber consists of a small fish tank, a cage and some filter floss. The cage which is slightly smaller than the fish tank separates the male and female during the night. The filter floss inside the fish tank serves as a replacement for vegetation and increases the amount of breeding couples.

In the morning of an injection day, the male and female of each breeding chamber were set together into the cage. 30 min later, the embryos of all 12 couples were collected through one strainer. Afterwards the embryos were held in an E3 buffer filled Petri dish at 27°C until the embryos reached the required stage.

3.2.2 PTU treatment to prevent pigmentation

To improve the signal of the *in situ* hybridization, 1-phenyl 2-thiourea (PTU) was used to inhibit the melanization process. PTU blocks all tyrosinase-dependent steps in the melanin pathway so that the embryos remain transparent. According to Karlsson, von Hofsten *et al*. (2001) the embryos were transferred 24 hpf into 100 µM PTU E3 buffer. Until the embryos reached the required stage they were held in PTU E3 buffer.

3.2.3 Paraformaldehyde fixing of embryos

Embryos at the required stage were fixed overnight in a freshly made 4 % paraformaldehyde (PFA) PBS solution. The next day, the embryos were washed twice in 1xPBS and transferred into 100 % methanol for whole mount RNA *in situ* hybridization or in 100 % ethanol for RNA *in situ* hybridization on paraffin sections.

For methanol storage, embryos were transferred in a 2 ml reaction tube and washed for 5 min with 100 % methanol. Finally the methanol was replaced with fresh 100 % methanol and the embryos were stored at -20 C.

For ethanol storage, embryos were transferred into a 2 ml microreaction tube and washed in increasing ethanol concentrations each time for 20 min (25 %, 50 % vol/vol ethanol/1xPBS, 75 %, vol/vol ethanol/DEPC water, 100 % ethanol). Afterwards, the embryos were stored at –20 C.

3.2.4 Whole mount RNA *in situ* hybridization

Whole mount *in situ* hybridization (WMISH) was used to analyze the spatial and temporal gene expression patterns in the embryo. During this process, the DIG label antisense probe hybridizes to its corresponding mRNA. Afterwards, the double stranded RNA is visualized with an alkaline phosphatase (AP) conjugated anti-DIG antibody. The protocol can be performed within three days and is based on Thisse and Thisse (2008).

On the first day, the PFA-fixed and methanol stored (-20°C) embryos were rehydrated. Afterwards, the embryos were permeabilized with proteinase K and hybridized with the probe overnight. The second day started with the removal of unbound probe by several washing steps, which were followed by overnight blocking with BSA to prevent unspecific binding of the anti-DIG antibody (anti-DIG AB). At the third day, the embryos were incubated with the antibody, followed by several washing steps and the staining of the embryos with 5-Bromo-4-chloro-3-indolyl phosphate p-toluidine salt (BCIP) and nitroblue tetrazolium (NBT).

The detailed protocol for the WMISH can be found in the supplement 7.1, page 113.

3.2.5 RNA *in situ* hybridization on paraffin section

Because of the low resolution of the WMISH, an *in situ* hybridization on paraffin section (IHPS) was performed. The probe and staining method is likewise the WMISH. To perform the sections, the PFA-fixed and in ethanol stored embryos were imbedded in paraffin. Afterwards, 5 µm thick sections of the embryos were cut with a microtome (Leica HM553 S). Next, the sections were deparaffinized, rehydrated and fixed in PFA. Then the labeled RNA probe was added onto a slide and incubated overnight. The next day, the unbound probe was washed off and the surface was blocked with BSA.

Afterwards, the slides were incubated overnight with the anti-DIG antibody. On the third day, the slides were washed and stained with BCIP/NBT. After the desired staining was reached, the coloring reaction was stopped by washing in PBS buffer. Finally, the slides were sealed with a coverslip.

The detailed protocol for the IHPS can be found in the supplement 7.2, page 114.

3.2.6 Microinjection of morpholinos

For the injection, a plate is needed to position the fertilized embryos. The injection plate was based on a Petri dish (92 mm) filled with a 1 mm layer of 1.5 % agarose. After the first layer is solidified, a second agarose layer was added in which a plastic mold was placed. Prior to injection, the plastic mold was removed and the embryo could be positioned into the resulting grooves. The teeth on the plastic mold have a pyramid shape with a 90° angle, a height of 1 mm and a base of 1.5 mm (Figure 9) (Westerfield 2000, Bill, Petzold *et al*. 2009).

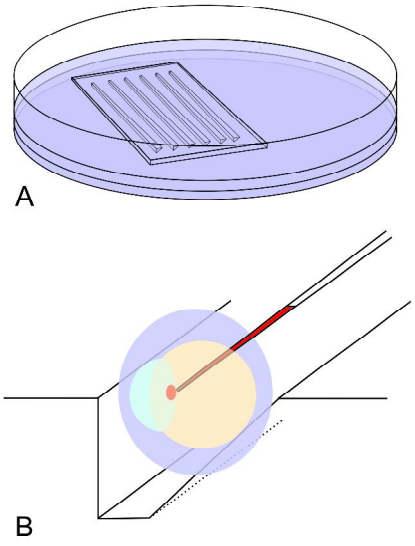

Figure 9 Injection procedure
A) injection plate, Petri dish filled with two layers of agarose. In the second layer a plastic mold is added. (Size of the plastic matrix can be found in "The Zebrafish Book" (Westerfield 2000) or at Bill, Petzold *et al.* (2009)). B) sketch of the injection into one-cell stage zebrafish embryo positioned on the injection tray.

The needles (glass filament outer diameter 1.0 mm, inner diameter 0.78 mm), needed for the injection, were fabricated using a micropipette puller (Shutter Instruments, settings: heat 550, pull 80, velocity 120, time 120). As visual control of the injection, the injection solution is mixed with phenol red (final concentration 0.05 %).

Approximately 150-170 embryos were transferred with a 1.5 ml plastic pipette onto the injection plate and positioned into the grooves. Next, the embryos were injected using an inverse microscope (Leica) with an attached NM151 micromanipulator (Leica) and a FemtoJet injection pump (Eppendorf) to adjust the injected volume to approximately one tenth of the cell.

After the injection, the eggs were rinsed with E3 buffer into a new Petri dish and incubated at 27°C until the required developmental stage was reached.

3.2.7 Microangiography, visualizing the cardiovascular system

For visualization of the blood flow a microangiography was performed. This technique is based on Weinstein, Stemple *et al.* (1995). For the injection, the same setup as described in the morpholino injection was used. The embryos were transferred onto an injection plate, anesthetized with tricaine and turned lateral. Next, approximately 5 nl of the fluorescent Rhodamine B dextran solution (5 mg/ml) were directly injected into the sinus venosus of the 3 day old embryos. Because of the high molecular weight of the coupled dextran, the Rhodamine B diffuses very slowly from the blood vessels into the tissue. Subsequent to the injection, the embryos were imaged using an Axiovert 200M microscope.

3.2.8 Size determination of zebrafish embryos

To identify differences in the cell count in the brain of the embryos, the head size and body length were measured as follows: embryos were anesthetized with tricaine (0.1 mg/ml) and positioned on an agarose injection tray using a shortened microloader tip (Eppendorf). Next, embryos were photographed using a stereomicroscope (Zeiss) and the length was measured with the AxioVision 4.8 software (Zeiss).

3.3 Statistical methods

To identify differences in the brain size, the head diameter was measured at 2 dpf, 3 dpf and 4 dpf. The reason for choosing the head size is that it is mainly based on the size of the brain. Since the embryos do not develop completely uniformly, the staging of the embryos is required to make the results comparable. Because this is a time-intensive process it was chosen to use the body length for comparability, because it is progressing approximately linear during the 2 - 4 dpf and is directly linked to the developmental stage of the embryos. For comparison, the head size and body length of the embryos were plotted and a regression function, which corresponds to the growth rate, was calculated (Excel 2003). Finally, the regression lines from the morpholino knockdown embryos and their corresponding control were tested for significant differences in their

distribution and slope (F-test, T-test). All statistical methods used in this thesis can be found in Angewandte Statistik (Sachs 2004).

3.3.1 Comparing the correlation coefficients

To test for a difference in the distribution of the head size/ body length regression, the r^2 of the morpholino knockdown embryos was compared to the SCMO injected embryos via a Fisher's z transformation. Therefore, the z values of the morpholino knockdown and the SCMO injected embryos were calculated according to formula 1. Afterwards the $\hat{z}$ was calculated (Formula 2). If $\hat{z}$ is lower than the significance threshold of 1.96 it can be assumed that $r_1 = r_2$. This would mean that there is no difference in the regression lines/growth rate between the knockdown and SCMO injected embryos.

$$z = \tfrac{1}{2} \ln \frac{1+r}{1-r}$$

Formula 1 Fisher's z transformation of the correlation coefficient r

$$\hat{z} = \frac{|z_1 - z_2|}{\sqrt{\frac{1}{n_1 - 3} + \frac{1}{n_2 - 3}}}$$

Formula 2 $\hat{z}$ calculation for *p*-value determination

3.3.2 Comparing the regression coefficients

In order to test if the slope (β) of the head size / body length regression of injected and control embryos have no significant difference, the Formula 5 was used. The mathematical explanation for the rest variance ($S^2_{y \cdot x}$) and the sum of the squared deviations (Q_x) are given in formula 3 and 4. If $\hat{t}$ is higher than the significance threshold of 1.99 (two-tailed) the null hypothesis H_0 $\beta_1 = \beta_2$ is rejected and the alternative hypothesis H_1 $\beta_1 \neq \beta_2$ is accepted (corresponds to a *p*-value of 0.05).

$$Q_x = \sum x^2 - \frac{\left(\sum x\right)^2}{n}$$

Formula 3 sum of the squared deviations

$$S_{y\cdot x}^2 = \frac{\sum (y - \hat{y})^2}{n - 2}$$

Formula 4 rest variance

$$\hat{t} = \frac{|b_1 - b_2|}{\sqrt{\frac{S_{y_1\cdot x_1}^2 (n_1 - 2) + S_{y_2\cdot x_2}^2 (n_2 - 2)}{n_1 + n_2 - 4} \left[\frac{1}{Q_{x_1}} + \frac{1}{Q_{x_2}} \right]}}$$

Formula 5 Comparison of two regression coefficients, null hypothesis a) $\beta_1 \leq \beta_2$ one-tailed or b) $\beta_1 = \beta_2$ two-tailed

4 Results

4.1 Identification of syntenic regions within the 16p11.2 locus

The evolutionary distance of 450 million years between humans and teleost fish required a selection of genes, to support the comparability between the identified phenotypes. Because of the known relation between evolutionary stable gene clusters and conserved developmental function throughout metazoan genomes, the zebrafish orthologs were investigated for syntenic clusters (Kikuta, Laplante *et al*. 2007).

As first step the zebrafish genome was investigated with the Ensembl genome browser (release 72: Jun 2013; Flicek, Ahmed *et al*. (2013)) for orthologs of 16p11.2 CNV. This identified 22 zebrafish orthologs to 27 human genes of the 16p11.2 CNV. Because of the additional whole-genome duplication of the teleost fish, 6 of the 22 genes are present as duplicates. For identification of the syntenic regions the Genomicus genome browser was used (database version 69.01, Figure 10, Louis, Muffato *et al*. (2013)).

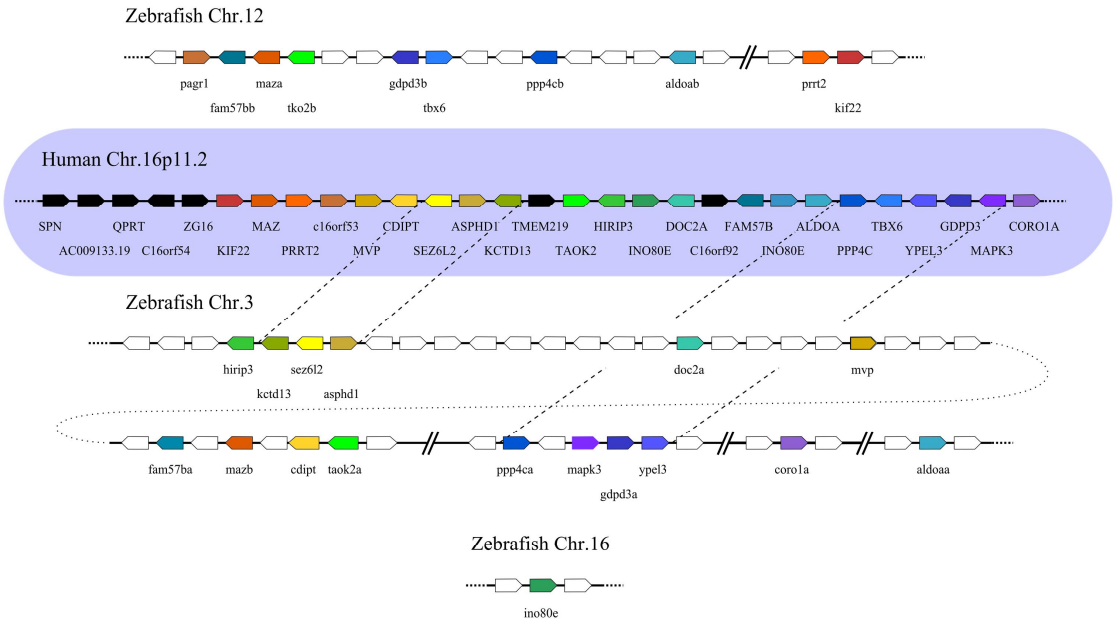

Figure 10 Gene map of the autism associated deletion in 16p11.2 and its corresponding orthologous genes in the zebrafish genome
Arrowheads represent the chromosomal order (5' to 3') and translational direction of the genes. Each orthologous gene is uniquely color coded. Black labeled human genes don't have an orthologous gene in the zebrafish genome. White colored zebrafish genes are nonorthologs to the autism-associated deletion in human 16p11.2. The two syntenic gene clusters on zebrafish chr.3 are linked by dotted lines with their human orthologs. The data used to plot this syntenic map is derived from the Genomicus genome browser database version 69.01 (Louis, Muffato *et al*. 2013).

This browser visualizes orthologous and paralogous copies of a gene in its genomic context to all available metazoan genomes. This analysis revealed that most of the genes were located on zebrafish chromosome 3 and 12. Interestingly, two syntenic clusters are formed on chromosome 3. The first gene cluster consists of the three genes *kctd13*, *sez6l2*, and *asphd1* and the second encompasses the four genes *ppp4ca*, *mapk3*, *gdpd3a*, and *ypel3*. Based on their syntenic structure, these genes were selected for further investigation. Because *gdpd3a* and *ppp4ca* have an orthologous copies, further analyses were required to decide, if the paralogs had to be included in the investigations to uncover a masking of the knockdown.

To achieve an additional overview of the zebrafish orthologs, the conservation on protein level was compared (Table 10). A strong conservation of a protein would indicate an equal mechanistically function. The protein sequences were aligned in both directions: human to zebrafish and zebrafish to human. The reason for this is that a difference in the amino acid sequence length would affect the calculated identity. The calculated amino acid sequence identity for the orthologous genes was varying from 22 % to 98 % with an average similarity of ~59 ± 21 % in both directions (Table 10). Besides the conservation between human and zebrafish orthologs, also the paralogous zebrafish genes were tested for their amino acid sequence identity. They showed a similar conservation pattern like the interspecies comparison, with nearly the same arithmetic mean in conservation of 65 ± 20 % (Table 11). Therefore the strong conservation of 93 % of the amino acid sequence between the zebrafish paralogs *ppp4ca* and *ppp4cb* is remarkable. This strong conservation of *ppp4cb* could mask the knockdown effect of *ppp4ca*. Therefore, *ppp4cb* was included in the further analysis.

The other gene with a paralog was *gdpd3a* which only showed 59 % identity of the protein sequence compared to its paralog *gdpd3b*. Further analyses of the alignment revealed, that the first 55 aa of *gdpd3*b were truncated (Figure 11). Therefore, *gdpd3*b was not included in this study.

Table 10 Alignment of human 16p11.2 genes to their zebrafish orthologs
Table is sorted for the alignment identity from low to high. Genes present in the first gene cluster are shaded in yellow and genes present in the second cluster are shaded in red. Gene names of the zebrafish paralogs are colored equally. The bottom row presents the average and the standard deviation.

zebrafish orthologs	similarity in %		Difference in alignment directions in %
	zebrafish on human	human on zebrafish	
prrt2	22	33	11
hirip3	26	28	2
maza	**30**	**64**	**34**
mazb	**40**	**40**	**0**
tbx24	40	20	20
asphd1	41	45	4
gdpd3a	**47**	**47**	**0**
gdpd3b	**48**	**48**	**0**
ino80e	48	51	3
kif22	48	50	2
taok2b	**49**	**52**	**3**
taok2a	**50**	**54**	**4**
sez6l2	52	53	1
kctd13	61	61	0
doc2a	63	62	1
fam57ba	**65**	**61**	**4**
fam57bb	**65**	**66**	**1**
mvp	66	68	2
coro1a	68	69	1
ypel3	68	90	22
c16orf53	69	21	48
cdipt	69	69	0
mapk3	83	81	2
aldoaa	**84**	**84**	**0**
aldoab	**84**	**84**	**0**
ppp4ca	**93**	**91**	**2**
ppp4cb	**98**	**98**	**0**
Average ± standard deviation	58.41 ± 19.69	58.89 ± 20.84	6.19 ± 11.63

Table 11 Alignment of paralogues zebrafish genes of the human 16p11.2 deletion region

Zebrafish genes		similarity in %	
a	b	a to b	b to a
ppp4ca	*ppp4cb*	93	92
aldoaa	*aldoab*	93	93
fam57ba	*fam57bb*	74	75
gdpd3a	*gdpd3b*	59	59
taok2a	*taok2b*	57	59
maza	*mazb*	39	83

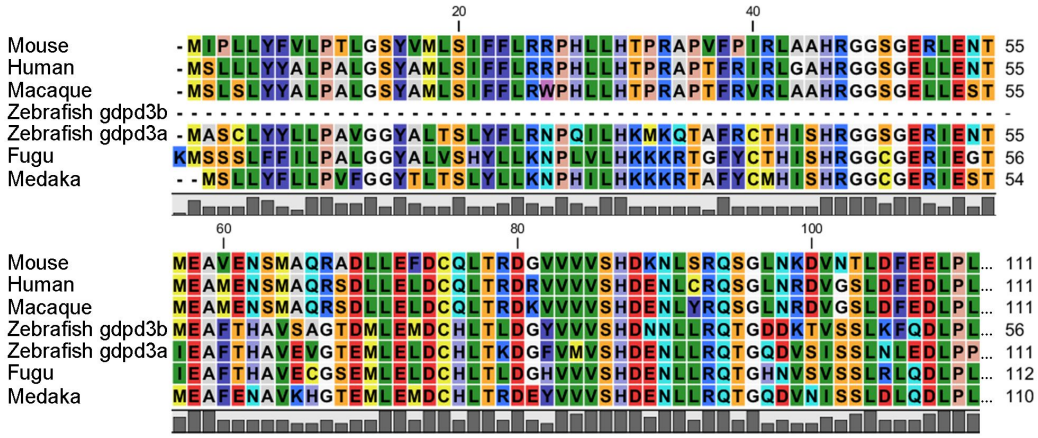

Figure 11 Truncation of zebrafish gene *gdpd3*b
Section of the protein alignment of zebrafish *gdpd3*a GI:47085996, *gdpd3*b GI:528495324; *gdpd3* fugu (*Takifugu rubripes*) ENSTRUG00000005467, *gdpd3* medaka (*Oryzias latipes)* ENSORLG00000011954, *gdpd3* macaque (*Macaca mulatta*) GI:302564980, *gdpd3* human (*Homo sapiens*) GI:146198639 and *gdpd3* mouse (*Mus musculus*) GI:110431345. Full alignment available in supplement Figure 64 page 117.

4.2 Expression pattern of the syntenic genes in zebrafish

The *in situ* hybridization is based on a digoxigenin (DIG) labeled antisense RNA probe binding to the mRNA of the gene of interest. Afterwards, the obtained double stranded RNA is targeted with an alkaline phosphatase (AP) conjugated anti-DIG antibody. In a coloring reaction the AP is used to visualize the spatial expression of the gene of interest. At first, the whole mount *in situ* hybridization (WMISH) was used to get an overview of the expression pattern. However, due to the increasing complexity of the embryos at 24 hpf, it was difficult to designate the stained tissues, especially the ones of the brain. Therefore, an *in situ* hybridization on brain and selected body sections was performed in addition to the WMISH. To ensure that the signal was caused by the hybridized DIG-labeled RNA and not by non-specific background interactions, each of the *in situ* experiments were accompanied by an *in situ* hybridization without DIG labeled antisense RNA. The results of WMISH and the IHPS are described in the following sections for each gene. Generally, all genes showed an ubiquitous expression within the head, only *sez6l2* was specifically localized in the brain of the embryos.

4.2.1 *asphd1* is ubiquitously expressed in head and intestine

The whole mount *in situ* hybridization showed a ubiquitous expression of *asphd1* in the trunk and a strong signal in head and intestine (Figure 12). This was confirmed by *in situ* hybridization on sections which also results in an ubiquitous expression in all parts of the brain, the intestine, and weak in muscles. (Figure 13)

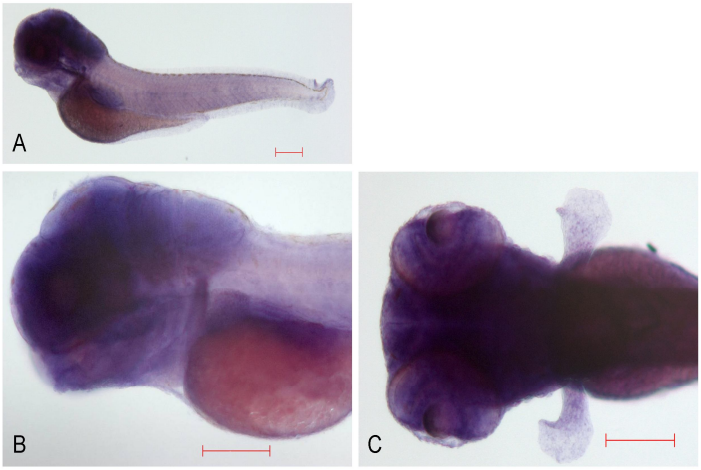

Figure 12 Whole mount *in situ* hybridization of *asphd1*
Whole mount *in situ* of *asphd1* on 3d old embryo, anterior left, A, B) lateral, C) ventral. The expression of *asphd1* (blue staining) is ubiquitous but strongest in the head and intestine, scale bar 200 µm

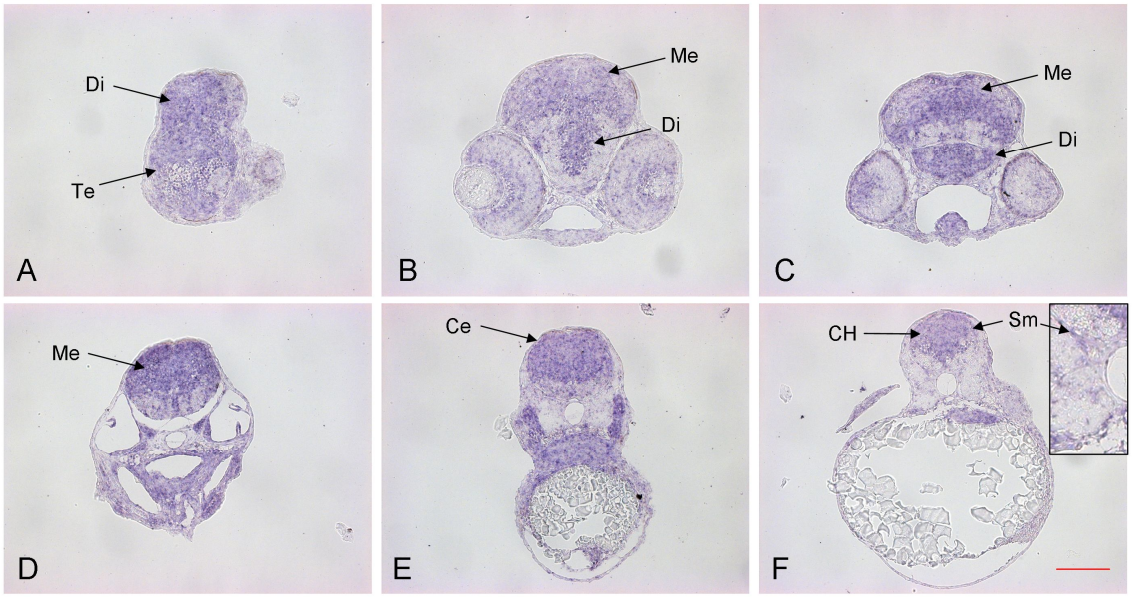

Figure 13 Ubiquitous expression of *asphd1* on transversal sections
A-F) transversal sections of a 3 day old embryo, from cranial to caudal. *asphd1* expression is stained blue, which is strongly visible in the whole head and less in the somitic muscle (Sm). Abbreviations: telencephalon (Te), diencephalon (Di), mesencephalon (Me), cerebellum (Ce) caudal hindbrain (CH), Magnification 100x scale bar 250 µm

4.2.2 *gdpd3a* is homogenously expressed in head, heart and intestine

The whole mount *in situ* hybridization of *gdpd3a* showed an expression in the head and heart of the embryos (Figure 14). This was confirmed by *in situ* hybridization on transversal sections, which showed an uniform expression pattern in all parts of the head, except the lenses, where no *gdpd3a* signal was observed. Additionally to the detection of the *gdpd3a* expression in the head, the *in situ* hybridization on sections also showed a *gdpd3a* expression in the heart and the developing internal organs like liver and gut which, in contrast, was not visible via WMISH (Figure 15).

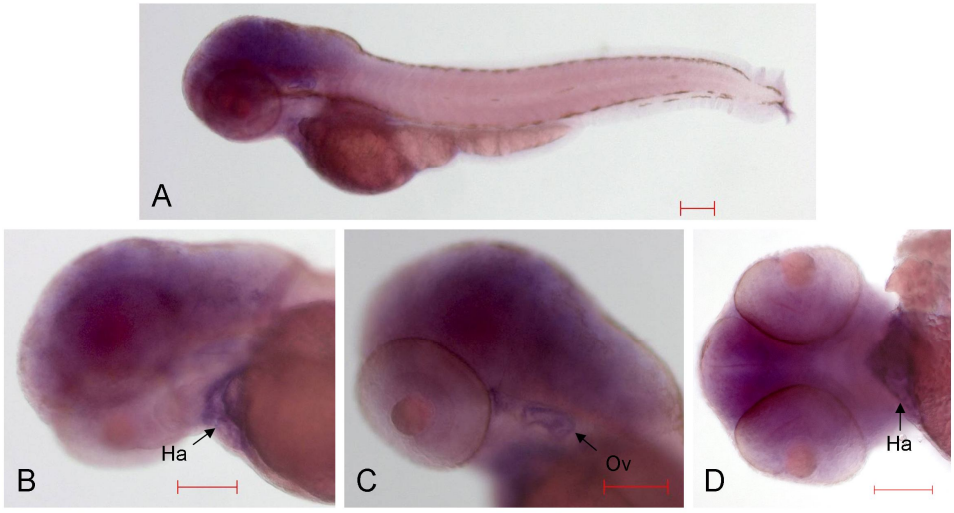

Figure 14 *gdpd3a* expression in the head and heart of a zebrafish embryo 3 dpf
In all pictures anterior is left A) whole embryo, B) head detailed lateral/ventral, C) head lateral/dorsal D) head and heart viewed ventral. *gdpd3a* expression (blue staining) in the whole head and heart (Ha). Also the otic vesicle (Ov) appears to be stained. Scale bar 200 µm

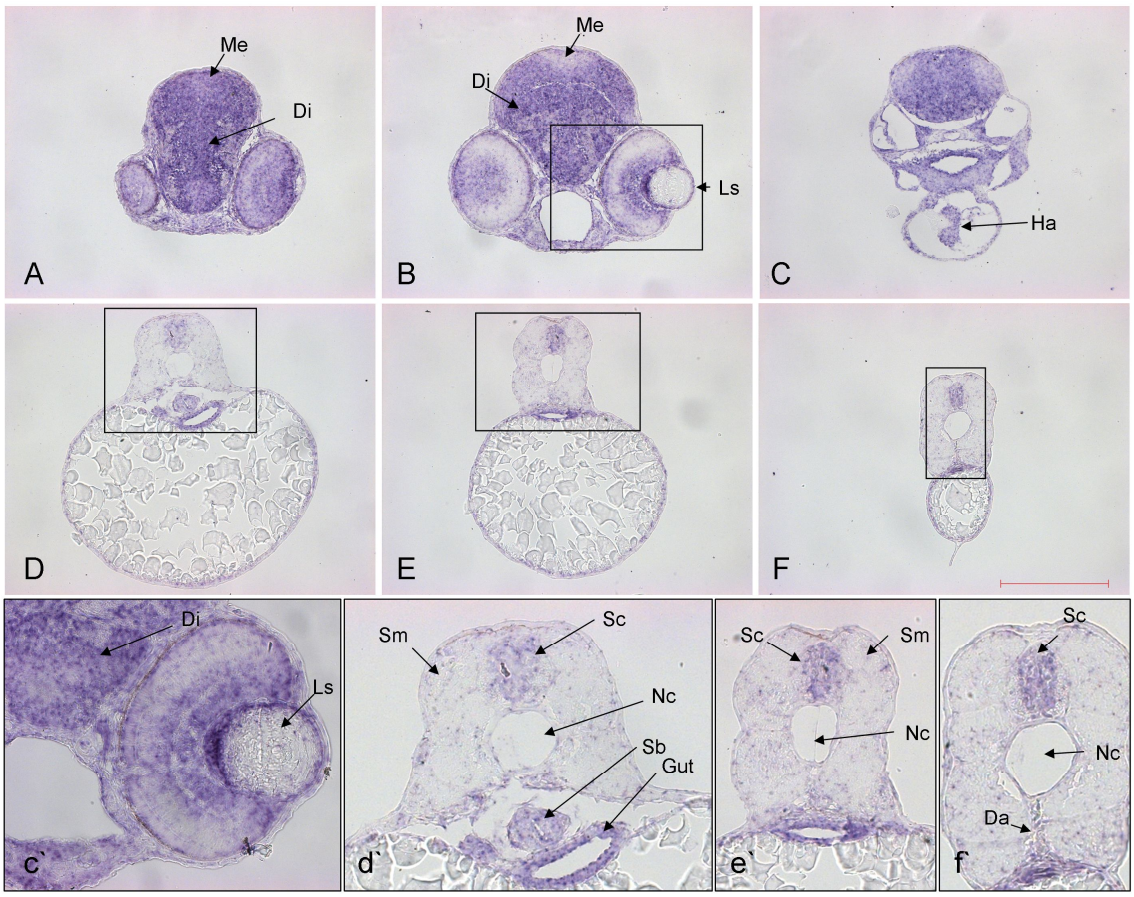

Figure 15 Transversal sections show *gdpd3a* in the head, spinal cord and intestine
A-F) transversal sections of a 3 day old embryo from cranial to caudal. A-C) *gdpd3a* signal is visible in the whole head and heart. D-F) *gdpd3a* signal in the spinal cord (Sc), swim bladder (Sb) and gut. Abbreviations: diencephalon (Di), dorsal aorta (Da), mesencephalon (Me), cerebellum (Ce), olfactori placode (Op), notochord (Nc), pectoral fin (Pf), somitic muscle (Sm). Magnification 100x, scale bar 200 µm

4.2.3 *kctd13* is uniformly expressed in the head and strongest in the heart

The whole mount *in situ* hybridization of *kctd13* showed, that its mRNA is located in the head and heart of the embryos at 3 dpf (Figure 16). This was confirmed by *in situ* hybridization on sections. The expression of the gene was uniformly distributed over the whole head. However, the signal of *kctd13* around the bulbus arteriosus and the proximal end of the pericardium was stronger compared to the surrounding (Figure 17). The bulbus arteriosus is a pear shaped chamber directly connected to the ventricle. This arterial structure can tolerate the high pressure of the heart and serves as a capacitor maintaining continuous blood flow (Bradford, Conlin *et al*. 2011).

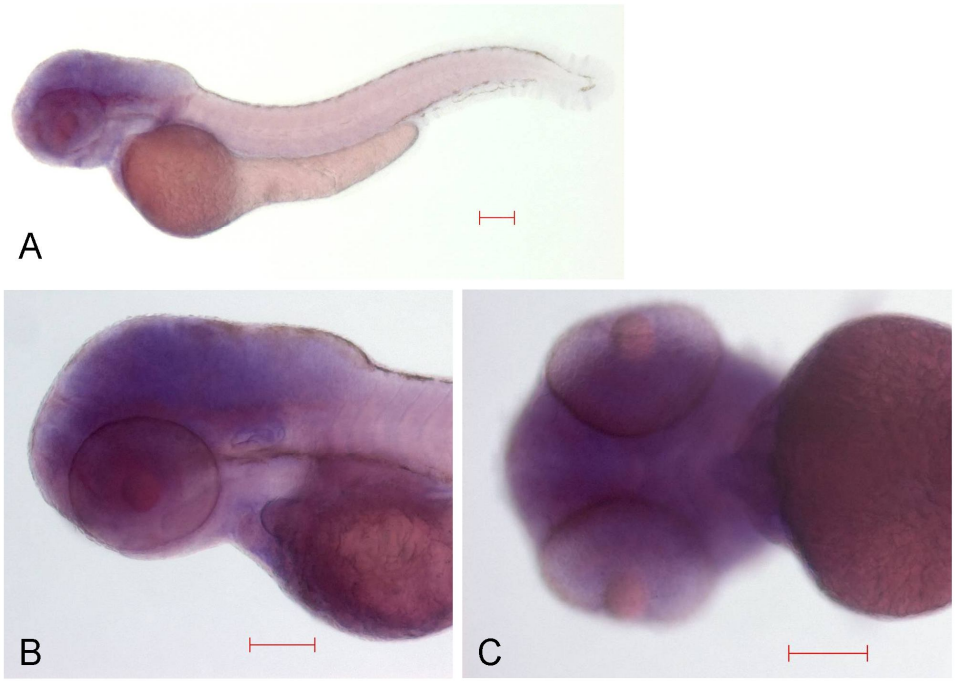

Figure 16 *kctd13* expression in the head of a zebrafish embryo 3 dpf
Embryos are orientated anterior left A) whole embryo lateral, B) head detailed lateral, C) head detailed viewed ventral. *kctd13* (blue staining) is expressed in the whole head and heart. Also the otic vesicle appears to be stained (C). Scale bar 200 µm

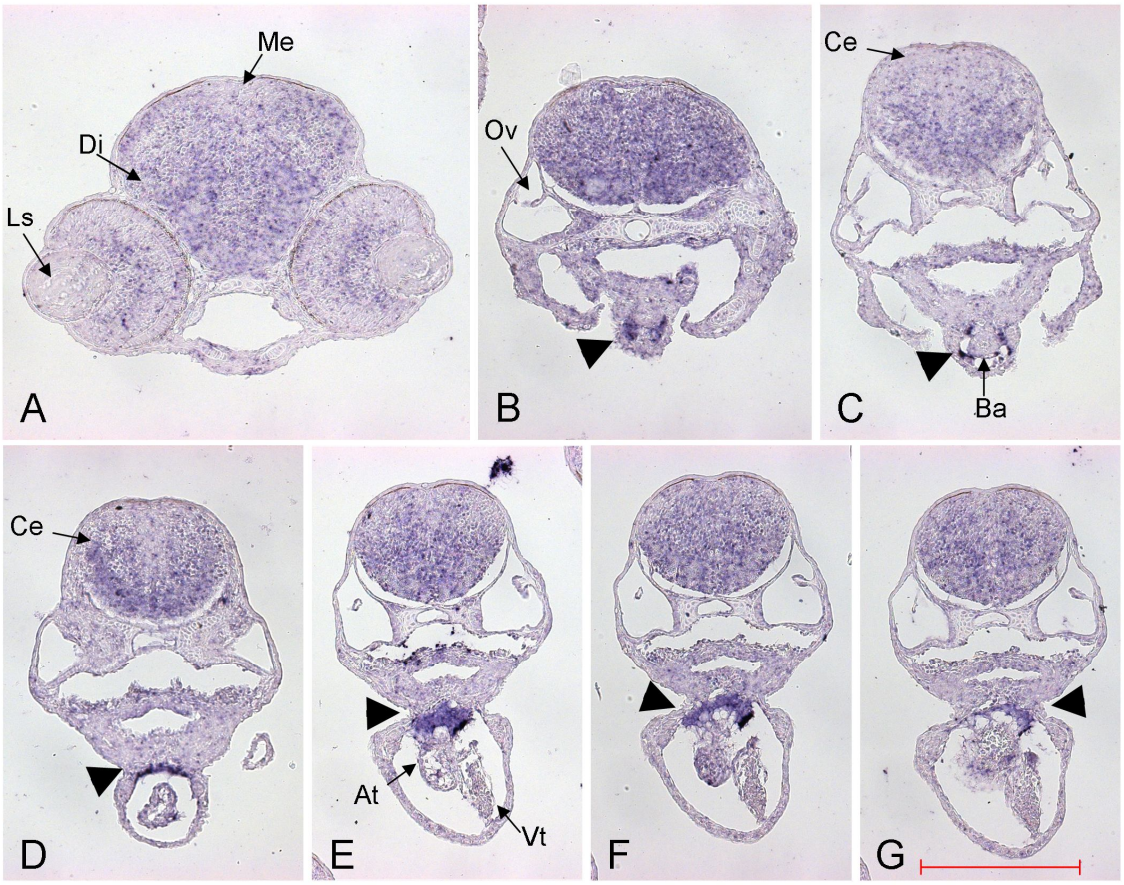

Figure 17 *kctd13*, ubiquitous expression in the head and strongest above the atrium
A-G) show transversal sections of a 3 day old embryo, from cranial to caudal. Stained in blue is the *kctd13* expression, which is visible in the whole head and heart. The expression is very strong around the bulbus arteriosus (Ba) and above the heart (arrowhead). Abbreviations: atrium (At), cerebellum (Ce), diencephalon (Di), lens (Ls), mesencephalon (Me), telencephalon (Te), ventricle (Vt). Magnification 100x, scale bar 250 µm

4.2.4 *mapk3* is expressed in head and heart

The whole mount *in situ* hybridization of *mapk3* showed a ubiquitous expression in the head, the heart, and the developing intestine of embryos 3 dpf (Figure 18). To localize the expression more precisely, an *in situ* hybridization on sections was performed. This confirmed the expression of *mapk3* in the head. Furthermore, the *mapk3* signal was also visible in the swim bladder, gut, pancreas liver, spinal cord, and pectoral fins. However, an expression of *mapk3* in the lenses was absent (Figure 19).

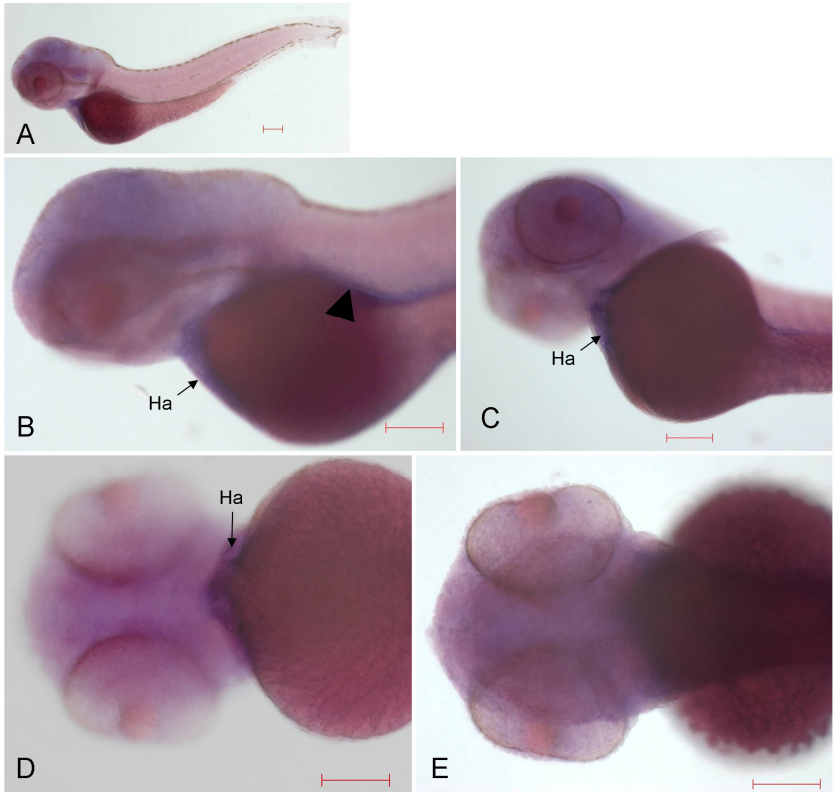

Figure 18 *mapk3* whole mount *in situ* hybridization 3 dpf
Anterior left, view orientation is: A) lateral, B) lateral left side, C) ventral/lateral D) ventral, E) dorsal. Blue staining represents the *mapk3* mRNA expression, which is visible in the whole head, the heart (Ha) and the developing intestine (arrowhead). Scale bar 200 µm

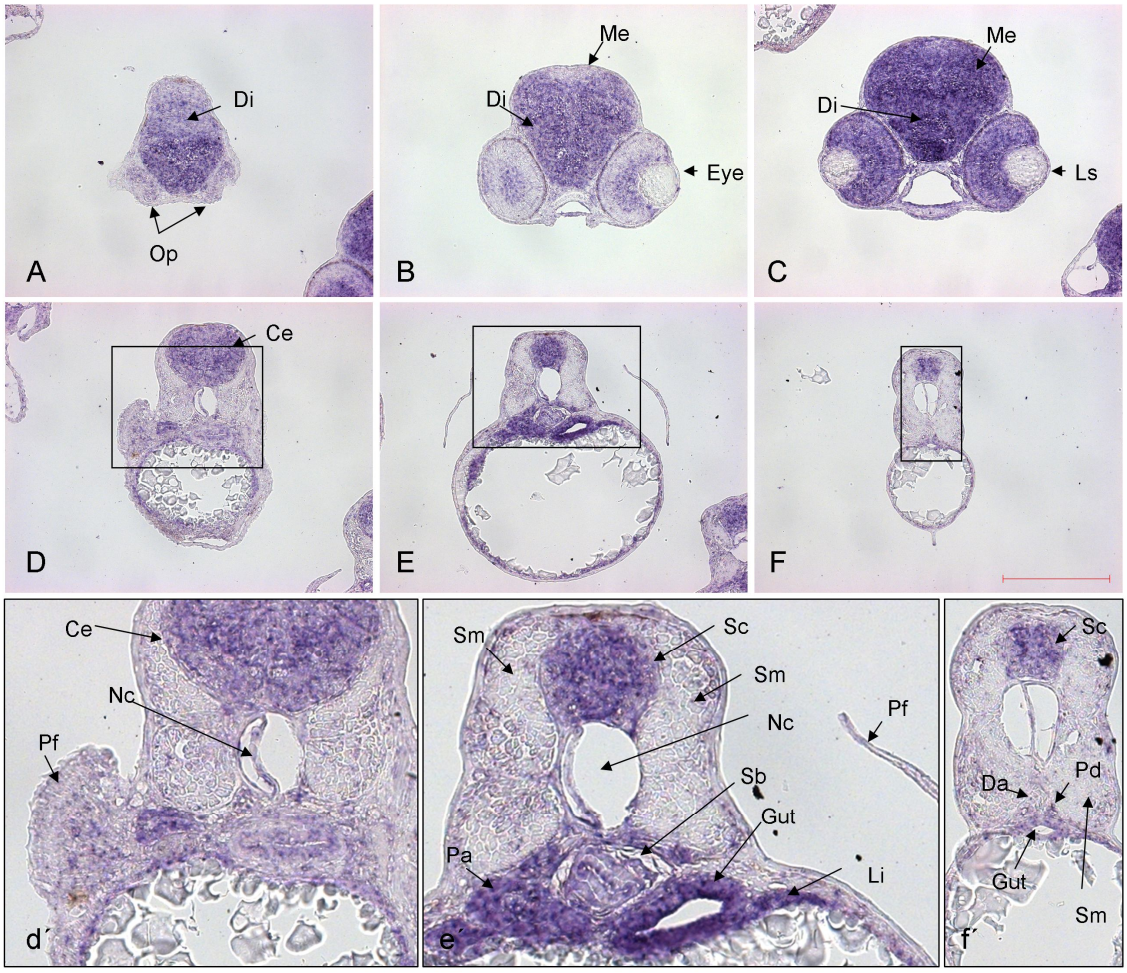

Figure 19 *mapk3 in situ* hybridization on transversal sections of embryos 3 dpf
A-G) transversal sections of a 3 day old embryo from cranial to caudal. The signal for *mapk3* is visible in the whole head except the lenses (A-C), and in the spinal cord (Sc), swim bladder (Sb), gut, pancreas (Pa), liver (Li) and light pectoral fins (Pf). Abbreviations: cerebellum (Ce), dorsal aorta (Da), diencephalon (Di), lens (Ls), mesencephalon (Me), notochord (Nc), olfactori placode (Op), heart (Ha), pectoral fin (Pf), somitic muscle (Sm), telencephalon (Te). Magnification 100x scale bar 200 µm

4.2.5 *ppp4ca* expression is present in head and intestine

The *ppp4ca* expression was observable in head, intestine and pectoral fins (Figure 20). The sections of the embryos showed that the expression of *ppp4ca* is uniformly distributed in all parts of the brain and the developing intestines like gut, liver and pronephric duct, as well as the pectoral fins. Notably, the expression of *ppp4ca* was very low in somitic muscles, which could be the reason why it is not visible in the WMISH (Figure 21).

Figure 20 *ppp4ca* expression in the head
Whole mount *in situ* hybridization of a *ppp4ca* probe on a 3d old zebrafish embryo, anterior left, A) lateral B) dorsal, *ppp4ca* expression is stained in blue in the head, intestine (arrowhead) and pectoral fins (Pf); scale bar 200 µm

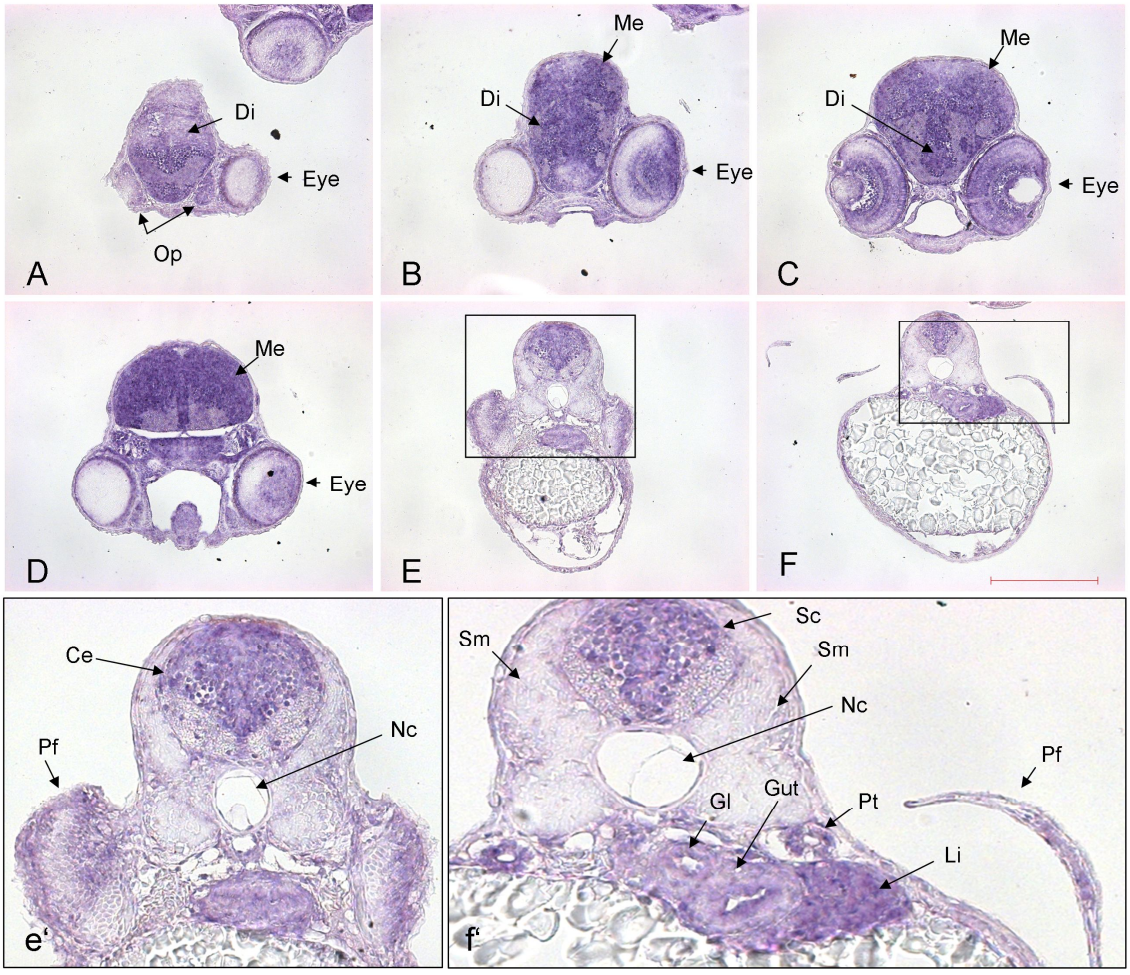

Figure 21 *ppp4ca in situ* hybridization on transversal sections of an embryo 3 dpf
A-F) transversal sections from cranial to caudal. The *ppp4ca* signal (blue) is visible in the whole head (A-D) and in the spinal cord (Sc), glomerulus (Gl), gut, pronephric duct (Pt), pectoral fins (Pf) and liver (Li). Abbreviations: cerebellum (Ce),diencephalon (Di), mesencephalon (Me), notochord (Nc), olfactori placode (Op), pectoral fin (Pf), somitic muscle (Sm), telencephalon (Te). Magnification 100x, scale bar 200 um

4.2.6 *ppp4cb* is expressed in head and intestine

The *ppp4cb in situ* hybridization resulted in a very strong signal of *ppp4cb* transcripts in the head of the embryos. The signal indicates a location in the brain, eye, ear, branchial arches, liver, gut and the swim bladder (Figure 22). To investigate the distribution of *ppp4cb* expression inside the embryos, transversal sections were stained (Figure 23).

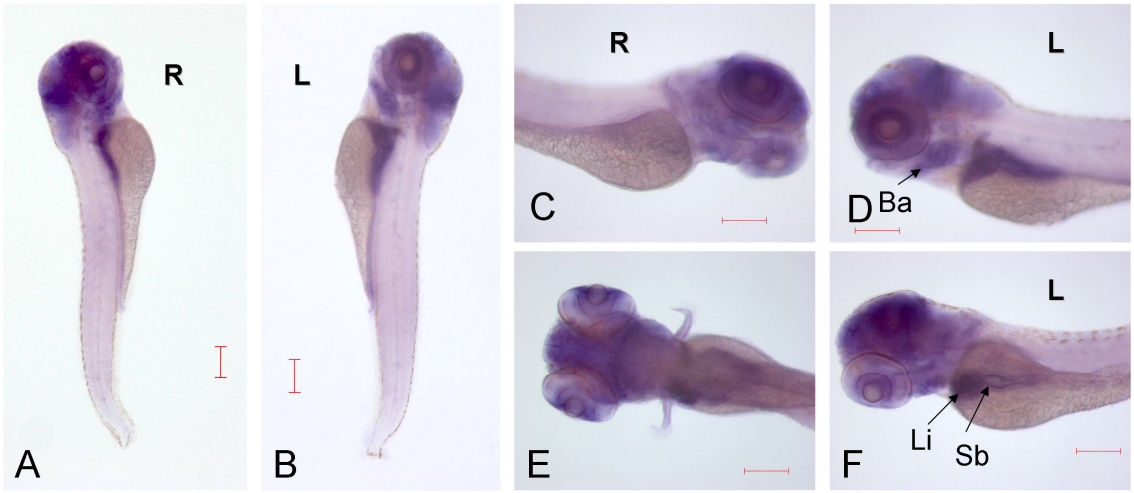

Figure 22 Whole mount *in situ* hybridization *ppp4cb*
Whole mount *in situ* hybridization of *ppp4cb* on a 4d old embryo A, B) lateral, anterior up C) anterior right D, E, F) anterior left. Photographed side right (R), left (L), the whole head is stained in blue, also the swim bladder (Sb), branchial arches (Ba) and liver (Li). Scale bar 200 µm

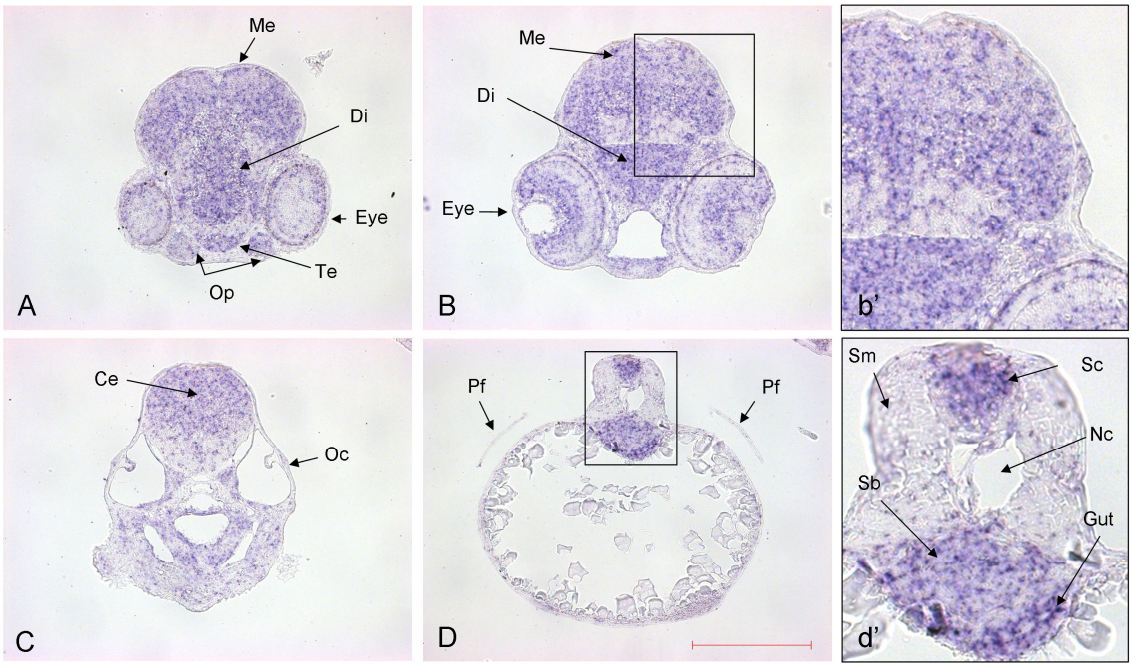

Figure 23 *ppp4cb in situ* hybridization on sections of embryo 3 dpf
A-D) transversal sections from cranial to caudal. The signal for *ppp4cb* expression (blue staining) is visible in the whole head, the spinal cord (Sc), swim bladder (Sb) and gut. Abbreviations: diencephalon (Di), cerebellum (Ce),mesencephalon (Me), notochord (Nc), olfactori placode (Op), pectoral fin (Pf), somitic muscle (Sm), telencephalon (Te). Magnification 100x, scale bar 200 µm

The above *in situ* hybridizations on sections show that the *ppp4cb* signal is uniformly distributed in the head. Additionally, the signal is visible in the spinal cord, swim bladder, gut and less prominent in the somitic muscle.

4.2.7 *sez6l2* is specifically expressed in neuronal tissue

The whole mount *in situ* hybridization showed a restricted *sez6l2* activity to the three parts of the brain: the diencephalon, midbrain and hindbrain (Figure 24). This is also confirmed by *in situ* hybridization in transversal sections. Importantly, the sections also showed that *sez6l2* is only expressed in the cell body of the neurons, which are forming the gray matter of the brain, and not in the axons. Besides the *sez6l2* activity in the brain, the sections also displayed a very diffuse expression in the trunk (Figure 25).

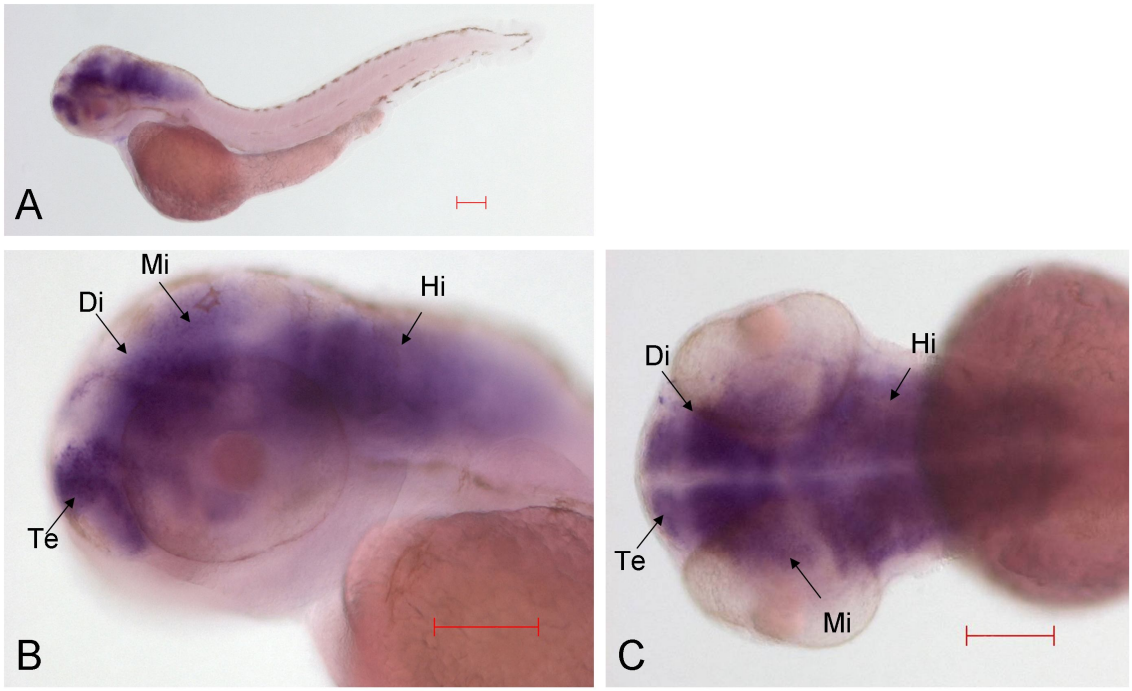

Figure 24 *sez6l2* expression in the brain of a zebrafish embryo 3 dpf
A) whole embryo lateral, anterior left, B) detailed view, head lateral, C) head viewed dorsal. Stained in blue are the *sez6l2* expressing parts of the brain, telencephalon (Te), diencephalon (Di), midbrain (Mi) and hindbrain (Hi), note the unstained parts between the brain segments. Scale bar 200 µm

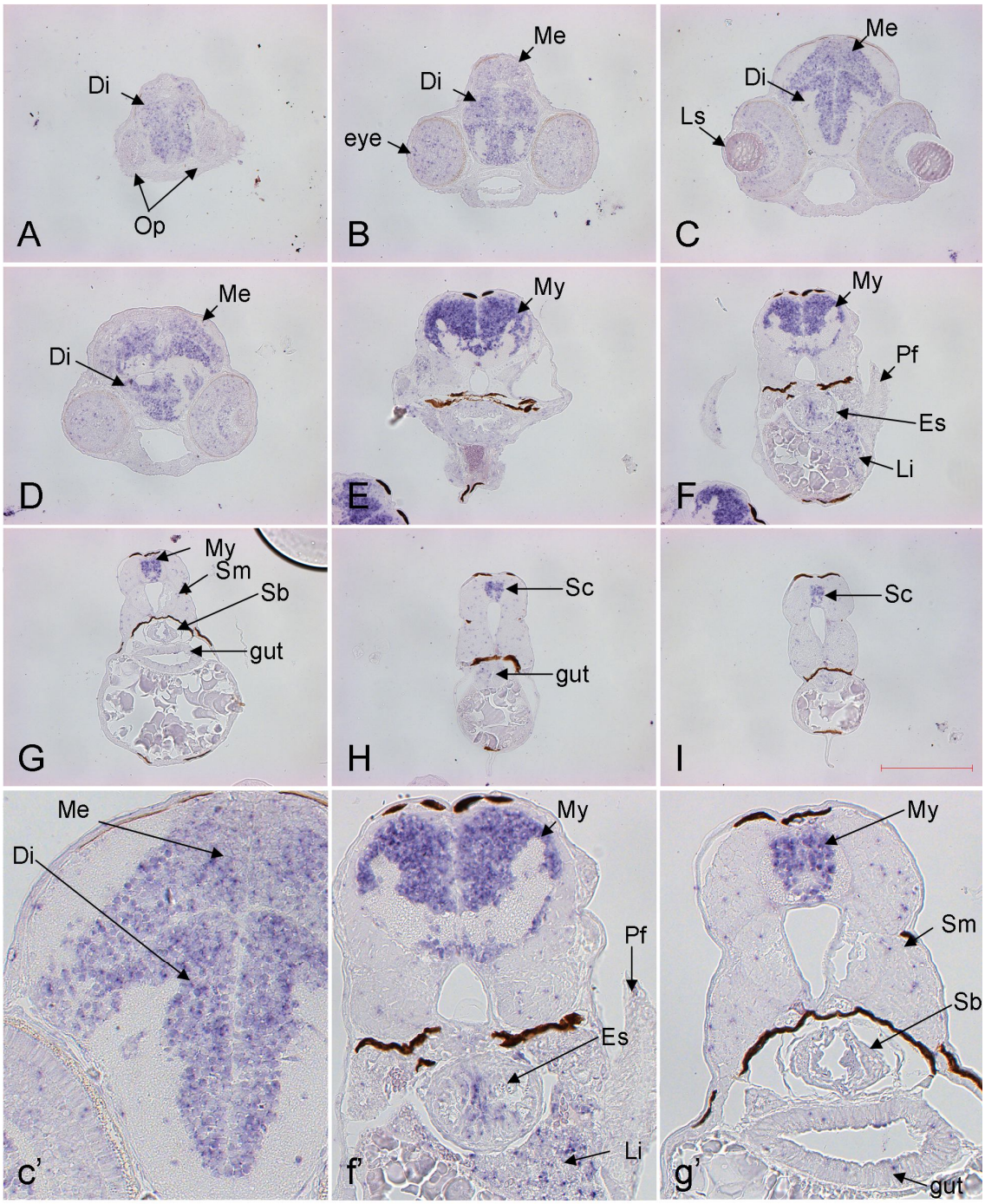

Figure 25 Specific brain expression of *sez6l2*
A-I) transversal sections from cranial to caudal, embryo 3 dpf. The signal for *sez6l2* expression (blue staining) is visible in all parts of the brain, the spinal cord (Sc) and pectoral fins (Pf) (A-I). Abbreviations:, diencephalon (Di), esophagus (Es), liver (Li), lens (Ls), mesencephalon (Me), myelencephalon (My), olfactori placode (Op), pectoral fin (Pf), somitic muscle (Sm), swim bladder (Sb). Magnification 100x, scale bar 200 µm

4.2.8 *ypel3* is uniformly expressed in the head, heart and pericardium

ypel3 is expressed in the head and the heart of the embryos (Figure 26). The expression in the head is diffuse and includes all parts of the head with the exception of the lenses. The pericardium and the heart showed the strongest expression of *ypel3* (Figure 27).

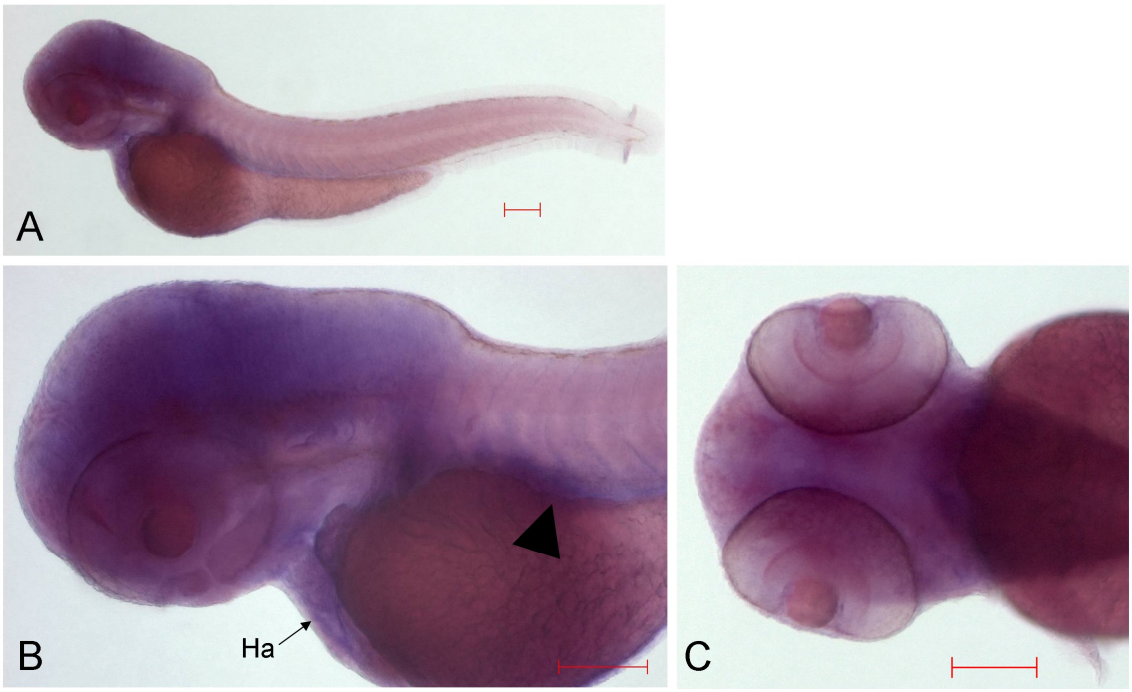

Figure 26 *ypel3* expression at the head of a zebrafish embryo 3 dpf
In all pictures anterior is left A) whole embryo lateral; head detailed B) lateral, C) head dorsal. Stained in blue is the *ypel3* expression in the whole head and heart (Ha). Also the otic vesicle and intestine (black arrow head) appear to be stained. Scale bar 200 µm

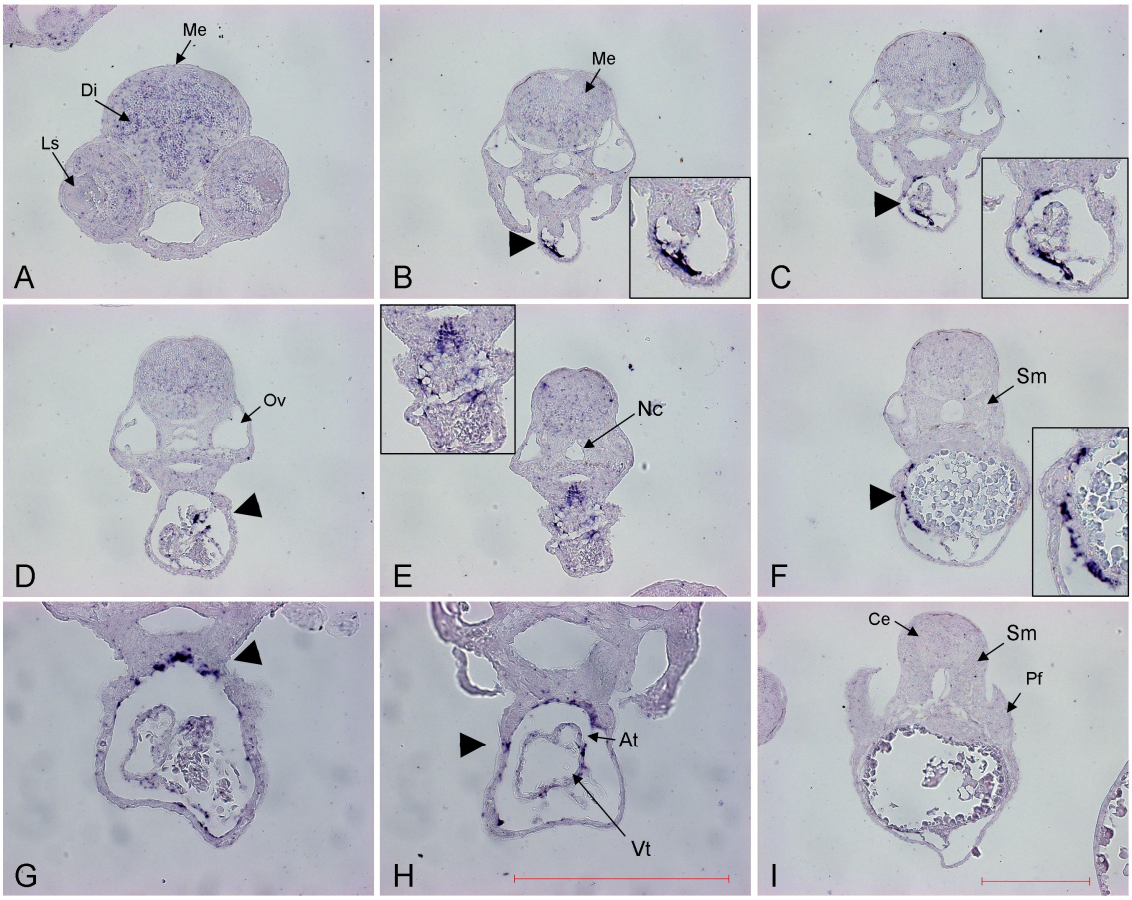

Figure 27 *ypel3* is ubiquitously expressed in the head and specifically at the heart
A-I) transversal sections of a 3 day old embryo from cranial to caudal. The signal for *ypel3* expression (blue staining) is visible in the whole head: diencephalon (Di), mesencephalon (Me), cerebellum (Ce) (A-F). Notably, there is also a strong signal at the heart and pericardium (arrowhead). Abbreviations: lens (Ls), notochord (Nc), otic vesicle (Ov), pectoral fin (Pf), somitic muscle (Sm). Magnification A-F, I) 200x, G, H) 400x, scale bar 200 µm

4.2.9 Summary of the *in situ* hybridization results

Generally, all target genes showed a ubiquitous expression in the head and brain. Therefore, all genes were selected for further investigation by morpholino knockdown. An exception was *sez6l2*, which was found to be localized specifically in the cell body of the brain cells. This was confirmed by *in situ* hybridization on sections which revealed an exclusive expression in the cell body of the neurons. Another specific expression is the very strong signal of *kctd13* and *ypel3* at the heart of the embryos. The expression patterns for all genes are summarized in Table 12.

Table 12 Summery of *in situ* hybridization experiments

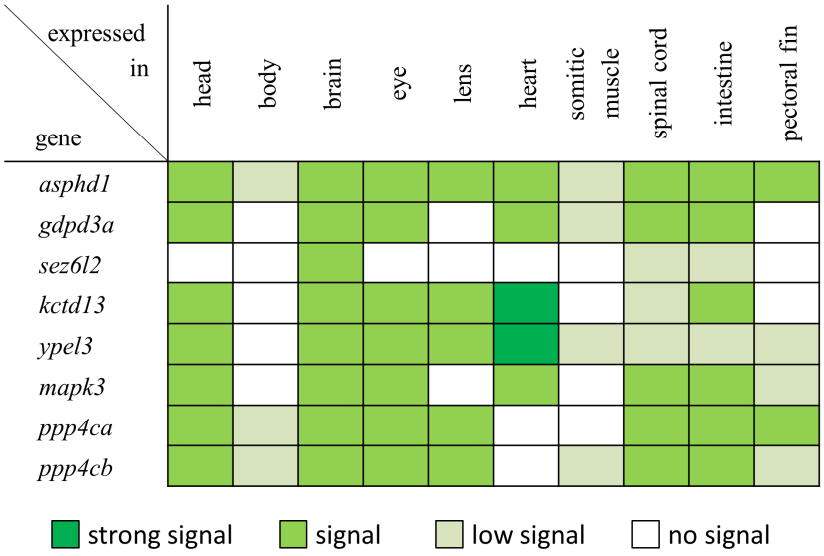

4.3 morpholino knockdown of the syntenic genes

The synthetic morpholino oligomers can achieve a gene knockdown by two different methods. For the first method the morpholino is designed complementary to the 5'UTR of the target gene to prevent the assembly of the ribosome. The second strategy is based on the interference of the RNA processing. Therefore, the morpholino is designed complimentary to a splice site of the gene of interest which causes a missense RNA. An advantage of this method is that a control of the missense RNA is possible by PCR. The main difficulty of the morpholino method is the delivery in to the cell, which in zebrafish experiments is most efficient by direct injection of the morpholino into the first cell of the embryo.

4.3.1 Morpholino injection procedure causes small developmental delay

To verify that the injection procedure itself does not cause an effect on the embryos, each experiment included an injection control. As control the standard control morpholino (SCMO) from GeneTools LLC was used. Embryos injected with the SCMO showed no anatomical change, but a developmental delay of approximately five hours. This short delay was also noticeable in the difference of body length and head size means (Figure 28). However, the difference was only significant for the 2 day old embryos (Bonferroni corrected *p*-value, body length $p = 6.13 \times 10^{-8}$, head size: $p = 0.0189$, Table 13 and Table 14). To verify that the difference in body length and head size was caused by the five hours developmental delay, the head size was plotted against body length (Figure 29). The regression lines, which represent the growth rate of the embryos, were added to both the uninjected and the SCMO injected data points. Both regression lines followed a linear progression with a difference in the gradient of only 0.0061 (uninjected: $y = 0.2006x - 148.99$, $r^2 = 0.8859$; SCMO: $y = 0.1984x - 141.97$, $r^2 = 0.8977$). To test if there was a significant difference in the correlation of the distributions, a Fisher's z transformation was performed and $\hat{z} = 0.689$ was calculated. Consequently, it can be assumed that the two correlation coefficients are equal ($z = 1.96$ corresponds to a *p*-value of 0.05). Therefore, the SCMO injected embryos showed no difference in the distribution of the growth rate compared to the uninjected. To test if the morpholino injection affects the growth rate, the regression coefficients of the regression lines were compared. The result was $\hat{t} = 0.260$, therefore the H_0 hypothesis

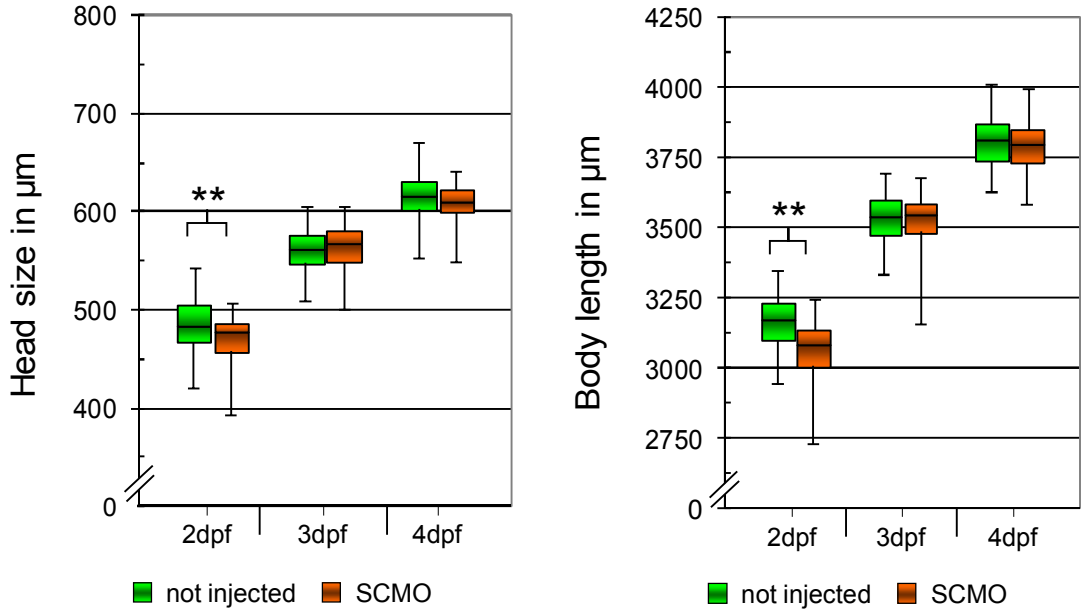

Figure 28 Growth difference between SCMO injected and uninjected embryos
Measured is the head size (left) and body length (right) of embryos two, three and four days of development. Most of the embryos showed no difference in head size or body length. Only the 2 d old SCMO injected embryos are significant smaller in body length and head size (** p-value < 0.01, two-tailed t-test), for the number of embryos used for comparison see Table 13 and Table 14.

$\beta_1 = \beta_2$ was accepted (t = 1.99 corresponds to $p = 0.05$). Consequently, the growth rates of SCMO injected and uninjected embryos showed no difference. This proves that the SCMO morpholino is not affecting the growth rate of the embryos.

Table 13 Head size comparison of uninjected and SCMO injected embryos
The number of measured embryos originates from two independent experiments. To test if the head size of the uninjected knockdown embryos differs significantly from the SCMO injected embryos a two-tailed student's t-test was performed. The p-value of the t-test was corrected for multiple testing using the Bonferroni method (n = 3).

dpf	**Head size** mean ± standard deviation		Number of measured embryos *uninjected* /SCMO	p-value (two-tailed student's t-test)	Corrected p-value (Bonferroni p_{ad} = n×p)
	uninjected	SCMO			
2	485.41 ± 28.52	471.03 ± 24.03	58/46	0.0063	0.0189
3	561.12 ± 20.63	562.62 ± 25.60	64/60	0.1482	0.4444
4	616.49 ± 26.54	609.22 ± 21.57	62/65	0.0973	0.2811

Table 14 Body length comparison of uninjected and SCMO injected embryos
The number of measured embryos originates from two independent experiments. To test if the head size of the uninjected knockdown embryos differs significantly from the SCMO injected embryos a two-tailed student's t-test was performed. The *p*-value of the t-test was corrected for multiple testing using the Bonferroni method (n = 3).

dpf	**Body length** mean ± standard deviation		Number of measured embryos uninjected /SCMO	*p*-value (two-tailed student's t-test)	Corrected *p*-value (Bonferroni $p_{ad} = n \times p$)
	uninjected	SCMO			
2	3169.74 ± 92.19	3059.90 ± 120.46	58/46	2.04×10^{-6}	6.13×10^{-6}
3	3536.77 ± 89.68	3520.77 ± 104.90	64/60	0.2494	0.7482
4	3812.19 ± 93.98	3791.64 ± 95.67	62/65	0.2245	0.6735

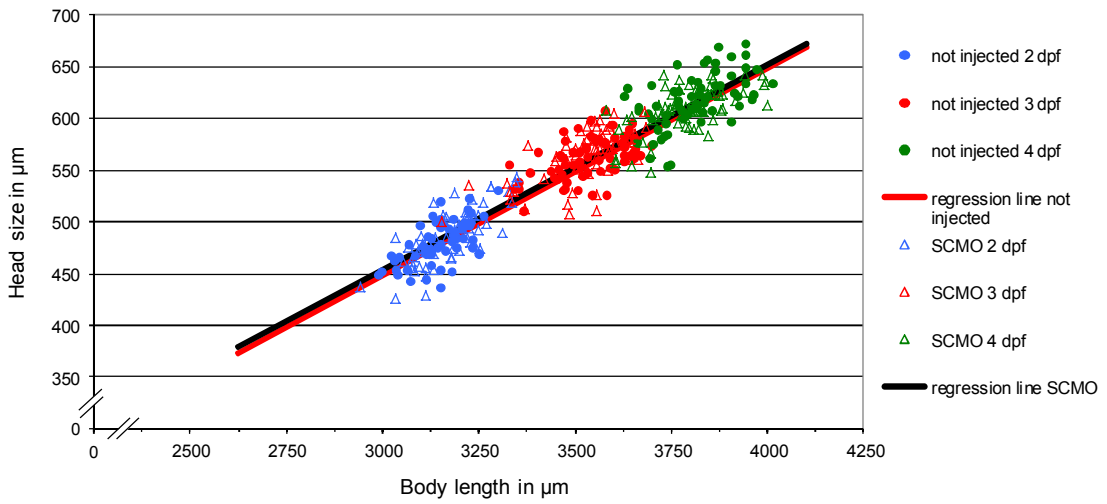

Figure 29 Effect of morpholino injection on body length and head size
Embryos measured at 2 dpf, 3 dpf and 4 dpf, regression line uninjected: y = 0.2006x – 148.99, $r^2 = 0.8859$, regression line SCMO: y=0.1848x – 90.96, $r^2 = 0.9103$, number of plotted embryos can be found in Table 13 and Table 14

4.3.2 *asphd1* knockdown causes edema in muscle and developmental delay

The comparison of *asphd1* and SCMO morpholino knockdown embryos showed no visible structural or behavioral difference (Figure 30). However, the *asphd1* knockdown embryos showed a developmental delay of approximately seven hours. This delay was also significant when comparing the head size and body length of knockdown and control embryos (corrected *p*-value $< 0.01 \times 10^{-5}$, Figure 31, Table 15 and Table 16). To confirm, that the significant difference in head size and body length is not affecting the growth rate, the head size was plotted over the body length. Afterwards a regression line from second to fourth day of embryo development was calculated for the *asphd1*

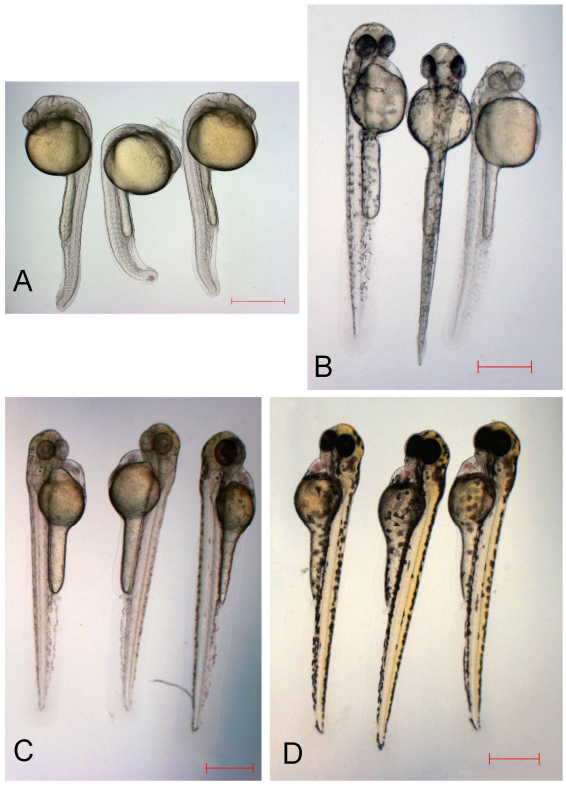

Figure 30 Development of *asphd1* knockdown embryos
Embryos positioned lateral, anterior up. A) 1 dpf B) 2 dpf C) 3 dpf D) 4 dpf, heart, head, eye and ear are developing normal like in the SCMO injected embryos (not shown), scale bars 500 µm.

knockdown embryos and the corresponding SCMO control (Figure 33). To test if the regression lines were different, the correlation coefficients were used in a Fisher's z transformation and the $\hat{z}$ was calculated. The result was a $\hat{z} = 1.73$ ($z = 1.96_{p=0.05}$), consequently there was no difference in the distribution of the *asphd1* knockdown and SCMO injected embryos. Furthermore, the slope of the regression lines was tested, which resulted in no significant difference ($\hat{t} = 0.406$; $t = 1.99_{p=0.05}$). Therefore, it is proven that the *asphd1* knockdown is not affecting the brain size of the embryos.

Interestingly, a detailed view at higher magnification revealed small edema in the somitic muscle (Figure 34). Similar edemas were also found in *ppp4ca* knockdown embryos, which display also difficulties in the formation of the blood system. Therefore, the *asphd1* knockdown embryos were screened for changes in the blood flow. This was done by observation of the erythrocyte movement within the posterior end of the tail, which revealed that the blood flow was fully established in the intersegmental vessels and extended to the distal end of the tail (Figure 32).

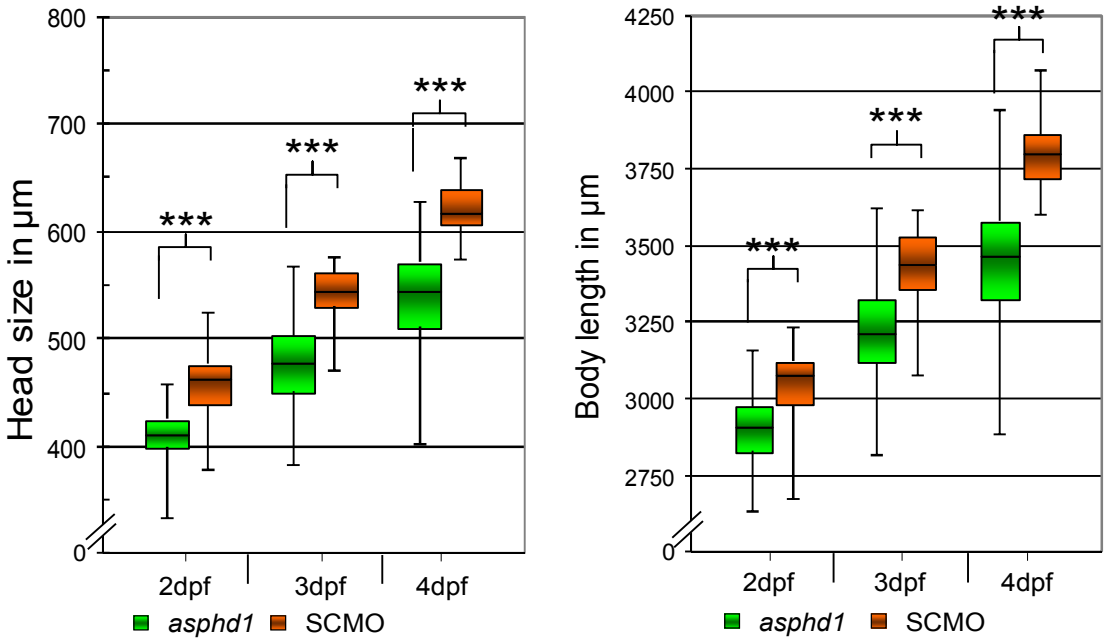

Figure 31 Box plot comparison of *asphd1* knockdown and SCMO injected embryos
head size (left) and body length (right). The number of embryos used per experiment and *p*-values can be found in Table 2 and Table 16, *** *p*-value < 0.01×10^{-5}

Table 15 Head size of *asphd1* and SCMO injected embryos at different time points
The number of measured embryos originates from two independent experiments. To test if the head size of the *asphd1* knockdown embryos differs significantly from the SCMO injected embryos a two-tailed student's t-test was performed. The *p*-value of the t-test was corrected for multiple testing using the Bonferroni method (n = 3).

dpf	**Head size** mean ± standard deviation		Number of measured embryos *asphd1* /SCMO	*p*-value (two-tailed student's t-test)	Corrected *p*-value (Bonferroni $p_{ad} = n \times p$)
	asphd1	SCMO			
2	408.33±24.77	456.68 ± 28.41	73/58	1.37×10^{-19}	4.12×10^{-19}
3	477.90±38.22	542.82 ± 24.89	133/72	2.13×10^{-32}	6.38×10^{-32}
4	538.92±43.30	620.62 ± 23.49	134/54	2.71×10^{-25}	8.12×10^{-25}

Table 16 Body length of *asphd1*and SCMO injected embryos at different time points
The number of measured embryos originates from two independent experiments. To test if the body length of the *asphd1* knockdown embryos differs significantly from the SCMO injected embryos a two-tailed student's t-test was performed. The *p*-value of the t-test was corrected for multiple testing using the Bonferroni method (n = 3).

dpf	**Body length** mean ± standard deviation		Number of measured embryos *asphd1* /SCMO	*p*-value (two-tailed students t-test)	Corrected *p*-value (Bonferroni $p_{ad} = n \times p$)
	asphd1	SCMO			
2	2899.68±114.01	3048.33±119.04	73/58	6.31×10^{-12}	1.89×10^{-11}
3	3220.29±144.85	3427.14±129.35	133/72	4.10×10^{-19}	1.23×10^{-18}
4	3452.87±190.39	3803.78±104.94	134/54	3.15×10^{-24}	9.45×10^{-24}

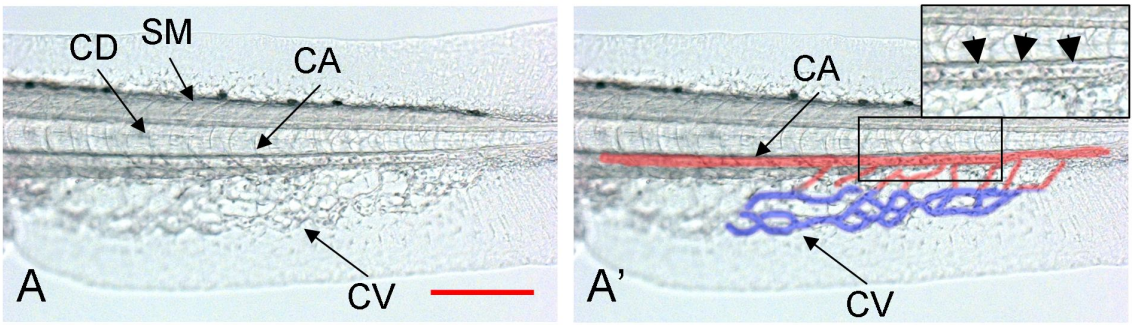

Figure 32 Normal blood flow in *asphd1* knockdown embryo
A) *asphd1* knockdown embryo with normal blood flow extending to the distal end of the tail. A') The caudal artery (CA) and caudal vein (CV) are highlighted in red and blue, respectively and are visible by movement of the erythrocytes under microscope. Detailed CA with erythrocytes (arrowheads). Scale bars 500 µm

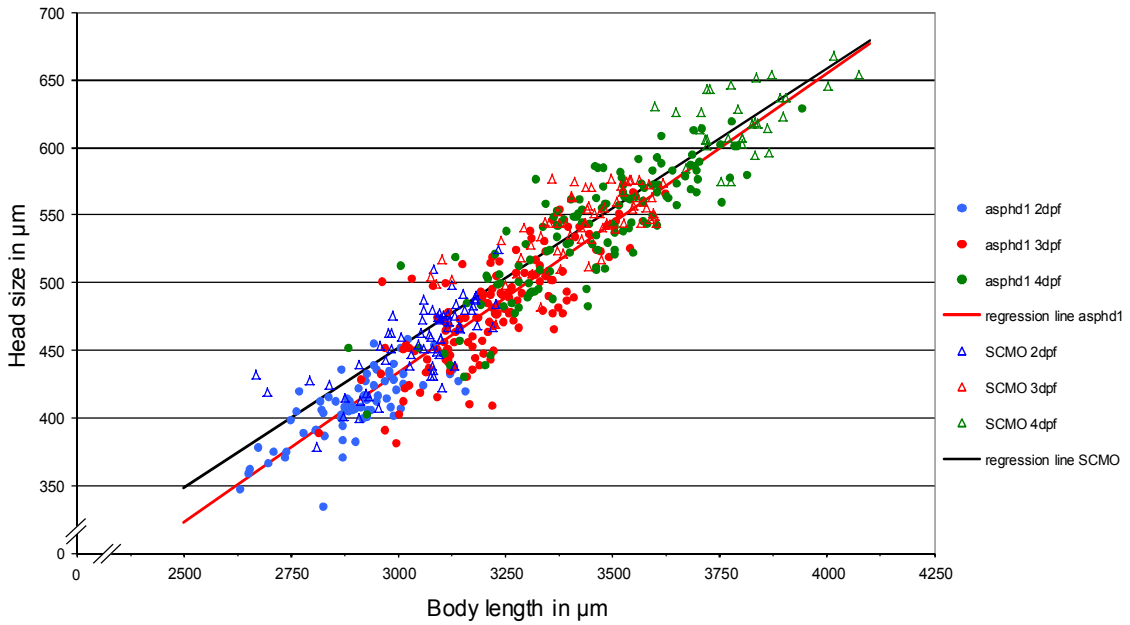

Figure 33 Growth rate comparison of *asphd1* and SCMO knockdown embryos
Plotted is head size to body length for 2d (blue), 3d (red) and 4d (green) old *asphd1* (point) and SCMO (triangle) knockdown embryos. Regression lines represent the growth rate from second to fourth day after fertilization SCMO (black): $y = 0.2071x - 169.99$, $r^2 = 0.8996$ and *asphd1* (red): $y = 0.2213x - 230.66$; $r^2 = 0.8633$

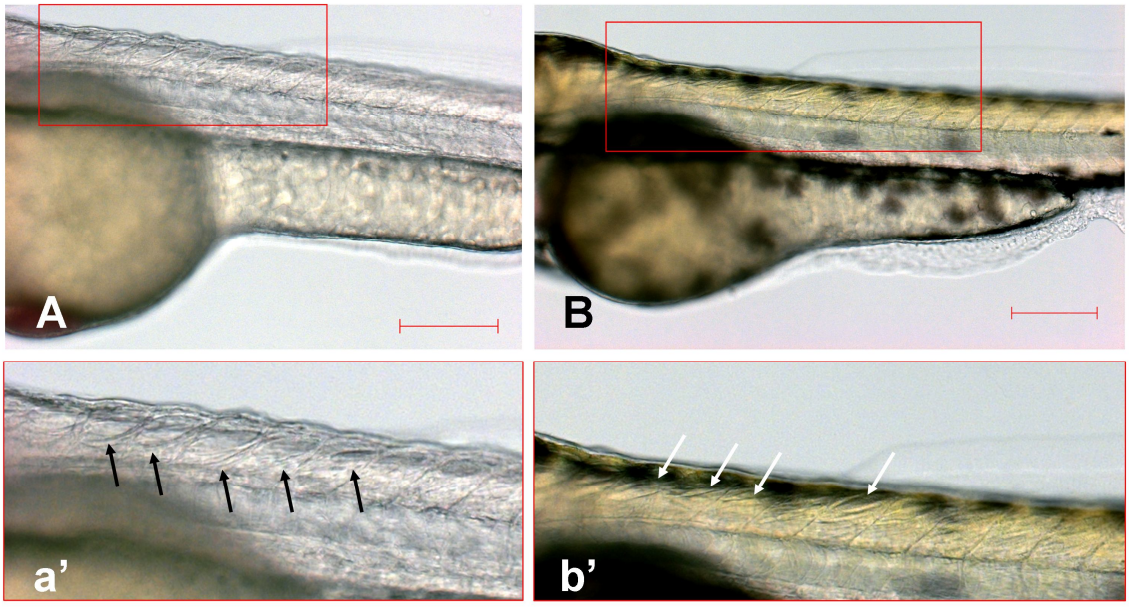

Figure 34 Edema in muscle of *asphd1* knockdown embryos
asphd1 knockdown embryo 3 dpf (A) and 4 dpf (B), embryos orientated lateral, anterior left, ventral down. Scale bar 200 µm. a' and b' represent sections, arrows indicate edema in the somitic muscle

4.3.3 *gdpd3a* knockdown leads to a developmental block at 18 somite stage

The *gdpd3a* knockdown was performed with a translational and a splice blocking morpholino. Interestingly, the morpholino against the 5'UTR induced no effect, whereas the splice blocking morpholino yielded a strong phenotype. At 24 hpf the knockdown embryos showed signs of cell death and denaturation. At 2 dpf, only 3 embryos out of approximately 300 developed normally (two independent experiments; survival rate SCMO: 116 out of 300) (Table 17). The other knockdown embryos died at the 18 somite stage, visible by complete denaturation (embryos were white, untransparent and started to lose structural integrity). Additionally, this was accompanied by deformations in head and trunk. Due to the deformation and the early death of the embryos, a measurement of the head size and body length was not performed.

To confirm the functionality of the splice site morpholino, a PCR with primers binding to the first and the third exon of the *gdpd3a* cDNA was performed. The PCR confirmed the loss of the 40 bp long exon 2 (Figure 36). Therefore, it can be expected that the *gdpd3a* phenotype is based on the effect of the splice site morpholino.

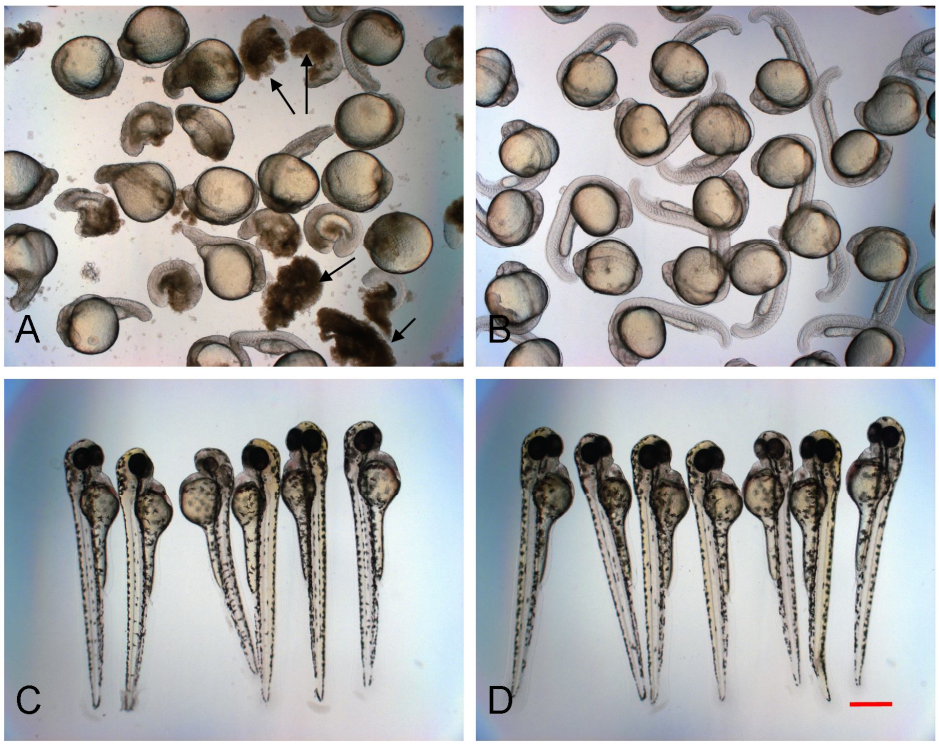

Figure 35 *gdpd3* splice site knockdown is lethal 24 hpf, 5'UTR knockdown embryos develop normally
A) *gdpd3* splice site morpholino knockdown 24 hpf, embryos unjustified, white arrows indicate denatured tissue, embryos show problems in head and trunk formation. B) SCMO injection 24 hpf. C) *gdpd3* 5'UTR morpholino knockdown, embryos develop normally, as in the corresponding SCMO injected embryos (D). Embryos positioned lateral, anterior up. Magnification 25x, scale bar 500 µm.

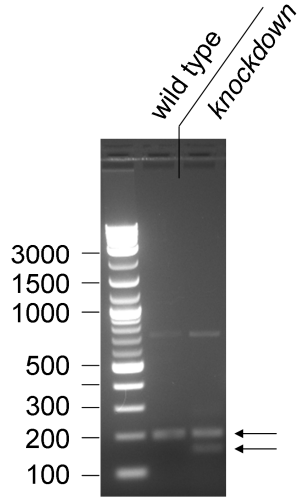

Figure 36 *gdpd3a* knockdown induces skipping of exon 2
PCR template was the cDNA of uninjected and *gdpd3a* splice site morpholino injected embryos. Primers binding to exon 1 and 3 of the *gdpd3a* mRNA are amplifying the expected 196 bp fragment. The morpholino used in the knockdown is blocking the splice site i2e3. Therefore, the PCR product is reduced by the length of exon 2 to the expected fragment size of 156 bp. Both fragments are marked with arrows. Marker: 2lod DNA ladder (NEB).

Table 17 *gdpd3a* slice site knockdown embryos dying between first and second day
Embryos injected with morpholino against the 5'UTR show no change in mortality rate. Whereas nearly all embryos injected with the splice site morpholino are dying.

morpholino type	morpholino concentration in mM	Number of surviving embryos 1 dpf (SCMO / uninjected)	Number of surviving embryos 2 dpf (SCMO / uninjected)	surviving embryos from 1 dpf to 2 dpf in %
5'UTR	0.8	133 (51/76)	108 (49/64)	81.20 (96/84)
5'UTR	1.6	106 (35/81)	75 (33/86)	70.75 (94/106)
Splice site i2e3	0.8	24 (37/50)	3 (36/45)	12.5 (97/90)
Splice site i2e3	0.8	7 (80/91)	0 (80/88)	0.00 (100/97)

4.3.4 Knockdown of *kctd13* causes head size enlargement

The injection of the *kctd13* knockdown morpholino did not cause structural changes on the embryonic development during the 4 dpf observation time (Figure 37). Moreover, the embryos developed at a similar pace as the controls. Therefore, the measurement of the head size and body length was directly comparable to the SCMO injected embryos. Interestingly, this comparison displayed a significant difference in the lenght of the four day old *kctd13* knockdown embryos (Figure 38). The measurement of the head size showed an increase of about 10 µm with a significance of $p = 0.000371$ (Bonferroni corrected p – value, Table 18). Conversely, the body length of the four day old *kctd13* knockdown embryos was 96 µm smaller when compared to the controls (Bonferroni corrected p –value $p = 0.00886$, Table 19). To test if this difference is affecting the growth ratio, the head size was plotted against the body length for each embryo (Figure 39). This plot demonstrates that the growth rate of the *kctd13* knockdown embryos is

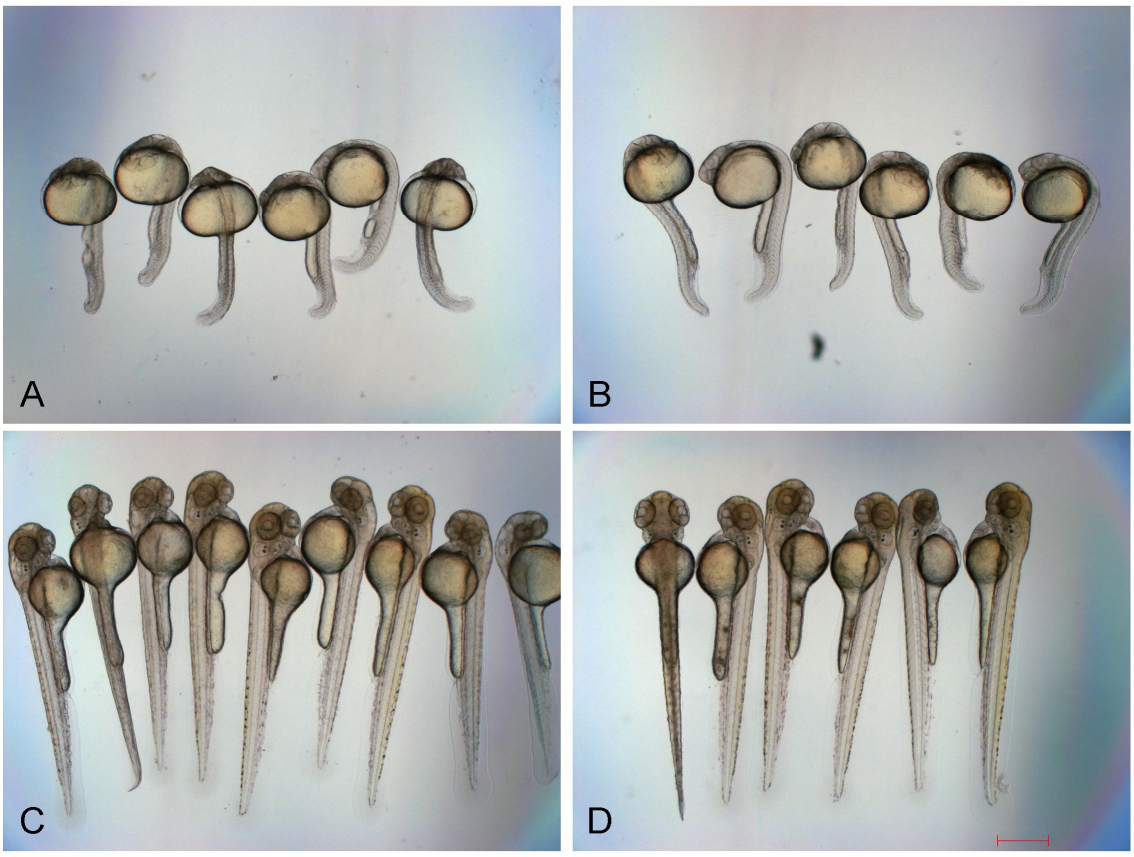

Figure 37 *kctd13* knockdown embryos
A) *kctd13* knockdown embryos 24 hpf, B) SCMO injected embryos 24 hpf, C) *kctd13* knockdown embryos 3 dpf, D) SCMO control 3 dpf; all embryos PTU treated, positioning is lateral, anterior up. Scale bar 500 µm

significantly higher ($\hat{t} = 3.73 > t = 1.99_{p=0.05}$). Moreover, the significance of the growth rate difference increases when comparing the *kctd13* knockdown embryos with the controls of all experiments performed within this thesis $\hat{t} = 6.97$ (Figure 40). Taken together, the *kctd13* morpholino injected embryos showed no structural differences in the brain or body development. However, the head size of the *kctd13* knockdown embryos was significantly larger compared to the controls. This indicates an increase in the cell mass of the brain or an enlargement of the brain ventricle.

Table 18 Head size of *kctd13* and SCMO injected embryos at different time points
The number of measured embryos originates from two independent experiments. To test if the head size of the *kctd13* knockdown embryos differs significantly from the SCMO injected embryos a two-tailed student's t-test was performed. The *p*-value of the t-test was corrected for multiple testing using the Bonferroni method (n = 2).

dpf	**Head size** mean ± standard deviation		Number of measured embryos *kctd13*/ SCMO	*p*-value (two-tailed student's t-test)	Corrected *p*-value (Bonferroni $p_{ad} = n \times p$)
	kctd13	SCMO			
3	522.60 ± 34.48	528.34 ± 23.45	107/66	0.195848	0.391695
4	619.68 ± 46.11	609.22 ± 21.56	88/65	0.000185	0.000371

Table 19 Body length of *kctd13* and SCMO injected embryos at different time points
The number of measured embryos originates from two independent experiments. To test if the body length of the *kctd13* knockdown embryos differs significantly from the SCMO injected embryos a two-tailed student's t-test was performed. The *p*-value of the t-test was corrected for multiple testing using the Bonferroni method (n = 2).

dpf	**Body length** mean ± standard deviation		Number of measured embryos *kctd13* /SCMO	*p*-value (two-tailed students t-test)	Corrected *p*-value (Bonferroni $p_{ad} = n \times p$)
	kctd13	SCMO			
3	3431.84 ± 146.05	3439.20 ± 121.21	107/66	0.72101	1.44201
4	3695.44 ± 185,57	3791.64 ± 95.67	88/65	0.00443	0.00886

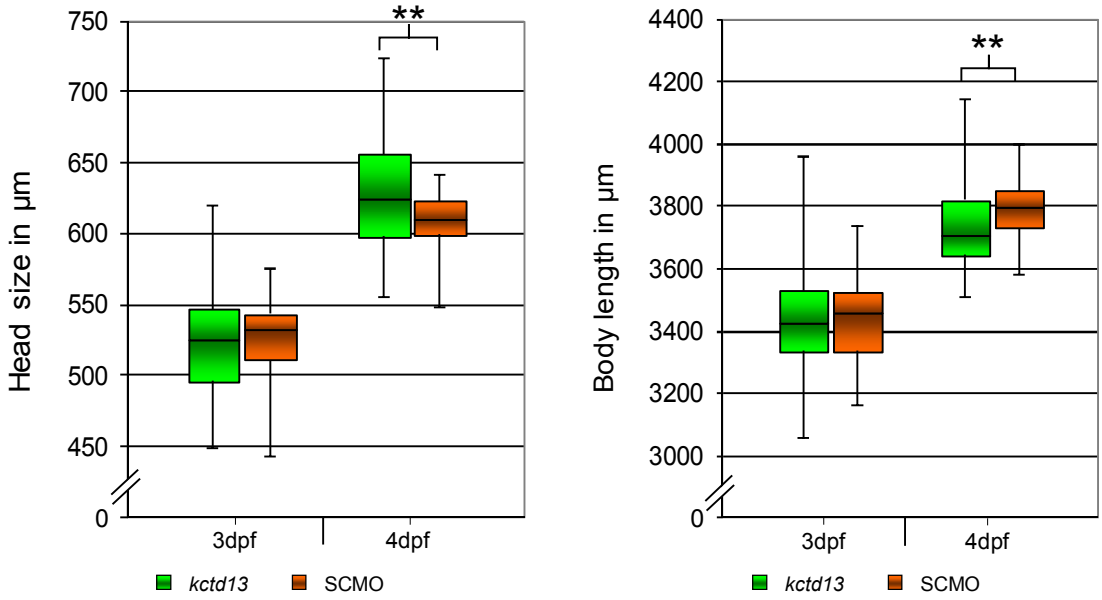

Figure 38 Head size and body length of *kctd13* knockdown embryos
Comparison of head size (left) and body length (right) between *kctd13* morpholino knockdown and SCMO injected embryos. *kctd13* knockdown present a significant enlargement in head size and a reduction in body length at 4 dpf(** *p*-value < 0.01). The number of embryos used per experiment and *p*-values can be found in Table 18 and Table 19.

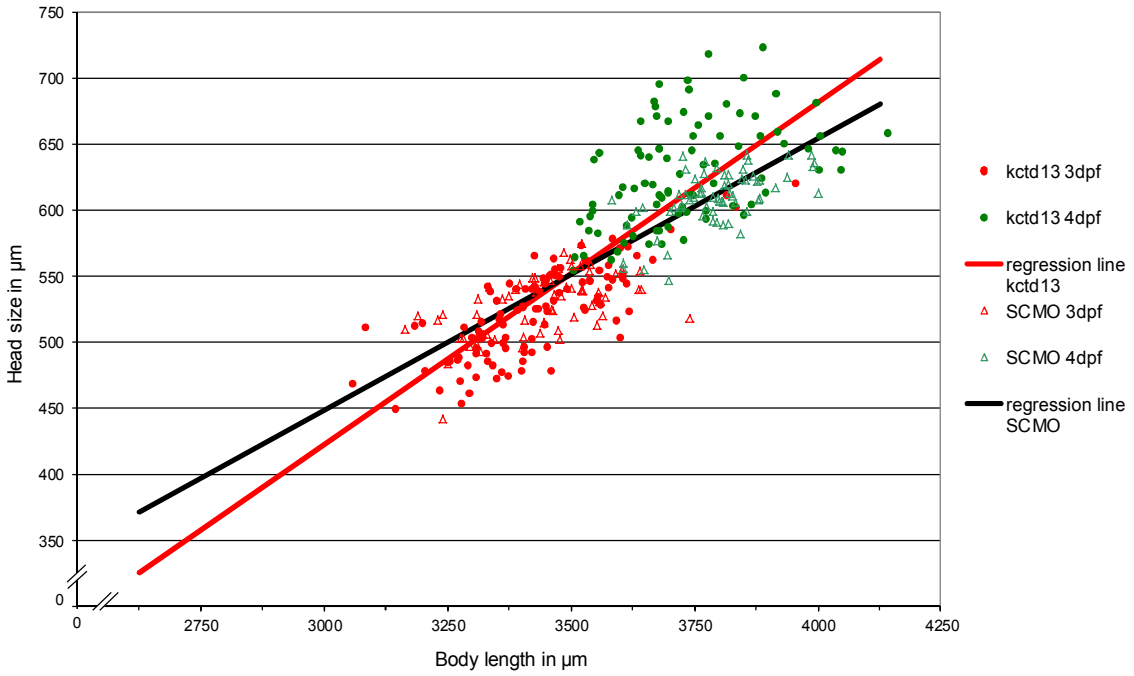

Figure 39 *kctd13* knockdown embryos body length to head size ratio plot
Plotted embryos are measured 3 (red) or 4 dpf (green). Regression lines represent the growth rate from third to fourth day post fertilization; SCMO (black): $y = 0.1989x - 150.40$, $r^2 = 0.8748$ and *kctd13* (red): $y = 0.2596x - 356.24$, $r^2 = 0.7138$. 4 dpf *kctd13* knockdown embryos show a bigger head size then the control embryos.

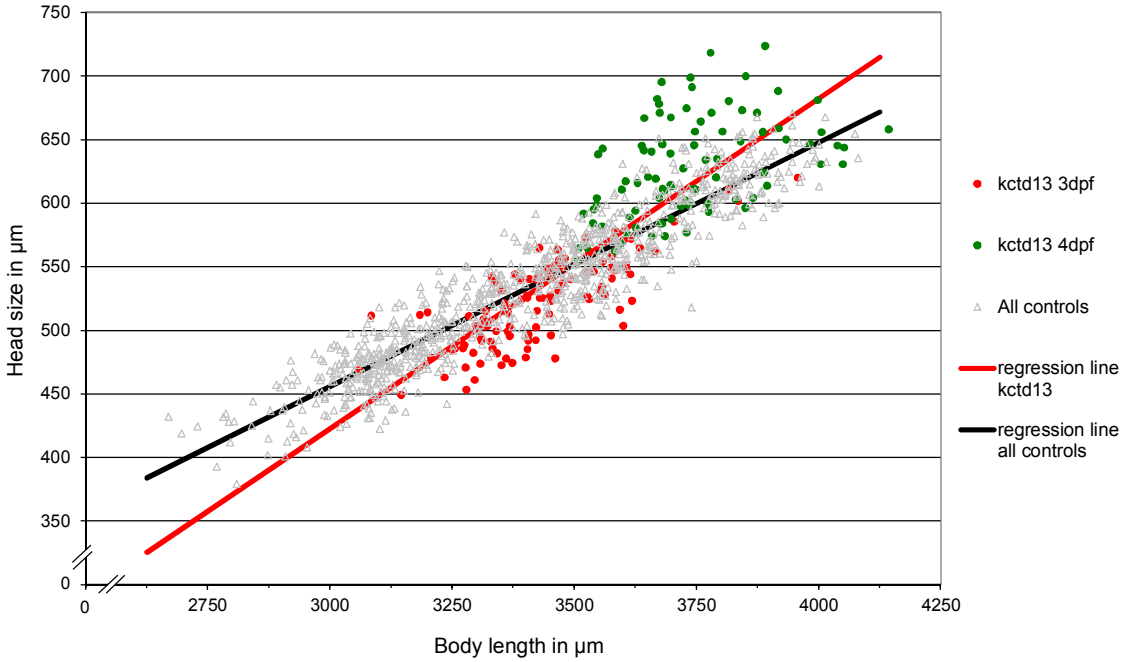

Figure 40 *kctd13* knockdown, body length to head size ratio plot compared with controls
Plotted embryos are measured 3 (red) or 4 dpf (green). Control embryos originate from all experiments and include SCMO and uninjected embryos measured at two, three and four days post fertilization. Regression lines represent the growth rate from second to fourth dpf; SCMO (black): $y = 0.1989x - 150.40$, $r^2 = 0.8748$ and third to fourth dpf *kctd13* (red): $y = 0.2596x - 356.24$, $r^2 = 0.7138$. Fourth dpf *kctd13* knockdown embryos show a bigger head size then all measured control embryos.

4.3.5 Knockdown of *mapk3* leads to severe deformations

At 1 dpf the *mapk3* knockdown embryos present a deformation of the notochord and tail in about 58 % of the embryos. In addition, the embryos were developmentally delayed (21- somite) compared to the SCMO controls (prim- 16). At 2 dpf most of the embryos still showed problems in axis formation as well as small heads and eyes. In the duct of Cuvier, where normally the blood is carried back to the heart, no blood is visible. At 3 dpf the embryos were between long pec and pec fin stage. They did not form erythrocytes and presented a swollen pericardium with a thin long-drawn-out heart. Nevertheless, the heart contracted and beat at a very low frequency.

The phenotype presented above was obtained with both morpholino types in 58 % of the embryos. In total, 390 embryos developed until 1 dpf in four independent experiments. However, after 3 dpf only 34 % of the embryos from day one were alive,

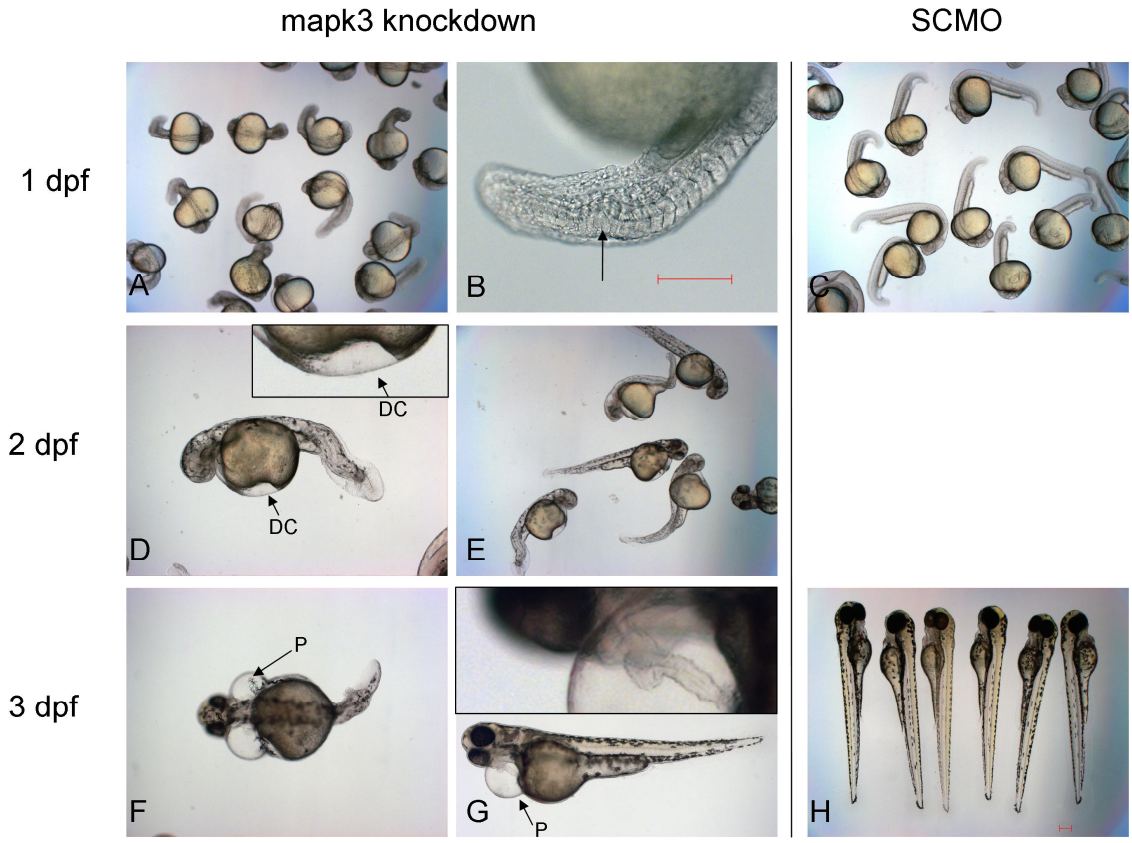

Figure 41 *mapk3* morpholino knockdown embryos at 1, 2 and 3 dpf
After 1 day of development the notochord of the *mapk3* knockdown embryos is deformed (B arrow). At the second day the embryos present small heads, reduced eyes and no blood flow (note the empty Duct of Cuvier (DC)). At 3 dpf still no blood is visible, the heart is thin and long-drawn-out. The pericardium (P) is swollen (arrow F, G). Magnifications (objective) B) 10x, D, F, G) 5x and A, C, E, H) 2.5x; scale bar 200 µm

of which 51 % showed the described phenotype. This and the enhancement of the phenotype by increasing the morpholino concentration led to the suggestion that the phenotype is dosage dependent (Table 20).

Table 20 Effect of *mapk3* knockdown
Number of morpholino injected embryos per experiment for *mapk3* ≈ 350, SCMO ≈ 175 and uninjected ≈ 175 embryos. Listed is the number of total and deformed embryos for each experiment at 1 dpf and 3 dpf.

morpholino type	morpholino concentration in mM	Number of total embryos **1 dpf** (SCMO / uninjected)	Number of deformed embryos **1 dpf** (SCMO / uninjected)	**1 dpf** deformed embryos in %	Number of embryos **3 dpf** (normal/ deformed)
5'UTR	1.6	128 (79 / 85)	123 (4 / 2)	96 (3/2)	3 / 11
5'UTR	0.8	82 (62 / 77)	23 (6 / 2)	28 (10/2)	24 / 15
Splice site e3i3	0.8	81 (45 / 55)	36 (13 / 2)	44 (28/4)	15 / 19
Splice site e3i3	0.8	99 (65 / 64)	45 (5 / 7)	45 (7/10)	22 / 23

4.3.6 *ppp4ca* knockdown induces atypical blood vessel formation and edema

The embryos injected with the *ppp4ca* morpholino against the 5'UTR and splice site share the major phenotypes in blood flow, muscle and swelling of the embryo. However, the loss of one otolith occured only in embryos injected with the translation blocking morpholino.

The first notable difference between the *ppp4ca* morpholino injected and control embryos became visible at 1 dpf. In contrast to the normal developed SCMO injected embryos (high pec), the *ppp4ca* knockdown embryos only attain the prim-22 stage, which corresponds to a developmental delay of approximately seven hours. During prim-22 stage, normally the angiogenesis is initialized which results in the full established blood circulation at 2 dpf. However, in the

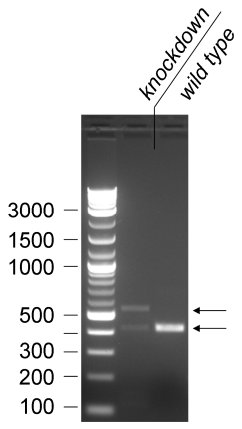

Figure 42 *ppp4ca* knockdown shows skipping of exon 2
Template for the PCR was cDNA from ppp4ca splice site morpholino knockdown and wild type embryos. The expected fragment size of untreated embryos was 551 bp. Embryos treated with the *ppp4ca* splice site morpholino show skipping of exon 2, PCR fragment at 424 bp. Marker 2lod DNA ladder (NEB).

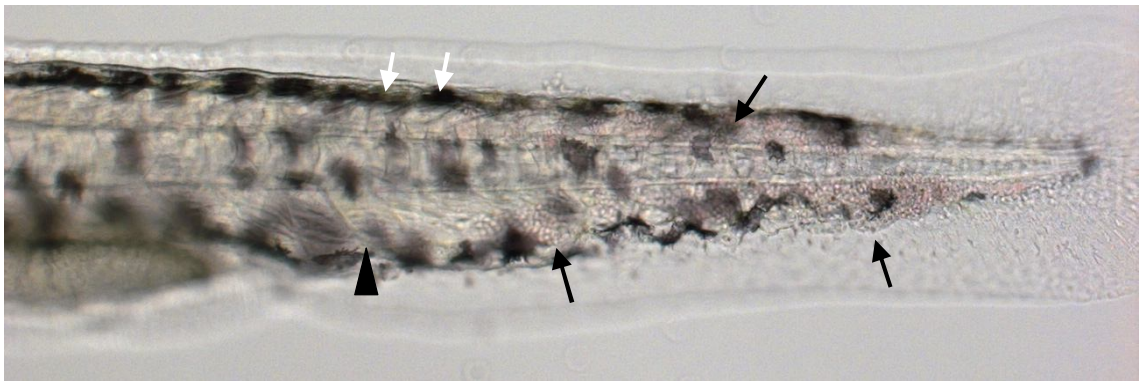

Figure 43 Tail of a *ppp4ca* morpholino injected embryo 3 dpf
Severe affected embryo, anterior left, erythrocytes accumulating in the tail (black arrow), also the muscle fibers appear thicker (black arrow head) and edema are visible within the muscle (white arrow).

two day old *ppp4ca* knockdown embryos the blood flow is interrupted at the posterior cardinal vein and the erythrocytes accumulate in the distal end of the tail (83.7 % n = 98; 2 independent experiments). At 3 dpf most of the *ppp4ca* knockdown embryos reached the long pec stage and accomplished the formation of the posterior cardinal vein (Figure 44, page 71). Nevertheless, the loop from the caudal artery to the caudal vein does not outreach the posterior end of the tail in which erythrocytes are still visible. A severely affected embryo with a strong accumulation of erythrocytes in the last third of the tail is depicted in Figure 43.

To test if the cardiovascular system of the *ppp4ca* knockdown embryos was affected by malformations of the blood vessels, a microangiography was performed. This method comprises the injection of a fluorescent dye into the ventricle to visualize the cardiovascular system. The outcome of the microangiography was that the dorsal aorta, the posterior cardinal vein and the intersegmental vessels developed normally. However, as expected the embryos showed no separation of the caudal artery and vein (Figure 45).

At 3 dpf, the control embryos developed normal and reached protruding mouth stage. In contrast, the *ppp4ca* knockdown embryos only developed until long pec to pec fin stage, where they arrested until they were euthanized at 5 dpf. In addition, the knockdown embryos developed phenotypically abnormal. For example, the muscle fibers got untransparent until the notochord was no longer visible. Furthermore, the interstitium between yolk and body, eye and body and the pericardium started to swell. The heart within the pericardium was stretched out, the pace was slow and continuously, but with no sign of any erythrocyte transport (Figure 44). In addition, the embryos did not respond to physical stimuli and start to lose their structural integrity.

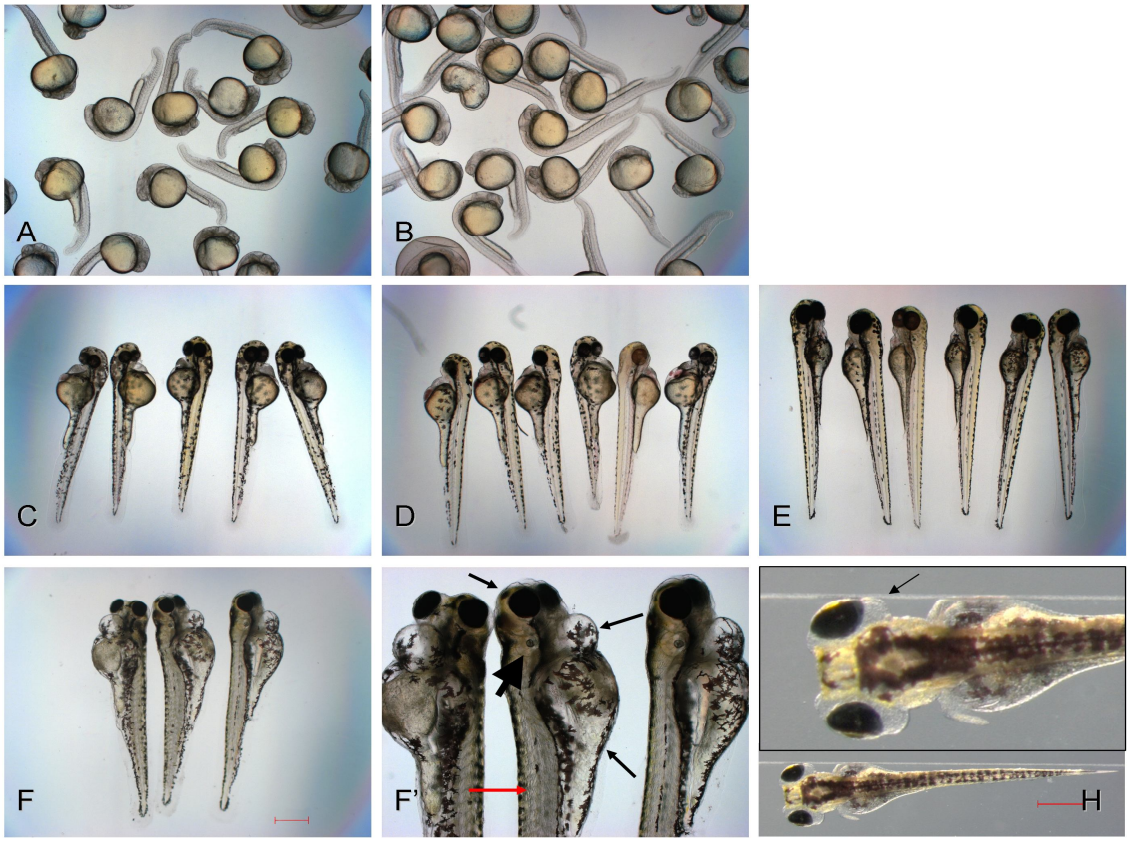

Figure 44 Different stages of *ppp4ca* morpholino injected embryos
A, C, F, F', H) *ppp4ca* knockdown embryos at different time points. B, D, E) control morpholino injected embryos. Embryos 24 hpf A) *ppp4ca* knockdown shows no difference to B) control embryos. C) *ppp4ca* knockdown embryo 3 dpf, development stage corresponding to control embryos at 2 dpf (D). E) control embryos 3 dpf at expected development stage (protruding mouth). F, H) *ppp4ca* knockdown embryos 5 dpf, developmental stage is between long pec and pec fin and equals 3 dpf. F') detailed view of F. Black arrows indicate swollen parts, interstitium between the yolk and body, eye and body and the pericardium; black arrowhead otolith; red arrow dense muscle. H) dorsal view on embryo 5 dpf anterior left. A - F) same magnification, scale bar 250 µm

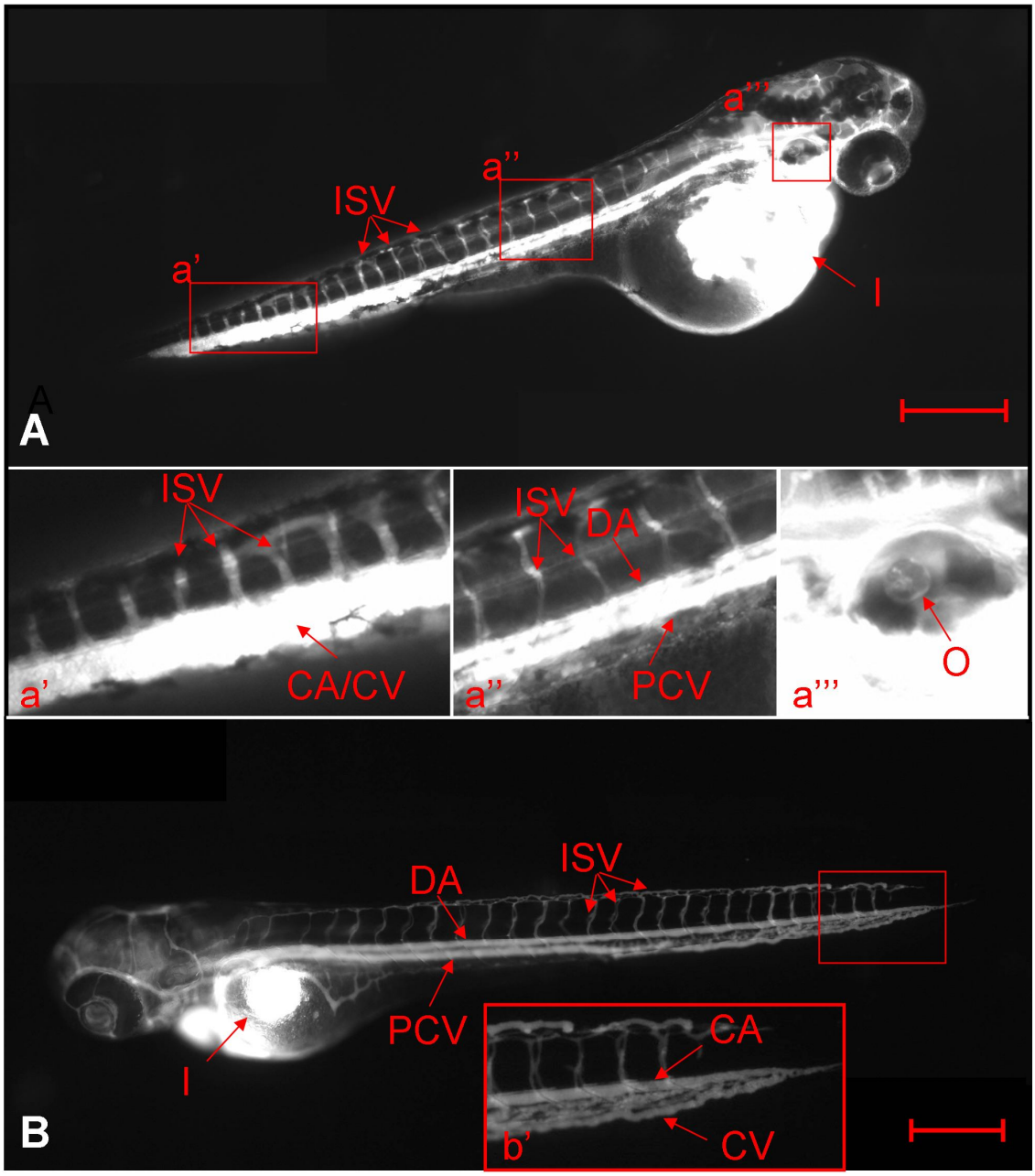

Figure 45 Microangiography of a *ppp4ca* knockdown embryoat 3 dpf
A) *ppp4ca* morpholino knockdown embryo, separation between caudal artery (CA) and caudal vein (CV) is not established. Dorsal aorta (DA), posterior cardinal vein (PCV) and intersegmental vessels (ISV) developed normally. In the *ppp4ca* knockdown embryo only one otolith (O) is present. B) Microangiography of an uninjected embryo 3 dpf. Injection site of the microangiography (I). Scale bar 250 µm

Interestingly, both morpholino types share the described phenotypical changes with one exception. The morpholino against the 5'UTR also induced the loss of at least one otolith per ear (88.2 %, embryos examined n = 145) (Figure 46). The loss is not completely penetrant, so that in some embryos the otolith loss was only present in one ear.

To identify changes in the brain size, the embryos were also measured for their head size and body length (Table 21, Table 22). Nevertheless, due to the large developmental delay, a direct comparison of the *ppp4ca* knockdown embryos with the SCMO injected embryos was not possible (Table 24, Figure 47, Figure 48). Therefore, the head size was plotted over the body length to compare the growth rate (Figure 49) (regression line for *ppp4ca* knockdown: y = 0.1763x - 63.25; SCMO: y = 0.1873x - 103.63). To confirm the similarity of the growth rates, a Student's t-test was performed on the slope of the regression lines. The calculated $\hat{t} = 1.27$ was lower than $1.99_{p=0.05}$, therefore it can be assumed, that there is no difference in the growth rate. This was also confirmed for the distribution of the growth rate, which showed no difference between the *ppp4ca* knockdown and the SCMO injected embryos ($\hat{z} = 0.2483$). Consequently, the knockdown of *ppp4ca* did not affect the brain size of the embryo.

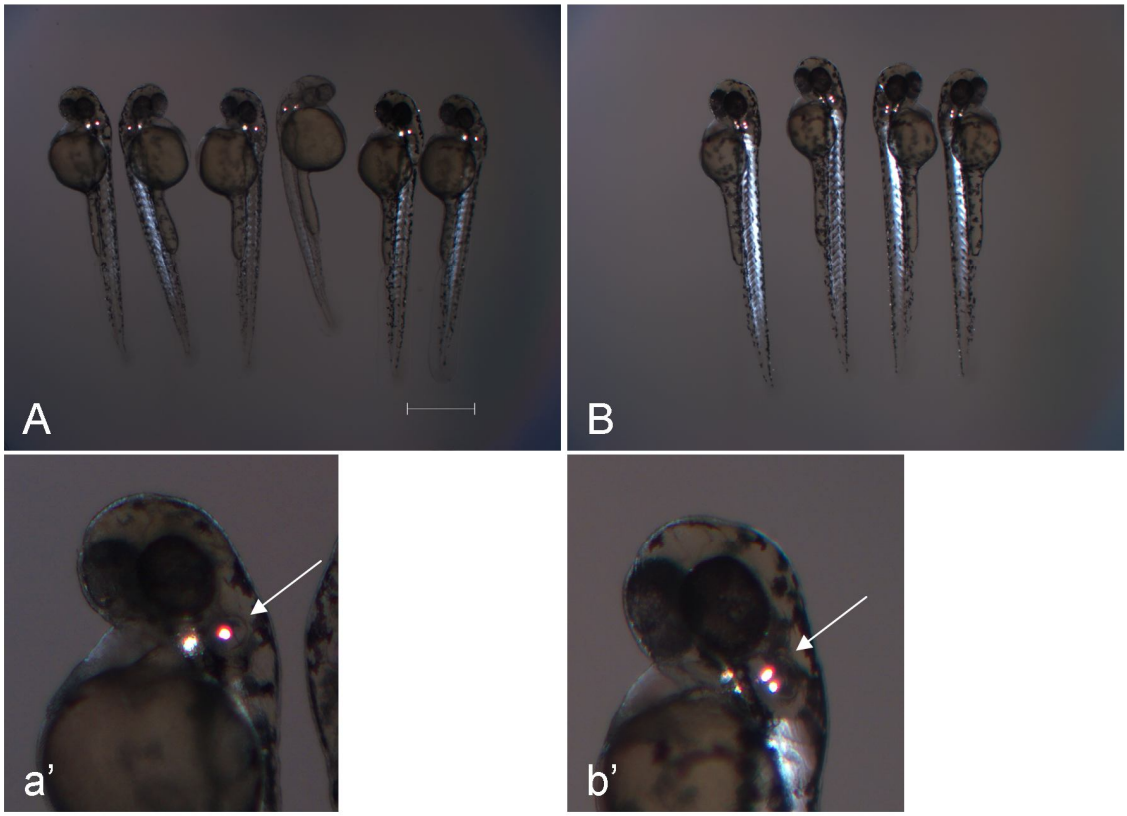

Figure 46 Otolith reduction in *ppp4ca* knockdown embryos
Knockdown embryos 2 dpf injected with morpholino against A) *ppp4ca* (5'UTR) and B) SCMO. Pictures taken in DIC mode, anterior - posterior axes in horizontal orientation. A' and B' are details, embryo orientate posterior up, ventral left, arrow indicates otolith in a') *ppp4ca* injected embryos present one otolith per ear, b') SCMO injected embryos two otolith per ear like the uninjected embryos (not shown). Scale bar 250 µm

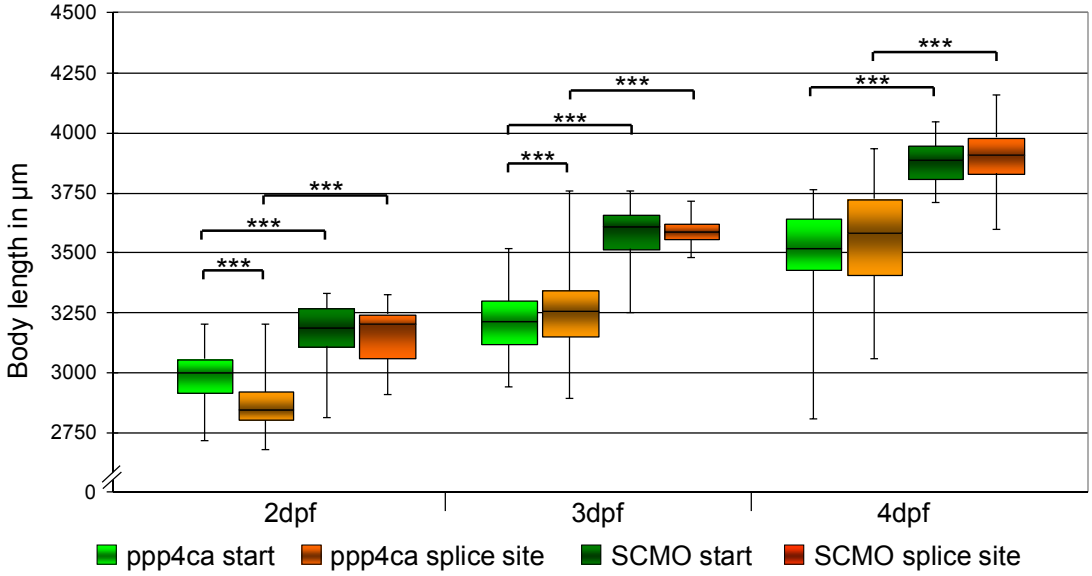

Figure 47 Body length comparison of *ppp4ca* 5'UTR and splice site morpholino injected embryos
Both *ppp4ca* knockdowns (5'UTR/ splice site) showed a significant reduction of the head size. The comparison of the head size between the *ppp4ca* 5'UTR and splice site morpholino injected embryos showed no difference. The number of embryos used per experiment and *p*-values can be found in Table 23, *** p-value $< 0.01 \times 10^{-5}$

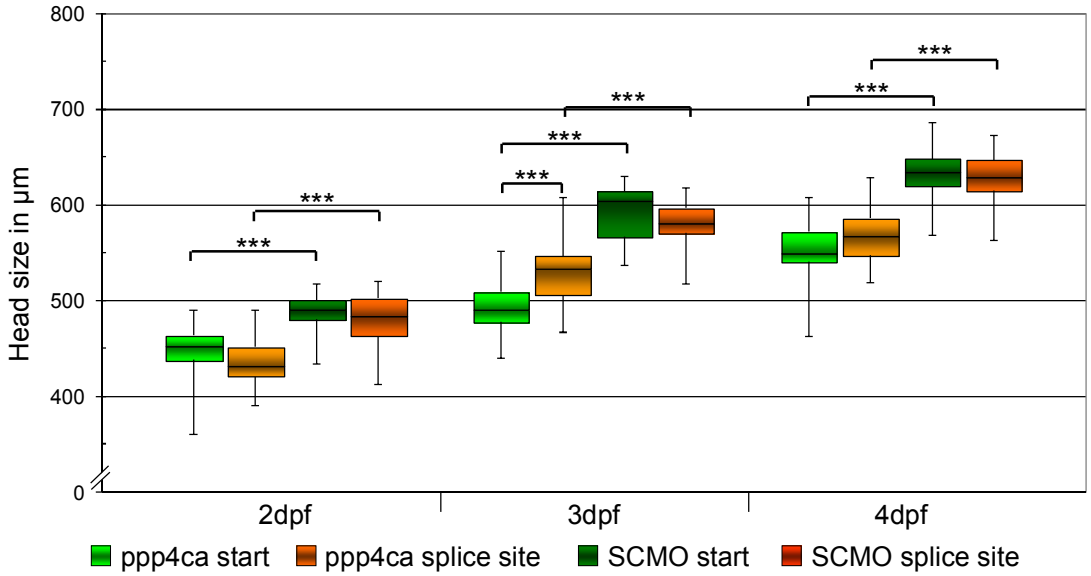

Figure 48 Head size comparison of *ppp4ca* 5'UTR and splice site morpholino injected embryos
Both *ppp4ca* knockdowns (5'UTR/ splice site) showed a significant reduction of the head size. The comparison of the head size between the *ppp4ca* 5'UTR and splice site morpholino injected embryos showed no difference. The number of embryos used per experiment and *p*-values can be found in Table 23, *** p-value $< 0.01 \times 10^{-5}$

Table 21 Body length of *ppp4ca* knockdown embryos and SCMO injected embryos
Given is the mean of the body length and standard deviation for embryos injected with the morpholino against the 5'UTR and the splice site of *ppp4ca* and the corresponding SCMO. The last column presents the number of measured embryos (*ppp4ca* 5'UTR / SCMO / *ppp4ca* splice site / SCMO).

dpf	Body length mean ± standard deviation				Number of embryos
	ppp4ca 5'UTR	SCMO	*ppp4ca* splice site	SCMO	
2	2892.20 ± 109.12	3090.94 ± 115.56	2820.49 ± 101.08	3015.43 ± 126,93	69/ 24/ 47/ 23
3	3123.23 ± 135.72	3485.91 ± 121.95	3153.30 ± 168.67	3561.69 ± 58.20	53/ 33/ 84/ 27
4	3401.05 ± 199.73	3798.54 ± 92.14	3383.61 ± 201.62	3825.00 ± 28,28	58/ 40/ 55/ 46

Table 22 Head size of *ppp4ca* knockdown embryos and SCMO injected embryos
Given is the mean of the head size and standard deviation for embryos injected with the morpholino against the 5'UTR and the splice site of *ppp4ca* and the corresponding SCMO. The last column presents the number of measured embryos (*ppp4ca* 5'UTR / SCMO / *ppp4ca* splice site / SCMO).

dpf	Head size mean ± standard deviation				Number of embryos
	ppp4ca 5'UTR	SCMO	*ppp4ca* splice site	SCMO	
2	433.15 ± 24.68	476.51 ± 20.63	424.21 ± 23.98	463.60 ± 26.75	69/ 24/ 47/ 23
3	479.50 ± 24.14	555.64 ± 26.90	498.49 ± 30.29	571.17 ± 21.43	53/ 33/ 84/ 27
4	544.22 ± 29.82	617.28 ± 25.37	548.67 ± 26.31	612.99 ± 28.28	58/ 40/ 55/ 46

Table 23 *p*-value comparison for *ppp4ca* and SCMO injected embryos
p-values for head size and body length comparison were calculated with Student's t-test

	2 dpf		3 dpf		4 dpf	
	head size	body length	head size	body length	head size	body length
ppp4ca 5'UTR; SCMO	5.70×10^{-11}	7.75×10^{-9}	7.84×10^{-20}	1.88×10^{-20}	1.37×10^{-22}	1.90×10^{-22}
ppp4ca splice site ; SCMO	5.11×10^{-7}	1.81×10^{-7}	1.68×10^{-20}	3.35×10^{-36}	4.40×10^{-20}	1.01×10^{-23}
ppp4ca 5'UTR; splice site	0.054	4.40×10^{-4}	8.63×10^{-5}	0.253	0.402	0.645
SCMO 5'UTR; splice site	0.072	0.039	0.016	0.003	0.461	0.238

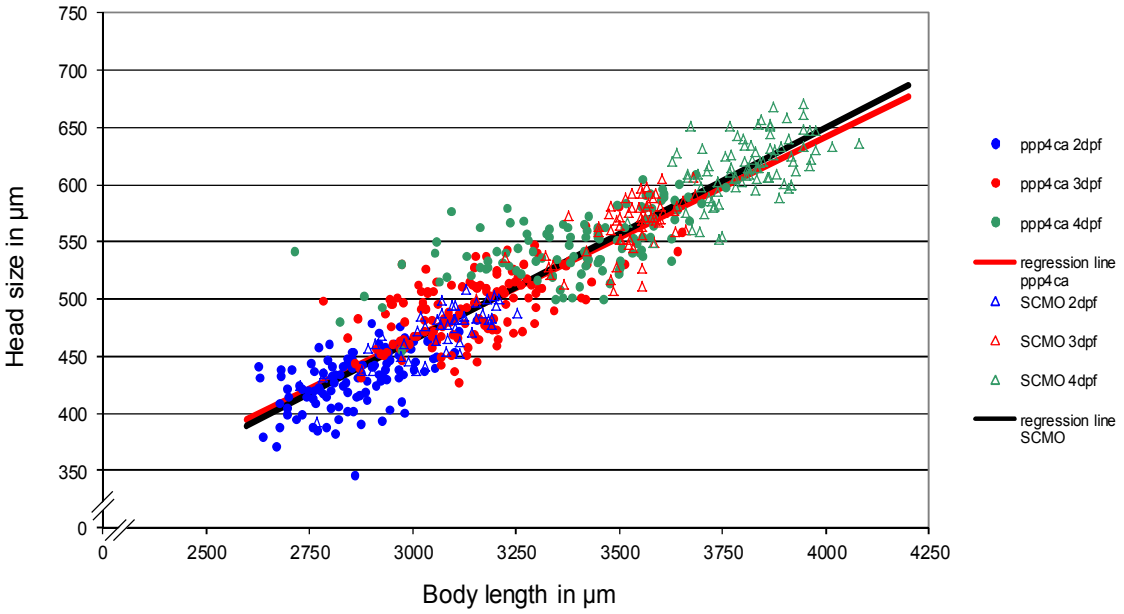

Figure 49 Head size to body length plot of *ppp4ca* knockdown embryos
Embryos are from two independent morpholino injection experiments (0.8 mM). Regression line *ppp4ca* knockdown: $y = 0.1763x - 63.25$, $r^2 = 0.742$; regression line controls: $y = 0.1873x - 103.63$, $r^2 = 0.870$

4.3.7 *ppp4cb* knockdown embryos present large edema

During the first day of development, approximately 50 % of the embryos injected with the morpholino against the 5'UTR of *ppp4cb* showed a developmental delay of up to 10 hours, whereas the rest of the embryos developed normally (Figure 51). During the next two days of development, the embryos showed a high mortality with a surviving rate of only 38 % at 3 dpf (165 embryos at 1 dpf, two independent experiments). In comparison, 88 % of the SCMO injected embryos survived during the same phase (137 embryos at 1 dpf, two independent experiments). In addition to the mortality, the *ppp4cb* 5'UTR morpholino knockdown embryos also showed a reduced body length and a swollen pericardium. The embryos, presenting these malformations, died during the next days. The remaining embryos developed normally until 5 dpf, where the pericardium, the eyes, and the interstitium between yolk and body started to swell. The heart inside the pericardium was long-drawn-out and slowly beating without transporting erythrocytes. The somitic muscle of the embryos, which are normally transparent, were untransparent and the muscle fibers appeared to be thicker than normal. Both of these abnormalities were comparable to the *ppp4ca* knockdown embryos. However, the loss of the otoliths was not recapitulated in the *ppp4cb* knockdown (Figure 51, Figure 52).

In contrast to the 5'UTR morpholino the splice site morpholino knockdown embryos showed, besides a short developmental delay at 1 dpf, no phenotypical changes. To test the functionality of the splice site morpholino, the skipping of exon 3 was analyzed by PCR. Surprisingly, the PCR for the knockdown and the control embryos only showed a band at 307 bp, which is the expected size with the included exon 3. Therefore, it can be assumed that the morpholino did not prevent the splicing. Consequently, only the *ppp4cb* 5'UTR morpholino injected embryos were used for measuring the head size and body length.

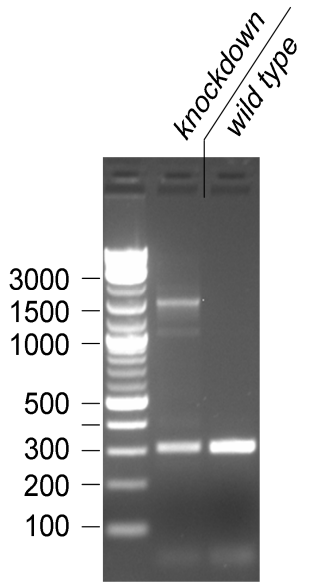

Figure 50 *ppp4cb* knockdown failed to induce exon skipping
Template for the PCR was cDNA from *ppp4cb* splice site morpholino knockdown and wild type embryo. The expected size of the unaffected mRNA was 307 bp. The *ppp4cb* morpholino binding to the e3i3 splice site should have induced the skipping of exon 3, leading to a lower band at 255 bp, but these band was not visible. The band at approximately 1500 bp represents the unspliced mRNA (1495 bp). Marker: 2lod DNA ladder (NEB).

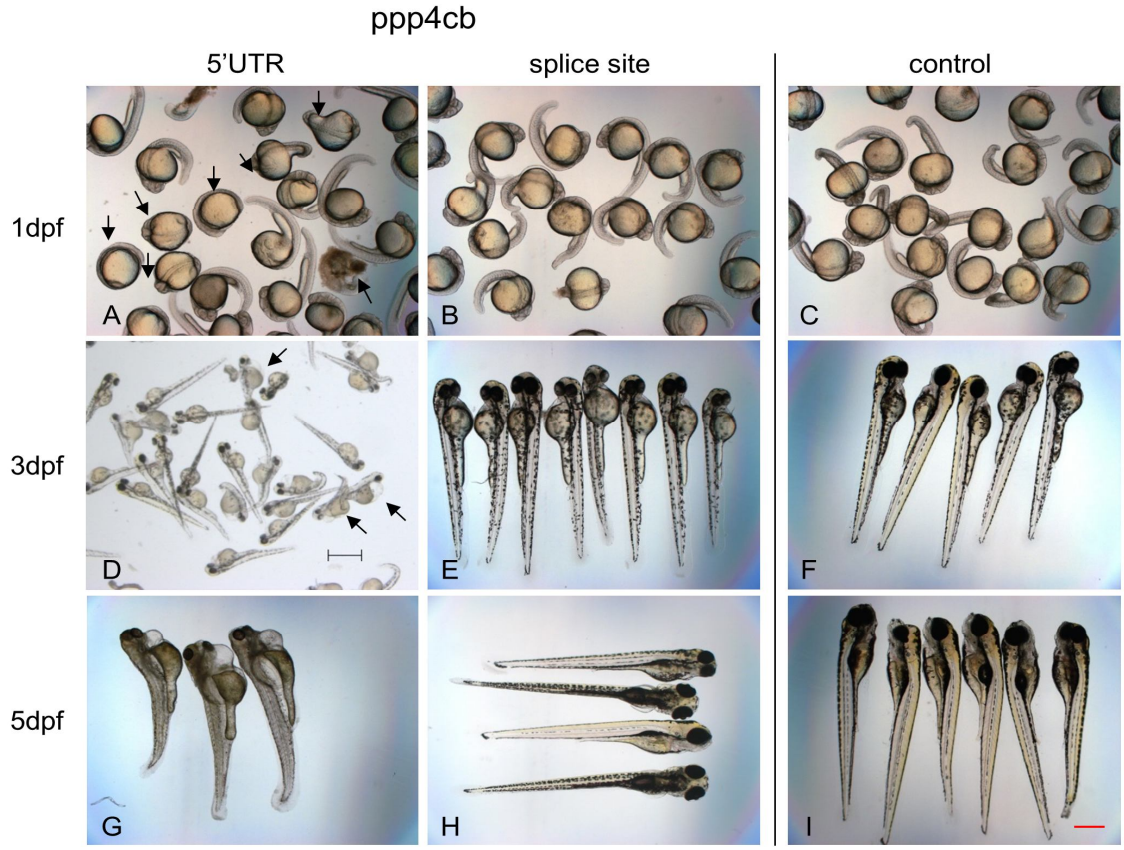

Figure 51 *ppp4cb* knockdown embryos display swelling
A-D) embryos without orientation, D-I) anterior up E) anterior left orientation. A) some *ppp4cb* knockdown embryos (5'UTR; 1 dpf) present a developmental delay of up to 10 h (arrows). D) At 3 dpf some *ppp4cb* knockdown embryos (5'UTR) were smaller and present a curved tail and swelling of the pericard (arrows). E) splice site morpholino injected embryos at 3 dpf showed a developmental delay of approximately 10 h (pec fin stage) compared to the control (F, mostly protruding mouth stage). G) At 5 dpf the embryos injected with the morpholino against the 5'UTR present a swollen pericardium, interstitium between yolk and body, and eye (detail in Figure 52). H) splice blocking morpholino injected embryos at 5 dpf, showed no difference to the controls (I). Magnification 25x, scale bar red 250 µm, D) scale bar black 1000 µm

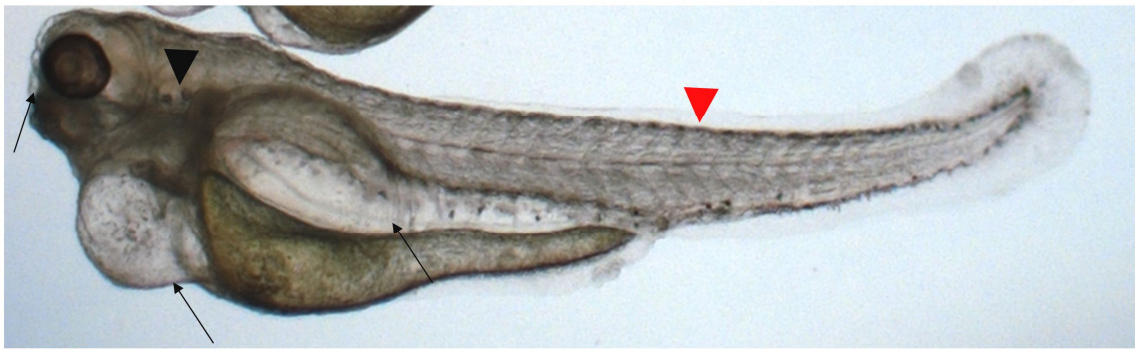

Figure 52 *ppp4cb* knockdown embryo at 5 dpf
Embryo orientated anterior left, swollen parts of the embryos like eye, pericardium and interstitium are indicated with arrows. Otic vesicles harbored two otoliths similar to the control (black arrowhead). The fibers of the somitic muscle appeared thicker than normal; note that the notochord is not visible through the muscle, which also represent edema (red arrowhead). (Detail of Figure 51 D)

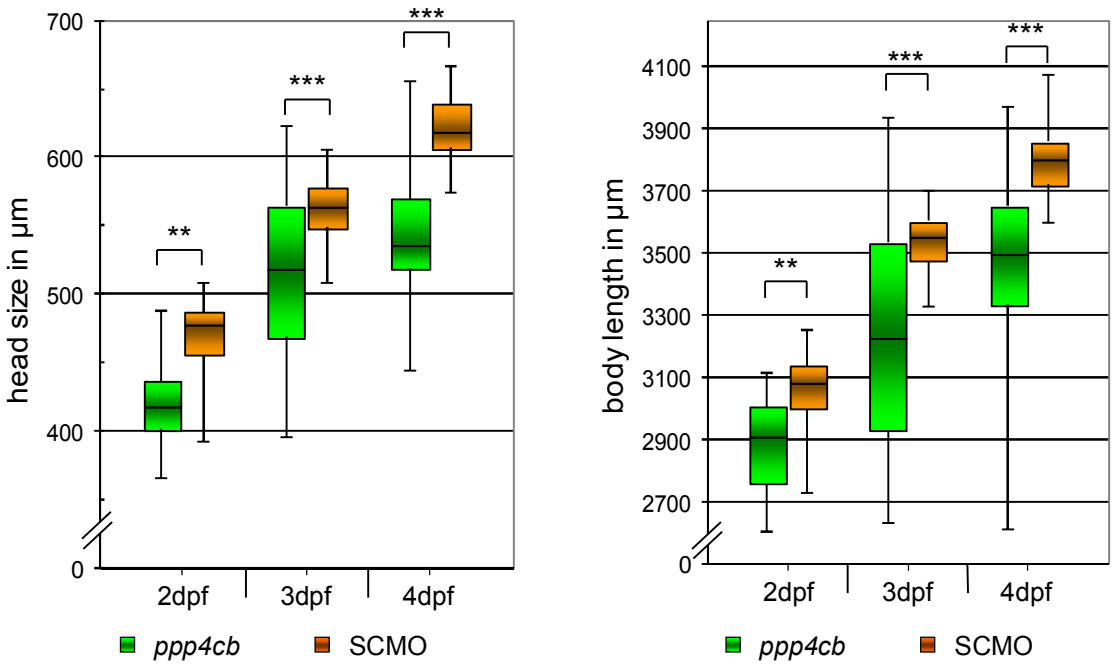

Figure 53 Head size and body length of *ppp4cb* knockdown embryos
Comparison of the head size (left) and body length (right) between *ppp4cb* morpholino knockdown and SCMO embryos. The number of embryos used per experiment and *p*-values can be found in Table 24 and Table 25. Embryos originated from two independent morpholino injections (0,8 mM). In all measurements the *ppp4cb* knockdown embryos were smaller in head size and body length than the corresponding control. ** *p*-value < 0.05, *** *p*-value < 0.01×10^{-5}

Table 24 Body length of *ppp4cb* and SCMO injected embryos at different time points
The number of measured embryos originates from two independent experiments. To test if the body length of the *ppp4cb* knockdown embryos differed significantly from the SCMO injected embryos a student's t-test was performed. The *p*-values of the t-test were corrected for multiple testing using the Bonferroni method (n = 3).

dpf	**Body length** mean ± standard deviation		Number of measured embryos *ppp4cb* /SCMO	*p*-value (two-tailed students t-test)	Corrected *p*-value (Bonferroni $p_{ad} = n \times p$)
	ppp4cb	SCMO			
2	2873.27 ± 164.84	3054.00 ± 125.85	18/47	6.28×10^{-4}	1.88×10^{-3}
3	3249.91 ± 358.72	3539.41 ± 87.35	55/32	1.45×10^{-8}	4.34×10^{-8}
4	3466.91 ± 314.24	3803.78 ± 104.94	44/47	2.57×10^{-7}	7.70×10^{-7}

Because of axis deformations, not all 5'UTR morpholino knockdown embryos could be used for the head size and the body length measurement. Hence, only normal appearing *ppp4cb* knockdown (5'UTR) and SCMO injected embryos are measured. The analysis of the measurement showed that the average body length and head size of the *ppp4cb* knockdown embryos was significantly smaller and the variance was much higher than in the SCMO injected embryos (Figure 53, Table 24, Table 25). To assess whether the ratio between head size and body length was changed in the *ppp4cb* knockdown

embryos, the head size was plotted against the body length (Figure 54). The resulting plot showed, that the distribution of the growth ratio was equally ($\hat{z} = 0.23$). In contrast to the distribution, the slope of the growth ratio showed a significant ($\hat{t} = 5.62$) difference. The slope of the *ppp4cb* regression line showed, that some of the embryos had shorter bodies and bigger heads at 3 dpf, whereas at 4 dpf some embryos presented smaller heads compared to the controls.

Because of the swelling phenotype, which was similar to the *ppp4ca* knockdown embryos at 5 dpf, a microangiography was performed to identify changes in the vascular system. Interestingly, the microangiography on *ppp4cb* knockdown embryos showed no changes in the vascular system (Figure 55, page 81).

Table 25 Head size of *ppp4cb* and SCMO injected embryos at different time points
The number of measured embryos originates from two independent experiments. To test if the head size of the *ppp4cb* knockdown embryos differed significantly from the SCMO injected embryos a two-tailed student's t-test was performed. The *p*-value of the t-test was corrected for multiple testing using the Bonferroni method (n = 3).

dpf	**Head size** mean ± standard deviation		Number of measured embryos *ppp4cb* /SCMO	*p*-value (two-tailed student's t-test)	Corrected *p*-value (Bonferroni $p_{ad} = n \times p$)
	ppp4cb	SCMO			
2	419.23 ± 30.64	470.19 ± 24.45	18/47	6.23×10^{-4}	1.88×10^{-3}
3	514.69 ± 55.41	562.98 ± 20.22	55/32	6.16×10^{-18}	1.85×10^{-8}
4	536.89 ± 40.05	620.62 ± 23.49	44/47	7.44×10^{-8}	2.23×10^{-7}

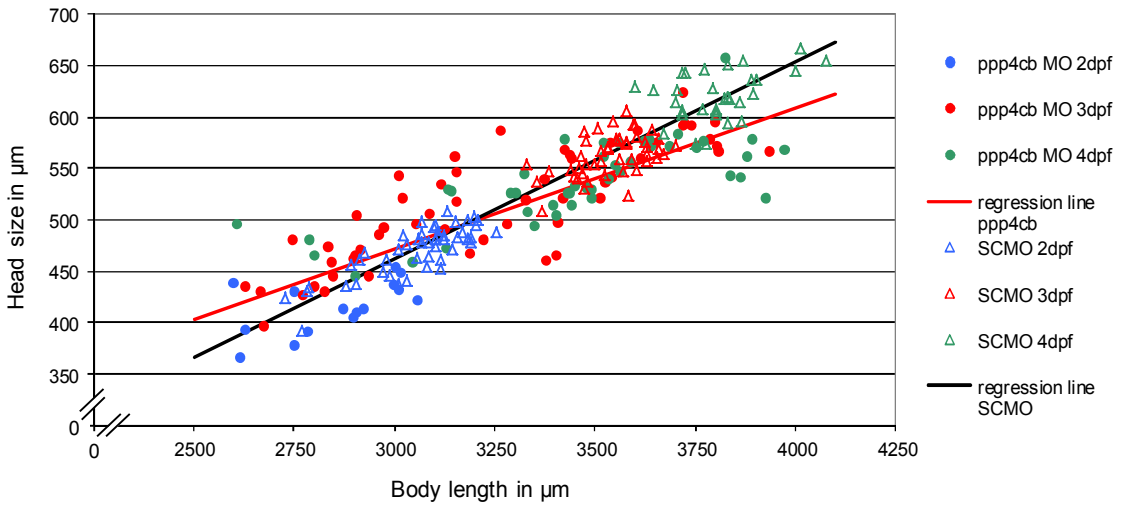

Figure 54 *ppp4cb* knockdown embryos, changing from small body with big heads to small heads
Embryo measurements are from two independent morpholino injections. *ppp4cb* knockdown embryos at 2 dpf are smaller than the control but fit the regression of the control embryos. At 3 dpf the embryos present a reduced body length and bigger head size compared to corresponding controls. At the fourth day this changes, the embryos still had a shorter body length, but the head size is smaller than in the controls. The result of this is a reduction in the slope of the *ppp4cb* knockdown regression line compared to the control. Regression line *ppp4cb* knockdown: $y = 0.1362\,x + 63.07$, $r^2 = 0.710$; regression line controls: $y = 0.19159x - 112.79$, $r^2 = 0916$

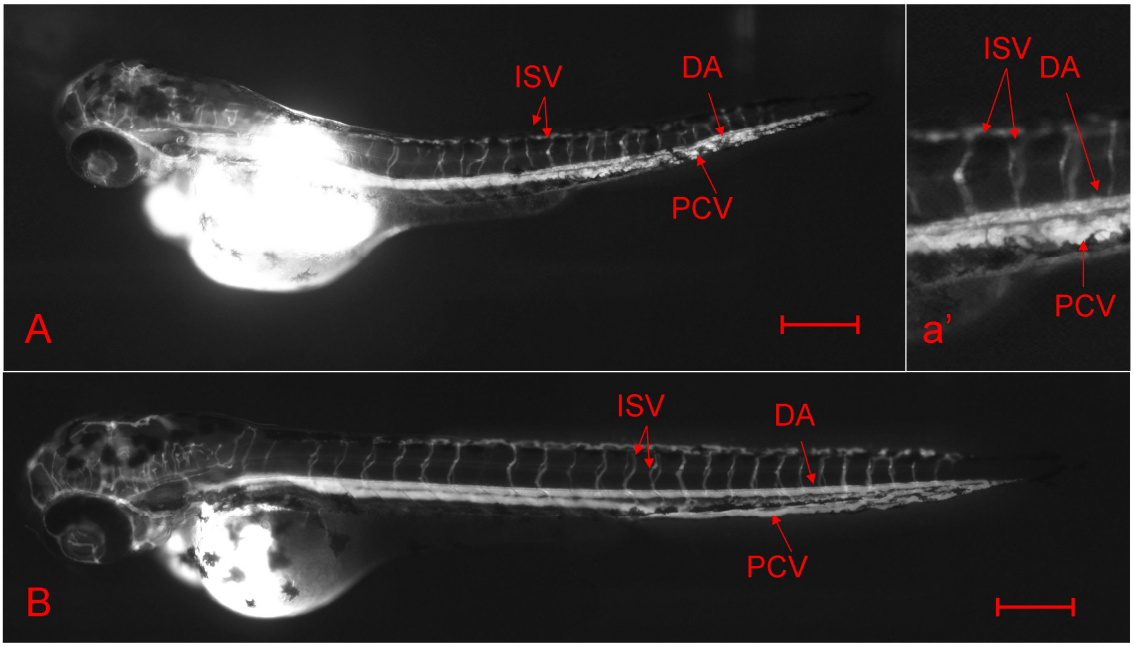

Figure 55 *ppp4cb* knockdown has no effect on blood vessel formation
Embryos 3 dpf, anterior left A) *ppp4cb* knockdown, B) control. Both present normally developed dorsal aorta (DA), posterior cardinal vein (PCV) and intersegmental vessels (ISV). Scale bar 200 µm

4.3.8 Knockdown of *sez6l2* reduces head size

The *sez6l2* knockdown embryos developed phenotypically normal. At 2 dpf, the *sez6l2* and the SCMO knockdown embryos reached the long pec stage. However, a small developmental delay of the *sez6l2* knockdown embryos was recognizable in eye size and pigmentation. At 3 dpf, the development of the *sez6l2* knockdown embryos reached the pec fin stage, whereas the controls already entered the protruding mouth stage. Compared to the control, which already developed to the protruding mouth stage, this is consistent with the developmental delay at 2 dpf. Because of no distinctive developmental marks at 4 dpf, the difference between the *sez6l2* knockdown and control embryos is not stageable. Nevertheless, it is still visible in a small difference of the yolk sac size (Figure 56).

To identify differences in the brain size of the *sez6l2* knockdown embryos, the head size and body length were measured as described in the methods section. The day-wise

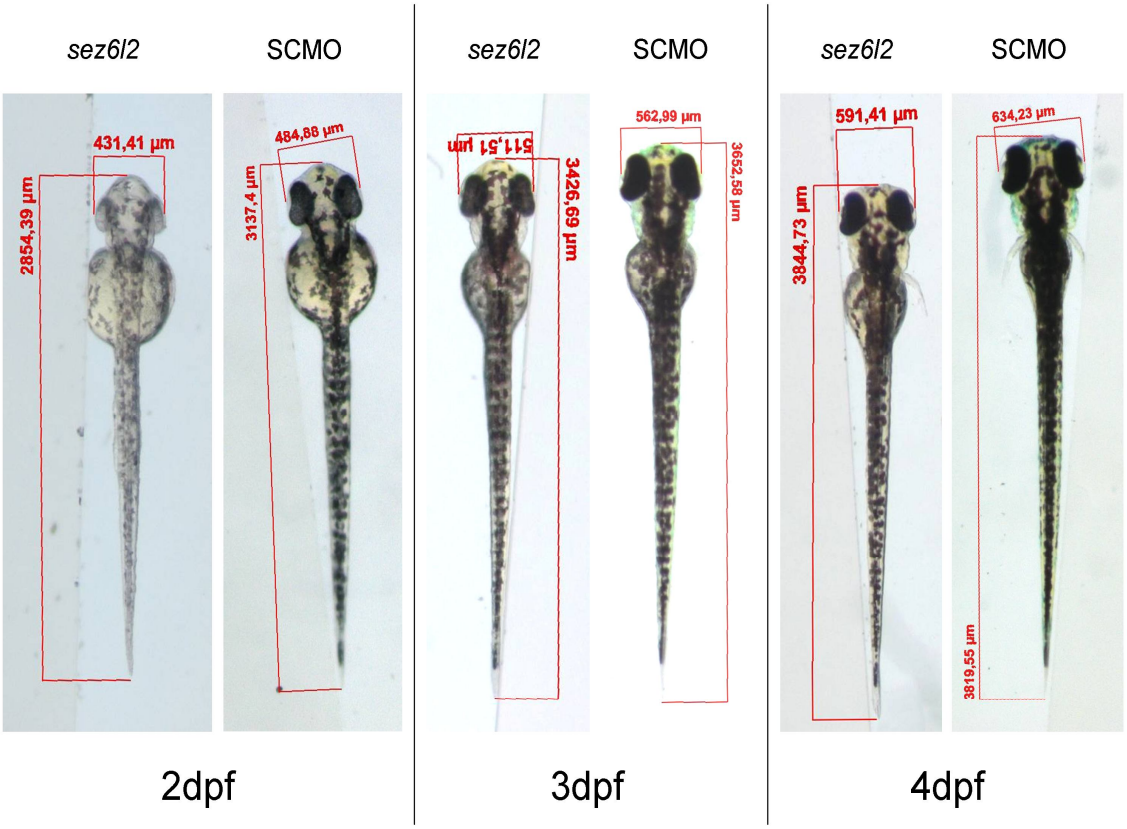

Figure 56 Comparison of *sez6l2* and SCMO knockdown embryos at 2 dpf, 3 dpf, and 4 dpf
The body length and head size for each embryo is shown next to it. Developmental stages of the embryos – 2 dpf *sez6l2* and SCMO long pec (note that the SCMO is further developed, compare eye size and pigmentation); – 3 dpf *sez6l2* pec fin close to protruding mouth, SCMO protruding mouth; – 4 dpf larva (the yolk sac of the *sez6l2* is bigger than in the SCMO knockdown illustrating the developmental delay)

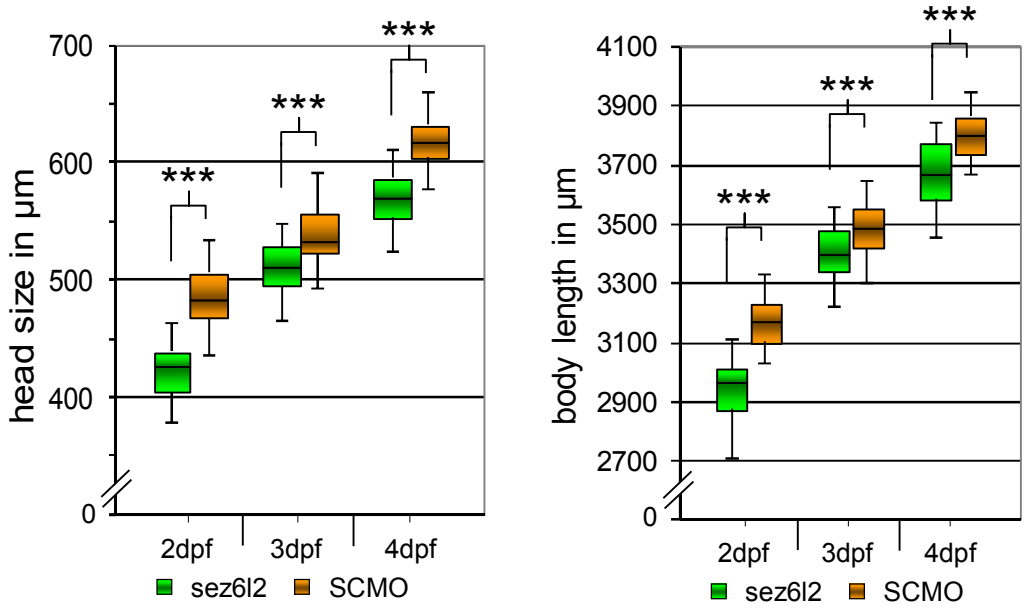

Figure 57 Head size and body length comparison of *sez6l2*
Comparison of head size (left) and body length (right) between *sez6l2* morpholino knockdown and SCMO embryos. The number of embryos used per experiment and *p*-values can be found in Table 26and Table 27. *** *p*-value < $1 \cdot \times 10^{-5}$

Table 26 Head size of *sez6l2* and SCMO injected embryos at different time points
The number of measured embryos originates from two independent experiments. To test if the head size of the *sez6l2* knockdown embryos differs significantly from the SCMO injected embryos a two-tailed student's t-test was performed. The *p*-value of the t-test was corrected for multiple testing using the Bonferroni method (n = 3).

dpf	**Head size** mean ± standard deviation		Number of measured embryos *sez6l2* /SCMO	*p*-value (two-tailed student's t-test)	Corrected *p*-value (Bonferroni $p_{ad} = n \times p$)
	sez6l2	SCMO			
2	422.66 ± 25.25	485.41 ± 28.52	122/58	5.36×10^{-26}	1.61×10^{-25}
3	509.82 ± 26.35	536.88 ± 22.88	108/72	1.05×10^{-11}	3.16×10^{-11}
4	568.98 ± 24.83	618.26 ± 25.26	102/54	4.33×10^{-21}	1.29×10^{-20}

comparison of the head size and body length (Figure 57) showed a significant reduction in both features of the *sez6l2* knockdown embryos (Table 26, Table 27). Nevertheless, the size reduction is supposed to occur from the short developmental delay of the embryos. To test this hypothesis, the head size was plotted against body length. Afterwards, the equations of the regression lines were calculated and plotted (Figure 58). The comparison of the two regression lines showed a significant reduction in the slope of *sez6l2* morpholino knockdown embryos ($\hat{t} \approx 1.27$). This shows that the head size, and therefore probably the brain size, is reduced in the *sez6l2* knockdown embryos.

Table 27 Body length of *sez6l2* and SCMO injected embryos at different time points
The number of measured embryos originates from two independent experiments. To test if the body length of the *sez6l2* knockdown embryos differs significantly from the SCMO injected embryos a two-tailed student's t-test was performed. The *p*-value of the t-test was corrected for multiple testing using the Bonferroni method (n = 3).

dpf	**Body length** mean ± standard deviation		Number of measured embryos *sez6l2* /SCMO	*p*-value (two-tailed students t-test)	Corrected *p*-value (Bonferroni $p_{ad} = n \times p$)
	sez6l2	SCMO			
2	2941.63 ± 117.37	3169.74 ± 92.19	122/58	8.71×10^{-29}	2.61×10^{-28}
3	3398.29 ± 104.75	3479.52 ± 96.18	108/72	2.91×10^{-07}	8.73×10^{-07}
4	3668.70 ± 126.00	3803.95 ± 89.56	102/54	2.25×10^{-13}	6.73×10^{-13}

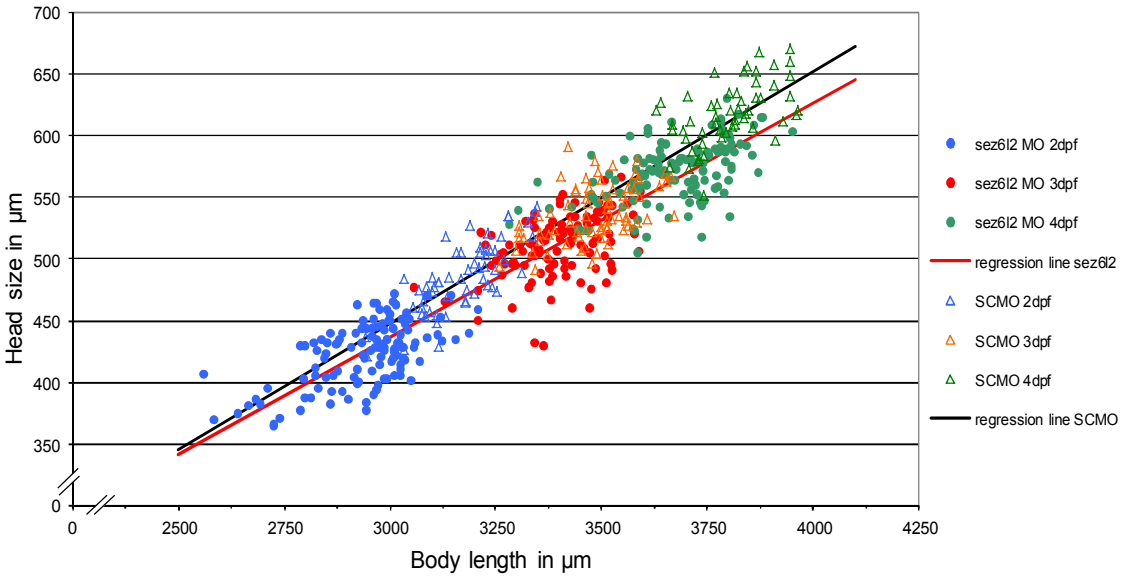

Figure 58 Growth rate comparison of *sez6l2* knockdown and SCMO injected embryos
Regression lines represent the growth rate from second to fourth day after fertilization. The reduced slope of the *sez6l2* morpholino knockdown regression line displays the reduction in head / body ratio. Regression line SCMO (blue): $y = 0.2041x - 165.09$, $r^2 = 0.864$; regression line *sez6l2*: $y = 0.1899x - 133.03$, $r^2 = 0.877$

4.3.9 *ypel3* knockdown is lethal at 1 dpf

The injection of both, the 5'UTR and the splice blocking morpholino against *ypel3* resulted in the same severe morphologically phenotype. At 1 dpf, the embryos reached the 20 somites stage and presented a bended chorda. At this stage 75 % of the embryos did not develop further and died between the 1-2 dpf (378 embryos, 3 independent experiments, Table 28). The surviving embryos presented a ventral curved shortened tail, a smaller head and body size, and lack the development of erythrocytes. At 3 dpf, the embryos reached the long pec stage. The heart of the embryos was thin, long drawn-out and hardly beating (Figure 60). Arrested in the long pec stage, the embryos started to die within the next day. In contrast to the high mortality rate of the *ypel3* morpholino injected embryos, the non-injection and SCMO embryos developed normally and showed survival rates of 98 % and 99 %, respectively. To confirm, that the morphological effects were based on the morpholino injection, the *ypel3* mRNA of the splice site morpholino knockdown embryos was assessed by PCR. The PCR proved the loss of the 44 bp large exon 3 and did thereby confirm the effect of the splice site morpholino (Figure 59).

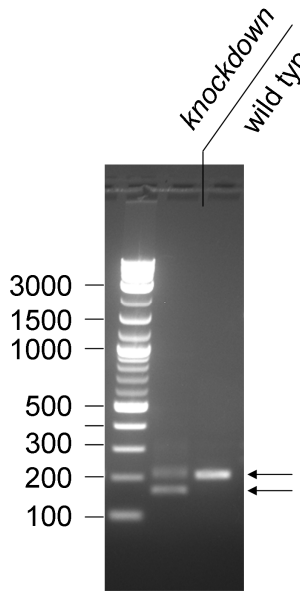

Figure 59 *ypel3* morpholino induces loss of exon 3
PCR on cDNA from wild type and *ypel3* splice site morpholino knockdown embryos. Primers are located in exon 2 and 4 (208 bp). Knockdown induces loss of exon 3. Therefore, the band is 44 bp shorter (164 bp)

Due to the high mortality rate, a lower morpholino concentration was tested (0.2 mM). Surprisingly, this concentration yielded in a complete loss of the phenotype. Therefore,

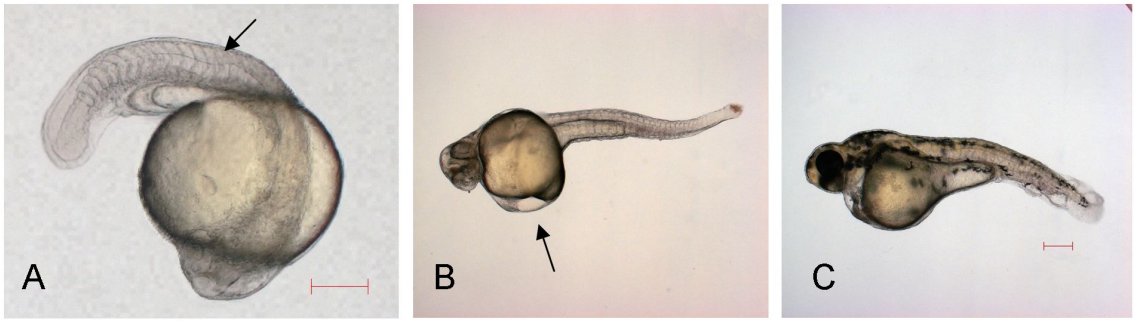

Figure 60 *ypel3* morpholino injected embryos after 1, 2 and 3 days of development
A) 1 dpf 20 somite stage, curved chorda marked by arrow B) 2 dpf high pec stage, curved tail and bloodless pericardium (arrow). C) 3 dpf, long pec stage, shorten tail and reduced body size. A) 100x magnification, B) and C) 50x magnification; scale bar 200 µm.

Table 28 Results of the *ypel3* morpholino injection

morpholino type	morpholino concentration in mM	Number of surviving embryos 1 dpf (SCMO / uninjected)	Number of surviving embryos 2 dpf (SCMO / uninjected)	of surviving embryos form 1 dpf to 2 dpf in%
5'UTR	0.8	95 (49/58)	31 (49/58)	32.63 (100/100)
Splice site e3i3	0.8	131 (77/92)	34 (77/90)	25.95 (100/98)
Splice site e3i3	0.4	132 (89/69)	39 (85/70)	29.61 96/101
Splice site e3i3	0.2	134 (53/61)	129 (52/60)	96.27 (98/98)

this concentration was not sufficient to block enough of the *ypel3* mRNA.

4.3.10 Summary of morpholino knockdown phenotypes

The morpholino knockdown embryos displayed various phenotypes which are summarized in Figure 61. The most important phenotype, which was found in nearly all knockdown embryos, was the developmental delay. Another interesting phenotype was the formation of edema in the pericardium, eye and interstitium which was found in

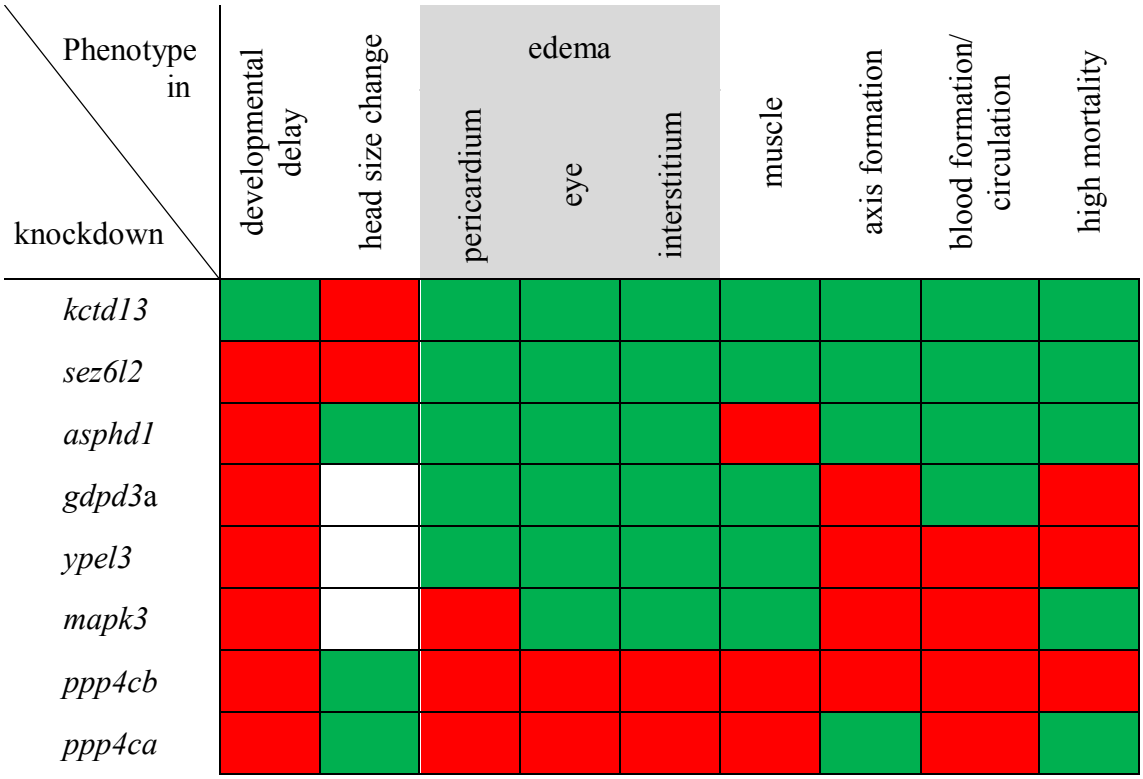

Figure 61 Phenotypes of the morpholino knockdown embryos
Red filling indicates difficulties in formation of tissues or differences to the corresponding control; green- developed like corresponding control; white- could not be defined.

mapk3, *ppp4ca* and *ppp4cb* knockdowns. As a muscle phenotype, deformations like thick muscle fibers or the appearance of small edemas inside the muscle were counted. A phenotype in blood formation / circulation was assessed when no blood was developed (*ypel3*), problems in the formation of the circulatory system (*ppp4ca*) occurred or the appearance of heart deformations. Notably, the swelling of the pericardium was always accompanied by the stretching of the heart, leading to a reduction or disruption of the blood flow. A knockdown was described as highly mortal, if the survival rate dropped below 40 % during the development or if all embryos died at a specific developmental stage.

5 Discussion

As result of this thesis, the four genes *KCTD13*, *SEZ6L2*, *MAPK3* and *PPP4C*, located in the human 16p11.2 region, have been identified to be potentially involved in ASD or accompanying symptoms. In addition, the crucial role of *ypel3* and *gdpd3a* during early zebrafish development, reflected by a high embryo mortality rate after their knockdown, makes them attractive for further analysis. More importantly, the results of this thesis approve the great potential of zebrafish as a model for neuronal diseases and specifically autism

5.1 KCTD13, a strong ASD candidate

At the beginning of this thesis, no *in situ* hybridization data was available for *kctd13*. Here it was shown that *kctd13* is expressed in the head of the embryos at 3 dpf. This phenotype was supported by Golzio, Willer *et al*. (2012). A so far undiscovered result was the strong expression of *kctd13* within the bulbus arteriosus, which was revealed by *in situ* hybridization on sections. Moreover, it was shown that the *kctd13* knockdown embryos displayed an enlargement of the heads. This was significantly confirmed by the direct comparison of the mean head size against the control embryos as well as in the plotted ratio of head size and body length. Interestingly, the head size enlargement phenotype was found to be initialized specifically at 4 dpf, which was supported by a publication by Golzio, Willer *et al.* (2012). They further showed, that the head size enlargement was accompanied by an increase in the cell mass of the brain. Another publication presenting a *kctd13* knockdown was published by Blaker-Lee, Gupta *et al.* (2012). This publication focused on the ventrical formation of the embryos (24 hpf) and showed that *kctd13* knockdown embryos have a reduced brain ventrical size and a less destinct midbrain-hindbrain boundary. Further, they discoverd a change in the axon trace formation.

Together the results of this thesis and other publications demonstrate that the *kctd13* knockdowns affect head size, ventricle and axon trace formation. Still it is unclear what the reasons are for this phenotypic expression. It is known that the *KCTD13* is interacting with the small subunit (p50) of the DNA polymerase delta (pol-δ) and the proliferating cell nuclear antigen protein (*PCNA*) (Waga and Stillman 1998, Kim,

Leventhal *et al*. 2011). The relation with the Pol δ and *PCNA* indicates a regulatory association in DNA replication and cell-cycle progression. This could be a possible reason for an increase of cells in the *kctd13* knockdowns, which would explain the head size enlargement. The question is if the change in the head size of the zebrafish can be associated with ASD. Strong indicators for this are the enlargement of the brain mass and the reduction of the ventricle, which leads to the prediction of a neurological function (Sawamoto, Wichterle *et al.* 2006, Gutzman and Sive 2010).

Further, the potential relation *KCTD13* with ASD is supported by another member of the *KCTD* family, which has a known connection to neuronal disorders. It has been shown that mutations in *KCTD7* are associated with the appearance of progressive myoclonic epilepsy (PME) a syndrome linked with myoclonic seizures, tonic-clonic seizures, and progressive neurological deterioration (Shahwan, Farrell *et al*. 2005, Van Bogaert, Azizieh *et al*. 2007, Azizieh, Orduz *et al*. 2011). Unfortunately, the mechanisms behind the PME are undiscovered. However, it is known that seizures are triggered by unpredictable interruptions of normal brain functions. All together, the effects of *kctd13* and *KCTD13* shown here and by others, as well as the connection of *KCTD7* with neuronal diseases, make this a strong candidate for an involvement in ASD. Nevertheless, further investigation is required to clarify the function of *kctd13*.

5.2 Head size reduction of sez6l2 knockdown embryos indicates association with ASD-like symptoms

Because of its expression in human and mouse fetal brain tissue, the *sez6l2* (*seizure related 6 homolog (mouse)-like 2*) was one of the strongest candidates within this study (Kumar, Marshall *et al.* 2009). Here it was shown, that *sez6l2* is expressed in the cell bodies of nerve cells located in brain, during zebrafish development. The similar spatial expression indicates an evolutionary conservation, which supports the comparability of the knockdown phenotype.

Interestingly, the *sez6l2* morpholino knockdown resulted in a head size reduction of the embryos. Since the diameter of an embryonic head is mainly based on the size of the brain, it can be expected that in *sez6l2* knockdown embryos the brain size is affected, which probably is comparable to the presence of microcephaly in ASD patients (Courchesne, Karns *et al*. 2001, Lainhart, Bigler *et al*. 2006). Unfortunately, the

publication by Konyukh, Delorme *et al*. (2011) does not contain specific information regarding individual symptoms of the patients, so that a relationship between head size and *SEZ6L2* cannot be confirmed in humans yet. Interestingly, the *SEZ6L2* gene shows a high frequency of potential damage causing sequence variations in the promoter and coding sequence, which are not only found in ASD patients, but also in healthy persons. A possible explanation for this could be the structure of the protein domains, which is repeated several times and therefore are possibly prone to the mutation. Another explanation is a multiple hit model, which is indicated by the non-mendelian inheritance of ASD. This model suggests that the co-occurrence of mutations in different genes could be the reason for the ASD formation. As a result of this model, *SEZ6L2* would only be one amongst many genes causing ASD formation.

Another point linking *SEZ6L2* with neuronal diseases is its strong homology to the *SRPX2* gene, which is associated with rolandic seizures - a syndrome causing oral and speech dyspraxia and mental retardation (Roll, Rudolf *et al.* 2006). Unfortunately, the molecular mechanisms of *SRPX2* are not known yet. However, the relation of *SRPX2* with a neuronal disorder and the discovered mutations of *SEZ6L2* in ASD patients support the relevance of *SEZ6L2* as a strong candidate for ASD.

5.3 The Ras/Raf/ERK1 pathway possibly links *MAPK3* with neuronal disorders

In this thesis it was demonstrated that *mapk3* is expressed in the brain and intestine of a three day old zebrafish embryo. This is comparable to the results of Krens, He *et al.* (2006), who also showed an expression of *mapk3* in the brain of zebrafish embryos at 2 dpf. Surprisingly, the morpholino knockdown phenotype described by Krens, He *et al.* (2008) is not completely congruent to the one presented here. Both knockdowns showed the same effect in axis formation. However, a complete loss of the tail could not be recapitulated in this thesis, even at a very high morpholino concentration of 1.6 mM. Additionally, the embryos presented defects during the formation of the notochord, heart and blood, which were also visible in the figures of the publication but had not been mentioned by Krens, He *et al.* Interestingly, the morpholino used by Krens, He *et al.* (2008) was positioned directly upstream of the 5'UTR morpholino used in this thesis, with an overlap of one base pair. Moreover, Krens, He *et al.* (2008) injected the same volume and used a lower concentration (0.4 mM). This indicates that the

difference in the complete loss of the tail is based on a difference in the binding affinity of the morpholino rather than in the used concentration. However, the main character of the knockdowns is equal to Krens, He *et al.* (2008). Additionally, Blaker-Lee, Gupta *et al.* (2012) also performed a *mapk3* knockdown and described the phenotype as "consistent" with Krens, He *et al.* (2008). However, the *mapk3* knockdown embryos presented by Blaker-Lee, Gupta *et al.* (2012) showed milder deformation than the one presented here. Furthermore, Blaker-Lee, Gupta *et al.* (2012) did not mention the swelling of the pericard or heart defects as described by Krens, He *et al.* (2008) and this thesis. Because of the 92 % sequence similarity of the Blaker-Lee, Gupta *et al.* (2012) morpholino with the one used in this thesis, it is unlikely that this difference is due to a lower binding affinity. Therefore, it must be concluded that the difference of the reported *mapk3* phenotypes are based on morpholino concentration or the injected amount. Taken together, the comparison of the knockdown phenotypes with Krens, He *et al.* (2008) and Blaker-Lee, Gupta *et al.* (2012) demonstrated the difficulty in interpreting the phenotypes and the comparison of the morpholino injection procedures. Nevertheless, the identical phenotype of the 5'UTR and the splice site morpholinos used in this thesis, which were injected in the same concentration and amount, proved the robustness of the system when performed at constant conditions.

The question remains if *MAPK3* is relevant for the manifestation of ASD. An indication for this, besides the effects on body axis and brain, is a deficiency in the axon tract development of the *mapk3* knockdown embryos (Blaker-Lee, Gupta *et al*. 2012). This direct effect on the neuronal system indicates a relevance for ASD. Additionally, *MAPK3*, which encodes the ERK1 protein, is part of the Ras/Raf/ERK1 pathway. This pathway was found to be involved in formation of the neuro-cardio-facial-cutaneous syndrome (NCFC; OMIM 115150). Patients with this syndrome exhibit mental retardation and multiple congenital anomalies such as macrocephaly, a distinctive face with prominent forehead, absence of eyebrows, heart defects, pulmonic stenosis and hypertrophic cardiomyopathy. Sequencing of patients with this syndrome showed, that mutations causing NCFC are located in BRAF, KRAS, MEK1 and MEK2, which act upstream of ERK1 (Roberts, Allanson *et al.* 2006). This and the phenotype of the NCFC syndrome indicate a possible relevance of *MAPK3* for ASD.

5.4 gdpd3a is suggested to be an important developmental regulator

The results of the *gdpd3 in situ* experiments presented an expressed in the whole head, intestine and heart of a three day old embryo. This is comparable to the results of Blaker-Lee, Gupta *et al.* (2012) who showed an expression in the head of an embryo 2 dpf.

The embryos of the *gdpd3a* splice site morpholino knockdown experiment showed a strong phenotype. The embryos presented developmental defects, abnormalities in head and trunk formation and disintegrate at 2 dpf, while only developing until the 18 somite stage. In contrast to this, the 5'UTR morpholino showed no phenotypic change, even at a high morpholino concentration of 1.6 mM. However, because of the PCR verified skipping of exon 2, the functionality of the splice site morpholino was proven and therefore it is reasonable to conclude that the visible phenotype is reflecting the loss of *gdpd3*. This is also supported by the publication of Blaker-Lee, Gupta *et al.* (2012), who observed a similar *gdpd3a* knockdown, affecting the formation of brain, head and pigmentation of the embryo. In contrast to this thesis, Blaker-Lee, Gupta *et al.* (2012) did not mention the dying of the embryos. An explanation for the survival of the *gdpd3a* knockdown embryos is possibly a difference in the binding affinity or the concentration of the morpholino. Since the morpholino used by Blaker-Lee, Gupta *et al* is overlapping in 15 bp with the 5'UTR morpholino used here (Figure 62), a difference in binding affinity can probably be excluded. Therefore, the disparity is likely to be based on concentration differences. Comparing the *gdpd3* and the *mapk3* knockdowns of Blaker-Lee, Gupta *et al.* (2012) with the ones in this study, their knockdown phenotype constantly show a lower manifestation, which supports the idea that a concentration differences have caused the phenotypical variations.

Generally, the question remains if *GDPD3* can be linked with ASD. Unfortunately, the

Figure 62 *gdpd3* morpholino comparison
Part of the 5'UTR and coding sequence of *gdpd3* around the 5'UTR (ATG marked red). Overlap of morpholinos used by Blaker-Lee, Gupta *et al.* (2012) (green) and this thesis (blue).

phenotype presented in this thesis cannot contribute to answer the question yet. However, the developmental arrest and lethality impressively show the importance of *gdpd3a* during a developmental key step. Therefore, it can be suggested that a change in the expression level or the complete missing of *gdpd3* must have a strong effect on human development as well. Furthermore, also other members of the *GDPD* family, have been shown to be important for differentiation like osteoblasts, motor neurons and the outgrowth of Neuro2A cells (Rao and Sockanathan 2005, Yanaka 2007, Yanaka, Nogusa *et al.* 2007, Lang, Zhang *et al.* 2008). These findings also emphasize the importance of *GDPD3* and also draw a connection to neuronal processes which are maybe a hint to ASD.

5.5 asphd1 knockdown induces edema in the muscle but cannot be linked with autism

To date, no whole mount *in situ* hybridization data was available for *asphd1*. In this thesis it is shown that the *asphd1* expression is ubiquitous in head, intestine and weak in somitic muscles of three day old embryos. To find out more about the function of *asphd1,* the reverse genetic morpholino knockdown tool was used. This approach showed a developmental delay in the *asphd1* knockdown embryos which was visible in the mean of head size and body length. However, the calculated regression showed that there is no difference in the head size of the *asphd1* knockdown embryos when compared to the control. Consequently, the brain size is not affected by the knockdown of *asphd1*. The only visible change in the knockdown is the presence of edema in the muscle similar to the *ppp4c* knockdown. Since the *ppp4c* knockdowns are known for difficulties in blood vessel formation, the vascular system of the *asphd1* knockdowns was investigated. The result was, that no changes or deformation in the blood vessel development were visible in the *asphd1* knockdowns. Therefore, the reason for the edema formation in the muscle is most likely not related to the circulatory system.

Further, the hydroxylase function of *asphd1*, which processes basal post-translational modifications, also cannot direct explain the edema formation. It is possible, that the loss of *asphd1* induced senescence or changes in the osmoregulation of the muscle (Hill, Bello *et al*. 2004). However, further research is required to understand the function of *asphd1*. Nevertheless, the experiments have shown that a link of *ASPHD1* to ASD is unlikely.

5.6 ypel3 - a senescence inducer

To date, it is known that YPEL3 is located at the centrosome during interphase (Hosono, Sasaki *et al.* 2004), but an expression in a whole organism has not been shown. Here, *in situ* hybridizations were used to show that *ypel3* is ubiquitously expressed in the head and even stronger in the pericardium and the heart of zebrafish embryo, which interestingly, is also morphologically affected in the *ypel3* morpholino knockdown. The heart is stretched out and beats at a low frequency. Furthermore, the embryos do not develop erythrocytes, present a small head, curved tail and high mortality rate between the 1 - 2 dpf during which time the embryos die and start to disintegrate indicating senescence. Surprisingly, the phenotype appears to be very sensitive to the morpholino concentration. The injection of 0.2 mM *ypel3* morpholino was not sufficient to induce the phenotype, whereas it was fully penetrant at 0.4 mM. This and the strong phenotype lead to the suggestion that *ypel3* dosage sensitive and involved in fundamental processes during embryonic development. An explanation for the senescence could be, that YPEL3 is acting downstream of p53. It has been shown in MCF-7 cells that upon induction of YPEL3 the cellular senescence increases, which could be a plausible link to the phenotype described in this thesis (Kelley, Miller *et al.* 2010). However, the mortality of the *ypel3* knockdown embryos and the relation of YPEL3 with p53 indicate no apparent relationship with ASD.

5.7 Two ppp4c paralogs, one phenotype, but no direct connection to ASD

ppp4c is a highly conserved protein known to be involved in many processes such as microtubule organization at centrosomes, maturation of spliceosomal snRNPs, as well as regulation of histone acetylation (Sunkel, Gomes *et al.* 1995, Melki 1997, Helps, Brewis *et al.* 1998, Matera 1999, Gubitz, Mourelatos *et al.* 2002, Sumiyoshi, Sugimoto *et al.* 2002, Zhang, Ozawa *et al.* 2005). However, its function during the development is uncertain.

The challenge, of analyzing *ppp4c,* was the presence of two *ppp4c* paraloges in the zebrafish genome, which originated from additional whole-genome duplication in the teleost fish. Here it was demonstrated that both *ppp4c* genes have a similar expression pattern in the head and the intestine of an embryo at 3 dpf. This is consistent with whole

mount *in situ* hybridizations conducted by Jia, Dai *et al.* (2012), which showed a specific expression in the head for both *ppp4c* paralogs at 2 dpf. Interestingly, an expression located at the vascular system, like it was published for mouse, was not detectable (embryonic day 17.5, Kalen, Wellgard *et al.*2009). This is probably based on the different developmental stages of the embryos.

Accompanying to the *in situ* hybridizations Kalen, Wallgard *et al.* (2009) presented a morpholino knockdown of *ppp4ca* and Jia, Dai *et al.* (2012) a knockdown of *ppp4ca* and *ppp4cb*. Both studies used two morpholinos against the 5'UTR of *ppp4ca*, of which one morpholino showed 80 % sequence identity (Figure 63). Surprisingly, the two described knockdown phenotypes were completely different. Jia, Dai *et al.* (2012) described a ventralization, leading to a reduction in head and tail formation at 24 hpf for both *ppp4c* genes, whereas Kalen, Wallgard *et al.* (2009) showed that the *ppp4ca*

Figure 63 *ppp4ca* 5'UTR morpholino comparison
Morpholinos used by Kalen, Wallgard *et al.* (2009) are indicated in different green shades and Jia, Dai *et al.* (2012) in blue shades, the morpholino used in this thesis is represented in grey, the transcription start is labeled in red.

knockdown embryos had difficulties in the formation of the loop from the caudal artery and caudal vein. To confirm one of the published knockdown phenotypes, the morpholino experiments were repeated for both *ppp4c* genes within this thesis. Therefore, two morpholinos, one against the 5'UTR and another against a splice site, were used for each *ppp4c* gene. Both the morpholino knockdowns showed difficulties in the formation of the caudal blood loop, which was consistent with the *ppp4ca* phenotype described by Kalen, Wallgard *et al.* (2009).

The publication by Kalen, Wallgard *et al.* (2009) also described, that the *ppp4ca* knockdowns had difficulties in the formation of intersegmental vessels, which was illustrated by microangiography of 2 dpf embryo. To confirm these results, the microangiography was repeated in this thesis. In contrast to Kalen, Wallgard *et al.*

(2009), the microangiography was performed at 3 dpf to compensate for the developmental delay of the *ppp4ca* knockdown embryos. The results of the microangiography confirmed the difficulties in the formation of the caudal blood loop. Nevertheless, in contrast to Kalen, Wallgard *et al.* (2009) the intersegmental vessels were fully developed in all tested embryos. The explanation for this difference is probably the developmental delay of the knockdown embryos. Assuming that the *ppp4ca* knockdown embryos of Kalen, Wallgard *et al.* (2009) showed the same developmental delay like the *ppp4ca* knockdowns in this thesis they would only have attained the prime 22 stage. This is the stage were the embryos are about to form the intersegmental vessel. Therefore, the embryos, which Kalen, Wallgard *et al.* (2009) investigated by microangiography, probably have been too young to present intersegmental blood vessels. Further, because of their observation time of 3 dpf Kalen, Wallgard *et al.* (2009) did not recognize the swelling between yolk and interstitium, around the eye, and the pericard as well as the formation of edema in muscle as part of the phenotype of the *ppp4ca* knockdown embryos at 5 dpf.

Notably, the phenotypes for both *ppp4ca* morpholino knockdown experiments, generated within this thesis, were nearly identical. However, there were two striking differences between the splice site and the 5'UTR morpholino knockdown phenotype. The 5'UTR morpholino knockdown additionally induced an effect on the loop formation from caudal artery to caudal vein and the loss of one otolith. Because of the overlapping knockdown effects of the two morpholinos and the conformity with the Kalen, Wallgard *et al.* (2009) publication, the loss of the otolith is expected to be an off target effect of the 5'UTR morpholino. Candidate genes, which would influence otolith formation, are for example *zomp-1*, which encodes for the otolith matrix protein-1 (Omp-1) or *zotolin-1* (Lainhart, Bigler *et al*. 2006). However, the detailed mechanism of the otolith loss is not known yet.

Compared to the *ppp4ca* knockdown, the knockdown of *ppp4cb* showed a much higher mortality rate. 50 % of the embryos were characterized by deformations and developmental delays that occured already at 1 dpf. Only 38 % of these embryos survived until the third day of development. Some of the embryos also displayed a swollen pericard at 3 dpf. These deformed embryos died quickly. At 5 dpf, the remaining embryos, which had developed normally before, also manifested a swelling of the pericard, around the eyes and between the interstitium above the yolk.

Additionally, also the muscle showed structural changes. These changes had also been observed in the *ppp4ca* knockdown. However, the effect on the blood vessel formation of the *ppp4ca* knockdown embryos was not recapitulated. Therefore, it can be concluded that the swelling of the *ppp4ca* knockdown embryos is not dependent on a change in the vascular system. The question is, which function of the *ppp4c* genes is responsible for the edema formation and the muscle alteration? Due to the wide variety of known and probably unknown functions of *ppp4c* it is difficult to suggest the causes for this phenotype. Possible reasons for the formation of edema like in the *ppp4c* knockdowns are for example problems in formation of the pronephric glomerulus or the calcium regulation (Fombonne 2010, Boyle, Boulet *et al*. 2011). Further investigation is required to identify causes for the edema formation in the *ppp4c* knockdown embryos.

The main question in this thesis was if the zebrafish orthologs of the human genes within the 16p11.2 region can be linked with an autism-like disease pattern. Both *ppp4c* genes showed strong influence on embryonic development. Nevertheless, a change in the head size was not found for the *ppp4ca* knockdown. Interestingly, the *ppp4cb* knockdowns, which were generally smaller in body length, showed an extreme variability in head size and body length. To find out if the head size was affected by the knockdown, the head size was plotted over the body length and compared to the control injected embryos. However, the result of this was not conclusive. The distribution of the growth rate of the embryos was equal, whereas the slope was significantly different. Consequently, an effect on the brain size cannot be confirmed.

Taken together the *ppp4c* knockdowns showed an induction of edema, muscle deformations and problems in formation of the caudal artery loop. Therefore, a direct link between the *ppp4c* genes and neuronal changes could not be shown. However, some patients with a 16p11.2 deletion also display malformations of the heart (Puvabanditsin, Nagar *et al*. 2010, Shen, Chen *et al*. 2011). The results of this thesis together with Kalen, Wallgard *et al.* (2009) indicate, that a loss of function mutation of the hemizygous *ppp4c* of patients with a 16p11.2 deletion could be the reason for this. This would also explain why not all patients with a 16p11.2 deletion have heart malformations. In order to prove this hypothesis, DNA sequencing of patients with a 16p11.2 deletion and heart defects should be performed. A confirmation of a mutation in the *ppp4c* locus of these patients would be the identification of a new gene involved in heart formation, which would open new ways in diagnostics and therapy.

5.8 Zebrafish compared with other disease models

The results of this thesis clearly demonstrate how useful the zebrafish is as a model for neurological diseases, even when lacking the most important diagnostic component of ASD, the language. The advantages of the zebrafish model are: a relatively easy and cheap maintaining, the availability of the complete genome sequence and a battery of genetic methods such as morpholino knockdown and Tol2 mutagenesis (Summerton and Weller 1997, Kwan, Fujimoto *et al.* 2007). Further, the zebrafish offers genetic resources, such as GFP reporter vectors, which enable the detailed analysis of a large number of non-coding regulatory elements (Woolfe, Goodson *et al.* 2005, Hufton, Mathia *et al.* 2009). Nevertheless, it is interesting to ask what alternative options researchers currently have that could help to enrich our understanding of ASD and how they compare to the zebrafish.

Cell cultures of human cell lines or primary cells from patients offer the evolutionary closest, but probably also the simplest model. It has a high potential to test for example the effects of noncoding mutations on transcription or expression levels (Comoletti, De Jaco *et al*. 2004). However, the low complexity of this system prevents an initial identification of potential ASD genes. Another possibility is D*rosophila melanogaster*, a fly that has already been used successfully to model human neurological disorders like Huntington's disease (Zhang, Feany *et al*. 2009) or schizophrenia (Dickman and Davis 2009). Therefore, the fruit fly is an excellent and often discussed model organism to investigate neurological disorders (Sawa 2009, O'Kane 2011). The most important advantage is the availability of a large number of mutants which offers the possibility for extensive forward genetic screens. Nevertheless, the large evolutionary distance between insects and vertebrates only allows a comparison of strongly conserved mechanisms. Therefore, it is not possible to investigate all ASD candidate genes in *Drosophila melanogaster*.

Compared to the fruit fly and zebrafish, the mouse is the evolutionary closest animal model to human. Consequently, the question is how the mouse compares to the other model organisms? The first issue noticeable, when working with mice, is the very high costs for maintaining and keeping. Additionally, generating a mice knockout is very time consuming. All these factors together make the mouse not the first choice for testing a large number of genes. However, a mouse model offers a larger spectrum of

social behavior. An example for this is the study about the postsynaptic protein SHANK3, a potential inducer for the Phelan-McDermid syndrome which is associated with ASD. In this study Peça, Feliciano *et al*. (2011) showed, that heterozygous *Shank3* knockout mice display self-injurious repetitive grooming and a deficiency in social interactions. Besides the behavioral phenotype, the *Shank3* mutant mice also exhibit electrophysiological changes and defects in striatal synapses and cortico-striatal circuits. This was confirmed by another *Shank3* study from 2011, in which the same social affiliations, the electrophysiological and the neuronal structural changes had been observed (Wang, McCoy *et al*. 2011). In addition, Wang, McCoy *et al*. showed deficits of *Shank3* mutant mice in a larger spectrum of behavioral perspectives, for example in ultrasonic vocalization, repetitive behavior, as well as learning and memory. Taken together, the results of Wang, McCoy *et al*. (2011) and Peça, Feliciano *et al*. (2011) impressively showed the potential of single gene analysis in mice. Nevertheless, the mouse offers the possibility to investigate larger deletions comprising several genes. A great example for this is a publication by Horev, Ellegood *et al*. (2011). They engineered two mouse strains, one carrying a deletion and the other one a duplication of the chromosomal region corresponding to the human 16p11.2 deletion. Both strains showed changes in the gene expression profiles, viability, brain architecture and also repetitive behavior. However, the strongest effect was found in mice carrying a heterozygous 16p11.2 like deletion (df/+). For example, the df/+ mice as well as the control mice showed an increased behavioral activity when transferred to a new environment. However, in contrast to the control, the df/+ mice presented a second burst of activity, while the control animals rested after investigation of their new territory. Further, the df/+ mice showed ceiling-climbing behavior restricted to specific locations and stereotypical movement. Both behaviors could be analogue to the ASD phenotype. Another important finding was an enlargement of the brain in df/+ mice measured by high resolution magnetic resonance imaging (MRI). This corresponds to the finding of macrocephaly in patients with 16p11.2 deletion (Shinawi, Liu *et al*. 2010, Schaaf, Goin-Kochel *et al*. 2011). Taken together, the df/+ mice offer the potential for further investigation of global 16p11.2 deletion effects.

Generally, cell culture, fruit fly and mouse models offer individual ways to investigate effects of genetic mutations. Nevertheless, the zebrafish offers the best mixture of fast reverse genetic testing and evolutionary distance to human. Therefore, it is probably the

most suitable model for large scale screens of potential ASD candidate genes. To date. 573 potential ASD candidate genes are listed in the autism database AutDB (Update September 2013). This demonstrates that there is a need for fast screening methods to identify potential ASD inducing genes that would enable us to dissect the molecular pathways that underline this complex disease, but also classify ASD patients in more specific groups, which in extent will help identifying additional ASD genes.

5.9 The future of the ASD quest

An interesting question is how the price reduction of whole-genome sequencing will change the identification of ASD causing genes. It is likely that, due to its much higher resolution, the next generation sequencing (NGS) will replace the aCGH method. However, this resolution increase will only help to advance our knowledge on the molecular pathways involved in ASD, if the method used to diagnose and categorize ASD patients progresses. In addition, both the aCGH and the NGS techniques will be most effective if applied on large patient cohorts. This will serve to overcome the complex genetic background of ASD.

A recent example for the usage of NGS technology in autism research is a publication by Shi, Zhang *et al.* (2013). They sequenced the complete genome of the members of a large family with two autistic children and 6 siblings. As result they identified over 3 million single nucleotide variances (SNV) per patient. After applying several filtering steps to analyze their data, they prioritized 33 non-coding SNVs. This illustrates two issues: first, even with single base pair resolution, it is difficult to identify potentially damaging mutations and second, even with this technique, a large number of potential genes will be found. Hence, a model to test all these candidates will still be needed, and as shown in this thesis zebrafish is a great candidate for this.

6 References

American Psychiatric Association (2013). Diagnostic and statistical manual of mental disorders: DSM-5. Washington, DC u.a., American Psychiatric Publ.

Autism Genome Project, C., P. Szatmari, A. D. Paterson, L. Zwaigenbaum, W. Roberts, J. Brian, X. Q. Liu, J. B. Vincent, J. L. Skaug, A. P. Thompson, L. Senman, L. Feuk, C. Qian, S. E. Bryson, M. B. Jones, C. R. Marshall, S. W. Scherer, V. J. Vieland, C. Bartlett, L. V. Mangin, R. Goedken, A. Segre, M. A. Pericak-Vance, M. L. Cuccaro, J. R. Gilbert, H. H. Wright, R. K. Abramson, C. Betancur, T. Bourgeron, C. Gillberg, M. Leboyer, J. D. Buxbaum, K. L. Davis, E. Hollander, J. M. Silverman, J. Hallmayer, L. Lotspeich, J. S. Sutcliffe, J. L. Haines, S. E. Folstein, J. Piven, T. H. Wassink, V. Sheffield, D. H. Geschwind, M. Bucan, W. T. Brown, R. M. Cantor, J. N. Constantino, T. C. Gilliam, M. Herbert, C. Lajonchere, D. H. Ledbetter, C. Lese-Martin, J. Miller, S. Nelson, C. A. Samango-Sprouse, S. Spence, M. State, R. E. Tanzi, H. Coon, G. Dawson, B. Devlin, A. Estes, P. Flodman, L. Klei, W. M. McMahon, N. Minshew, J. Munson, E. Korvatska, P. M. Rodier, G. D. Schellenberg, M. Smith, M. A. Spence, C. Stodgell, P. G. Tepper, E. M. Wijsman, C. E. Yu, B. Roge, C. Mantoulan, K. Wittemeyer, A. Poustka, B. Felder, S. M. Klauck, C. Schuster, F. Poustka, S. Bolte, S. Feineis-Matthews, E. Herbrecht, G. Schmotzer, J. Tsiantis, K. Papanikolaou, E. Maestrini, E. Bacchelli, F. Blasi, S. Carone, C. Toma, H. Van Engeland, M. de Jonge, C. Kemner, F. Koop, M. Langemeijer, C. Hijmans, W. G. Staal, G. Baird, P. F. Bolton, M. L. Rutter, E. Weisblatt, J. Green, C. Aldred, J. A. Wilkinson, A. Pickles, A. Le Couteur, T. Berney, H. McConachie, A. J. Bailey, K. Francis, G. Honeyman, A. Hutchinson, J. R. Parr, S. Wallace, A. P. Monaco, G. Barnby, K. Kobayashi, J. A. Lamb, I. Sousa, N. Sykes, E. H. Cook, S. J. Guter, B. L. Leventhal, J. Salt, C. Lord, C. Corsello, V. Hus, D. E. Weeks, F. Volkmar, M. Tauber, E. Fombonne, A. Shih and K. J. Meyer (2007). "Mapping autism risk loci using genetic linkage and chromosomal rearrangements." Nat Genet **39**(3): 319-328.

Azizieh, R., D. Orduz, P. Van Bogaert, T. Bouschet, W. Rodriguez, S. N. Schiffmann, I. Pirson and M. J. Abramowicz (2011). "Progressive myoclonic epilepsy-associated gene KCTD7 is a regulator of potassium conductance in neurons." Mol Neurobiol **44**(1): 111-121.

Bailey, J. A., Z. Gu, R. A. Clark, K. Reinert, R. V. Samonte, S. Schwartz, M. D. Adams, E. W. Myers, P. W. Li and E. E. Eichler (2002). "Recent segmental duplications in the human genome." Science **297**(5583): 1003-1007.

Basu, S. N., R. Kollu and S. Banerjee-Basu (2009). "AutDB: a gene reference resource for autism research." Nucleic Acids Res **37**(Database issue): D832-836.

Bedell, V. M., S. E. Westcot and S. C. Ekker (2011). "Lessons from morpholino-based screening in zebrafish." Brief Funct Genomics **10**(4): 181-188.

Bentires-Alj, M., M. I. Kontaridis and B. G. Neel (2006). "Stops along the RAS pathway in human genetic disease." Nat Med **12**(3): 283-285.

Berberich, S. J., A. Todd and R. Tuttle (2011). "Why YPEL3 represents a novel tumor suppressor." Front Biosci **16**: 1746-1751.

Bernhardt, R. R., A. B. Chitnis, L. Lindamer and J. Y. Kuwada (1990). "Identification of spinal neurons in the embryonic and larval zebrafish." J Comp Neurol **302**(3): 603-616.

Bill, B. R., A. M. Petzold, K. J. Clark, L. A. Schimmenti and S. C. Ekker (2009). "A primer for morpholino use in zebrafish." Zebrafish **6**(1): 69-77.

Blaker-Lee, A., S. Gupta, J. M. McCammon, G. De Rienzo and H. Sive (2012). "Zebrafish homologs of genes within 16p11.2, a genomic region associated with brain disorders, are active during brain development, and include two deletion dosage sensor genes." Dis Model Mech **5**(6): 834-851.

Blau, N., F. J. van Spronsen and H. L. Levy (2010). "Phenylketonuria." Lancet **376**(9750): 1417-1427.

Boyle, C. A., S. Boulet, L. A. Schieve, R. A. Cohen, S. J. Blumberg, M. Yeargin-Allsopp, S. Visser and M. D. Kogan (2011). "Trends in the prevalence of developmental disabilities in US children, 1997-2008." Pediatrics **127**(6): 1034-1042.

Bradford, Y., T. Conlin, N. Dunn, D. Fashena, K. Frazer, D. G. Howe, J. Knight, P. Mani, R. Martin, S. A. Moxon, H. Paddock, C. Pich, S. Ramachandran, B. J. Ruef, L. Ruzicka, H. Bauer Schaper, K. Schaper, X. Shao, A. Singer, J. Sprague, B. Sprunger, C. Van Slyke and M. Westerfield (2011). "ZFIN: enhancements and updates to the Zebrafish Model Organism Database." Nucleic Acids Res **39**(Database issue): D822-829.

Bretaud, S., Q. Li, B. L. Lockwood, K. Kobayashi, E. Lin and S. Guo (2007). "A choice behavior for morphine reveals experience-dependent drug preference and underlying neural substrates in developing larval zebrafish." Neuroscience **146**(3): 1109-1116.

Chitnis, A. B. and J. Y. Kuwada (1990). "Axonogenesis in the brain of zebrafish embryos." J Neurosci **10**(6): 1892-1905.

Christoffels, A., E. G. Koh, J. M. Chia, S. Brenner, S. Aparicio and B. Venkatesh (2004). "Fugu genome analysis provides evidence for a whole-genome duplication early during the evolution of ray-finned fishes." Mol Biol Evol **21**(6): 1146-1151.

Chubb, J. E., N. J. Bradshaw, D. C. Soares, D. J. Porteous and J. K. Millar (2008). "The DISC locus in psychiatric illness." Mol Psychiatry **13**(1): 36-64.

Cohen, P. (2002). "The origins of protein phosphorylation." Nat Cell Biol **4**(5): E127-130.

Cohen, P. T., A. Philp and C. Vazquez-Martin (2005). "Protein phosphatase 4--from obscurity to vital functions." FEBS Lett **579**(15): 3278-3286.

Comoletti, D., A. De Jaco, L. L. Jennings, R. E. Flynn, G. Gaietta, I. Tsigelny, M. H. Ellisman and P. Taylor (2004). "The Arg451Cys-neuroligin-3 mutation associated with autism reveals a defect in protein processing." J Neurosci **24**(20): 4889-4893.

Corda, D., T. Kudo, P. Zizza, C. Iurisci, E. Kawai, N. Kato, N. Yanaka and S. Mariggio (2009). "The developmentally regulated osteoblast phosphodiesterase GDE3 is glycerophosphoinositol-specific and modulates cell growth." J Biol Chem **284**(37): 24848-24856.

Courchesne, E., C. M. Karns, H. R. Davis, R. Ziccardi, R. A. Carper, Z. D. Tigue, H. J. Chisum, P. Moses, K. Pierce, C. Lord, A. J. Lincoln, S. Pizzo, L. Schreibman, R. H.

Haas, N. A. Akshoomoff and R. Y. Courchesne (2001). "Unusual brain growth patterns in early life in patients with autistic disorder: an MRI study." Neurology **57**(2): 245-254.

Darland, T. and J. E. Dowling (2001). "Behavioral screening for cocaine sensitivity in mutagenized zebrafish." Proc Natl Acad Sci U S A **98**(20): 11691-11696.

Dehal, P. and J. L. Boore (2005). "Two rounds of whole genome duplication in the ancestral vertebrate." PLoS Biol **3**(10): e314.

Dickman, D. K. and G. W. Davis (2009). "The schizophrenia susceptibility gene dysbindin controls synaptic homeostasis." Science **326**(5956): 1127-1130.

Draper, B. W., P. A. Morcos and C. B. Kimmel (2001). "Inhibition of zebrafish fgf8 pre-mRNA splicing with morpholino oligos: a quantifiable method for gene knockdown." Genesis **30**(3): 154-156.

Drerup, C. M., H. M. Wiora, J. Topczewski and J. A. Morris (2009). "Disc1 regulates foxd3 and sox10 expression, affecting neural crest migration and differentiation." Development **136**(15): 2623-2632.

Durand, C. M., C. Betancur, T. M. Boeckers, J. Bockmann, P. Chaste, F. Fauchereau, G. Nygren, M. Rastam, I. C. Gillberg, H. Anckarsater, E. Sponheim, H. Goubran-Botros, R. Delorme, N. Chabane, M. C. Mouren-Simeoni, P. de Mas, E. Bieth, B. Roge, D. Heron, L. Burglen, C. Gillberg, M. Leboyer and T. Bourgeron (2007). "Mutations in the gene encoding the synaptic scaffolding protein SHANK3 are associated with autism spectrum disorders." Nat Genet **39**(1): 25-27.

Fernandez, B. A., W. Roberts, B. Chung, R. Weksberg, S. Meyn, P. Szatmari, A. M. Joseph-George, S. Mackay, K. Whitten, B. Noble, C. Vardy, V. Crosbie, S. Luscombe, E. Tucker, L. Turner, C. R. Marshall and S. W. Scherer (2010). "Phenotypic spectrum associated with de novo and inherited deletions and duplications at 16p11.2 in individuals ascertained for diagnosis of autism spectrum disorder." J Med Genet **47**(3): 195-203.

Flicek, P., I. Ahmed, M. R. Amode, D. Barrell, K. Beal, S. Brent, D. Carvalho-Silva, P. Clapham, G. Coates, S. Fairley, S. Fitzgerald, L. Gil, C. Garcia-Giron, L. Gordon, T. Hourlier, S. Hunt, T. Juettemann, A. K. Kahari, S. Keenan, M. Komorowska, E. Kulesha, I. Longden, T. Maurel, W. M. McLaren, M. Muffato, R. Nag, B. Overduin, M. Pignatelli, B. Pritchard, E. Pritchard, H. S. Riat, G. R. Ritchie, M. Ruffier, M. Schuster, D. Sheppard, D. Sobral, K. Taylor, A. Thormann, S. Trevanion, S. White, S. P. Wilder, B. L. Aken, E. Birney, F. Cunningham, I. Dunham, J. Harrow, J. Herrero, T. J. Hubbard, N. Johnson, R. Kinsella, A. Parker, G. Spudich, A. Yates, A. Zadissa and S. M. Searle (2013). "Ensembl 2013." Nucleic Acids Res **41**(Database issue): D48-55.

Folstein, S. and M. Rutter (1977). "Infantile autism: a genetic study of 21 twin pairs." J Child Psychol Psychiatry **18**(4): 297-321.

Fombonne, E. (2010). "Estimated prevalence of autism spectrum conditions in Cambridgeshire is over 1%." Evid Based Ment Health **13**(1): 32.

Gauthier, J., N. Champagne, R. G. Lafreniere, L. Xiong, D. Spiegelman, E. Brustein, M. Lapointe, H. Peng, M. Cote, A. Noreau, F. F. Hamdan, A. M. Addington, J. L. Rapoport, L. E. Delisi, M. O. Krebs, R. Joober, F. Fathalli, F. Mouaffak, A. P. Haghighi, C. Neri, M. P. Dube, M. E. Samuels, C. Marineau, E. A. Stone, P. Awadalla, P. A. Barker, S. Carbonetto, P. Drapeau, G. A. Rouleau and S. D. Team (2010). "De

novo mutations in the gene encoding the synaptic scaffolding protein SHANK3 in patients ascertained for schizophrenia." Proc Natl Acad Sci U S A **107**(17): 7863-7868.

Gerlai, R., D. Chatterjee, T. Pereira, T. Sawashima and R. Krishnannair (2009). "Acute and chronic alcohol dose: population differences in behavior and neurochemistry of zebrafish." Genes Brain Behav **8**(6): 586-599.

Gibson, T. J. and J. Spring (2000). "Evidence in favour of ancient octaploidy in the vertebrate genome." Biochem Soc Trans **28**(2): 259-264.

Golzio, C., J. Willer, M. E. Talkowski, E. C. Oh, Y. Taniguchi, S. Jacquemont, A. Reymond, M. Sun, A. Sawa, J. F. Gusella, A. Kamiya, J. S. Beckmann and N. Katsanis (2012). "KCTD13 is a major driver of mirrored neuroanatomical phenotypes of the 16p11.2 copy number variant." Nature **485**(7398): 363-367.

Gronke, R. S., W. J. VanDusen, V. M. Garsky, J. W. Jacobs, M. K. Sardana, A. M. Stern and P. A. Friedman (1989). "Aspartyl beta-hydroxylase: in vitro hydroxylation of a synthetic peptide based on the structure of the first growth factor-like domain of human factor IX." Proc Natl Acad Sci U S A **86**(10): 3609-3613.

Gubitz, A. K., Z. Mourelatos, L. Abel, J. Rappsilber, M. Mann and G. Dreyfuss (2002). "Gemin5, a novel WD repeat protein component of the SMN complex that binds Sm proteins." J Biol Chem **277**(7): 5631-5636.

Gutzman, J. H., E. G. Graeden, L. A. Lowery, H. S. Holley and H. Sive (2008). "Formation of the zebrafish midbrain-hindbrain boundary constriction requires laminin-dependent basal constriction." Mech Dev **125**(11-12): 974-983.

Gutzman, J. H. and H. Sive (2009). "Zebrafish brain ventricle injection." J Vis Exp(26).

Gutzman, J. H. and H. Sive (2010). "Epithelial relaxation mediated by the myosin phosphatase regulator Mypt1 is required for brain ventricle lumen expansion and hindbrain morphogenesis." Development **137**(5): 795-804.

Helps, N. R., N. D. Brewis, K. Lineruth, T. Davis, K. Kaiser and P. T. Cohen (1998). "Protein phosphatase 4 is an essential enzyme required for organisation of microtubules at centrosomes in Drosophila embryos." J Cell Sci **111 (Pt 10)**: 1331-1340.

Hill, A. J., S. M. Bello, A. L. Prasch, R. E. Peterson and W. Heideman (2004). "Water permeability and TCDD-induced edema in zebrafish early-life stages." Toxicol Sci **78**(1): 78-87.

Holland, P. W., J. Garcia-Fernandez, N. A. Williams and A. Sidow (1994). "Gene duplications and the origins of vertebrate development." Dev Suppl: 125-133.

Horev, G., J. Ellegood, J. P. Lerch, Y. E. Son, L. Muthuswamy, H. Vogel, A. M. Krieger, A. Buja, R. M. Henkelman, M. Wigler and A. A. Mills (2011). "Dosage-dependent phenotypes in models of 16p11.2 lesions found in autism." Proc Natl Acad Sci U S A **108**(41): 17076-17081.

Hosono, K., T. Sasaki, S. Minoshima and N. Shimizu (2004). "Identification and characterization of a novel gene family YPEL in a wide spectrum of eukaryotic species." Gene **340**(1): 31-43.

Hubbard, M. J. and P. Cohen (1993). "On target with a new mechanism for the regulation of protein phosphorylation." Trends Biochem Sci **18**(5): 172-177.

Hufton, A. L., D. Groth, M. Vingron, H. Lehrach, A. J. Poustka and G. Panopoulou (2008). "Early vertebrate whole genome duplications were predated by a period of intense genome rearrangement." Genome Res **18**(10): 1582-1591.

Hufton, A. L., S. Mathia, H. Braun, U. Georgi, H. Lehrach, M. Vingron, A. J. Poustka and G. Panopoulou (2009). "Deeply conserved chordate noncoding sequences preserve genome synteny but do not drive gene duplicate retention." Genome Res **19**(11): 2036-2051.

Hughes, A. L., J. da Silva and R. Friedman (2001). "Ancient genome duplications did not structure the human Hox-bearing chromosomes." Genome Res **11**(5): 771-780.

Hyatt, T. M. and S. C. Ekker (1999). "Vectors and techniques for ectopic gene expression in zebrafish." Methods Cell Biol **59**: 117-126.

Jia, S., F. Dai, D. Wu, X. Lin, C. Xing, Y. Xue, Y. Wang, M. Xiao, W. Wu, X. H. Feng and A. Meng (2012). "Protein phosphatase 4 cooperates with Smads to promote BMP signaling in dorsoventral patterning of zebrafish embryos." Dev Cell **22**(5): 1065-1078.

Johnson, G. L. and R. Lapadat (2002). "Mitogen-activated protein kinase pathways mediated by ERK, JNK, and p38 protein kinases." Science **298**(5600): 1911-1912.

Jones, J. R., C. Skinner, M. J. Friez, C. E. Schwartz and R. E. Stevenson (2008). "Hypothesis: dysregulation of methylation of brain-expressed genes on the X chromosome and autism spectrum disorders." Am J Med Genet A **146A**(17): 2213-2220.

Jorde, L. B., A. Mason-Brothers, R. Waldmann, E. R. Ritvo, B. J. Freeman, C. Pingree, W. M. McMahon, B. Petersen, W. R. Jenson and A. Mo (1990). "The UCLA-University of Utah epidemiologic survey of autism: genealogical analysis of familial aggregation." Am J Med Genet **36**(1): 85-88.

Kabashi, E., E. Brustein, N. Champagne and P. Drapeau (2010). "Zebrafish models for the functional genomics of neurogenetic disorders." Biochimica et biophysica acta **1812**(3): 335-345.

Kalen, M., E. Wallgard, N. Asker, A. Nasevicius, E. Athley, E. Billgren, J. D. Larson, S. A. Wadman, E. Norseng, K. J. Clark, L. He, L. Karlsson-Lindahl, A. K. Hager, H. Weber, H. Augustin, T. Samuelsson, C. K. Kemmet, C. M. Utesch, J. J. Essner, P. B. Hackett and M. Hellstrom (2009). "Combination of reverse and chemical genetic screens reveals angiogenesis inhibitors and targets." Chem Biol **16**(4): 432-441.

Karlsson, J., J. von Hofsten and P. E. Olsson (2001). "Generating transparent zebrafish: a refined method to improve detection of gene expression during embryonic development." Marine biotechnology (New York, N.Y.) **3**(6): 522-527.

Kelley, K. D., K. R. Miller, A. Todd, A. R. Kelley, R. Tuttle and S. J. Berberich (2010). "YPEL3, a p53-regulated gene that induces cellular senescence." Cancer Res **70**(9): 3566-3575.

Kelley, K. D., K. R. Miller, A. Todd, A. R. Kelley, R. Tuttle and S. J. Berberich (2010). "YPEL3, a p53-Regulated Gene that Induces Cellular Senescence." Cancer research: 3566-3575.

Kent, W. J., C. W. Sugnet, T. S. Furey, K. M. Roskin, T. H. Pringle, A. M. Zahler and D. Haussler (2002). "The human genome browser at UCSC." Genome Research **12**(6): 996-1006.

Kikuta, H., M. Laplante, P. Navratilova, A. Z. Komisarczuk, P. G. Engstrom, D. Fredman, A. Akalin, M. Caccamo, I. Sealy, K. Howe, J. Ghislain, G. Pezeron, P. Mourrain, S. Ellingsen, A. C. Oates, C. Thisse, B. Thisse, I. Foucher, B. Adolf, A. Geling, B. Lenhard and T. S. Becker (2007). "Genomic regulatory blocks encompass multiple neighboring genes and maintain conserved synteny in vertebrates." Genome Res **17**(5): 545-555.

Kim, Y. S., B. L. Leventhal, Y.-J. Koh, E. Fombonne, E. Laska, E.-C. Lim, K.-A. Cheon, S.-J. Kim, Y.-K. Kim, H. Lee, D.-H. Song and R. R. Grinker (2011). "Prevalence of autism spectrum disorders in a total population sample." Am J Psychiatry **168**(9): 904-912.

Kim, Y. S., B. L. Leventhal, Y. J. Koh, E. Fombonne, E. Laska, E. C. Lim, K. A. Cheon, S. J. Kim, Y. K. Kim, H. Lee, D. H. Song and R. R. Grinker (2011). "Prevalence of autism spectrum disorders in a total population sample." Am J Psychiatry **168**(9): 904-912.

Kimmel, C. B. (1993). "Patterning the brain of the zebrafish embryo." Annu Rev Neurosci **16**: 707-732.

Kimmel, C. B., W. W. Ballard, S. R. Kimmel, B. Ullmann and T. F. Schilling (1995). "Stages of embryonic development of the zebrafish." Dev Dyn **203**(3): 253-310.

Kimmel, C. B., S. L. Powell and W. K. Metcalfe (1982). "Brain neurons which project to the spinal cord in young larvae of the zebrafish." J Comp Neurol **205**(2): 112-127.

Konyukh, M., R. Delorme, P. Chaste, C. Leblond, N. Lemiere, G. Nygren, H. Anckarsater, M. Rastam, O. Stahlberg, F. Amsellem, I. C. Gillberg, M. C. Mouren-Simeoni, E. Herbrecht, F. Fauchereau, R. Toro, C. Gillberg, M. Leboyer and T. Bourgeron (2011). "Variations of the candidate SEZ6L2 gene on Chromosome 16p11.2 in patients with autism spectrum disorders and in human populations." PloS one **6**(3): e17289.

Kramer-Zucker, A. G., F. Olale, C. J. Haycraft, B. K. Yoder, A. F. Schier and I. A. Drummond (2005). "Cilia-driven fluid flow in the zebrafish pronephros, brain and Kupffer's vesicle is required for normal organogenesis." Development **132**(8): 1907-1921.

Krens, S. F., S. He, G. E. Lamers, A. H. Meijer, J. Bakkers, T. Schmidt, H. P. Spaink and B. E. Snaar-Jagalska (2008). "Distinct functions for ERK1 and ERK2 in cell migration processes during zebrafish gastrulation." Dev Biol **319**(2): 370-383.

Krens, S. F., S. He, H. P. Spaink and B. E. Snaar-Jagalska (2006). "Characterization and expression patterns of the MAPK family in zebrafish." Gene Expr Patterns **6**(8): 1019-1026.

Krens, S. F. G., S. He, H. P. Spaink and B. E. Snaar-Jagalska (2006). "Characterization and expression patterns of the MAPK family in zebrafish." Gene expression patterns : GEP **6**(8): 1019-1026.

Kumar, R. a., S. KaraMohamed, J. Sudi, D. F. Conrad, C. Brune, J. a. Badner, T. C. Gilliam, N. J. Nowak, E. H. Cook, W. B. Dobyns and S. L. Christian (2008). "Recurrent 16p11.2 microdeletions in autism." Human molecular genetics **17**(4): 628-638.

Kumar, R. A., C. R. Marshall, J. A. Badner, T. D. Babatz, Z. Mukamel, K. A. Aldinger, J. Sudi, C. W. Brune, G. Goh, S. Karamohamed, J. S. Sutcliffe, E. H. Cook, D. H.

Geschwind, W. B. Dobyns, S. W. Scherer and S. L. Christian (2009). "Association and mutation analyses of 16p11.2 autism candidate genes." PloS one **4**(2): e4582.

Kwan, K. M., E. Fujimoto, C. Grabher, B. D. Mangum, M. E. Hardy, D. S. Campbell, J. M. Parant, H. J. Yost, J. P. Kanki and C. B. Chien (2007). "The Tol2kit: a multisite gateway-based construction kit for Tol2 transposon transgenesis constructs." Dev Dyn **236**(11): 3088-3099.

Lainhart, J. E., E. D. Bigler, M. Bocian, H. Coon, E. Dinh, G. Dawson, C. K. Deutsch, M. Dunn, A. Estes, H. Tager-Flusberg, S. Folstein, S. Hepburn, S. Hyman, W. McMahon, N. Minshew, J. Munson, K. Osann, S. Ozonoff, P. Rodier, S. Rogers, M. Sigman, M. A. Spence, C. J. Stodgell and F. Volkmar (2006). "Head circumference and height in autism: a study by the Collaborative Program of Excellence in Autism." Am J Med Genet A **140**(21): 2257-2274.

Lang, Q., H. Zhang, J. Li, H. Yin, Y. Zhang, W. Tang, B. Wan and L. Yu (2008). "Cloning and characterization of a human GDPD domain-containing protein GDPD5." Mol Biol Rep **35**(3): 351-359.

Lanz-Mendoza, H., R. Bettencourt, M. Fabbri and I. Faye (1996). "Regulation of the insect immune response: the effect of hemolin on cellular immune mechanisms." Cell Immunol **169**(1): 47-54.

Lavaissiere, L., S. Jia, M. Nishiyama, S. de la Monte, A. M. Stern, J. R. Wands and P. A. Friedman (1996). "Overexpression of human aspartyl(asparaginyl)beta-hydroxylase in hepatocellular carcinoma and cholangiocarcinoma." J Clin Invest **98**(6): 1313-1323.

Levy, D., M. Ronemus, B. Yamrom, Y. H. Lee, A. Leotta, J. Kendall, S. Marks, B. Lakshmi, D. Pai, K. Ye, A. Buja, A. Krieger, S. Yoon, J. Troge, L. Rodgers, I. Iossifov and M. Wigler (2011). "Rare de novo and transmitted copy-number variation in autistic spectrum disorders." Neuron **70**(5): 886-897.

Lewis, D. A. and P. Levitt (2002). "Schizophrenia as a disorder of neurodevelopment." Annu Rev Neurosci **25**: 409-432.

Lin, S. L., S. J. Chang and S. Y. Ying (2006). "First in vivo evidence of microRNA-induced fragile X mental retardation syndrome." Mol Psychiatry **11**(7): 616-617.

Louis, A., M. Muffato and H. Roest Crollius (2013). "Genomicus: five genome browsers for comparative genomics in eukaryota." Nucleic Acids Res **41**(Database issue): D700-705.

Marshall, C. R., A. Noor, J. B. Vincent, A. C. Lionel, L. Feuk, J. Skaug, M. Shago, R. Moessner, D. Pinto, Y. Ren, B. Thiruvahindrapduram, A. Fiebig, S. Schreiber, J. Friedman, C. E. J. Ketelaars, Y. J. Vos, C. Ficicioglu, S. Kirkpatrick, R. Nicolson, L. Sloman, A. Summers, C. A. Gibbons, A. Teebi, D. Chitayat, R. Weksberg, A. Thompson, C. Vardy, V. Crosbie, S. Luscombe, R. Baatjes, L. Zwaigenbaum, W. Roberts, B. Fernandez, P. Szatmari and S. W. Scherer (2008). "Structural variation of chromosomes in autism spectrum disorder." American journal of human genetics **82**(2): 477-488.

Matera, A. G. (1999). "Nuclear bodies: multifaceted subdomains of the interchromatin space." Trends Cell Biol **9**(8): 302-309.

Mathur, P. and S. Guo (2010). "Use of zebrafish as a model to understand mechanisms of addiction and complex neurobehavioral phenotypes." Neurobiol Dis **40**(1): 66-72.

Melki, J. (1997). "Spinal muscular atrophy." Curr Opin Neurol **10**(5): 381-385.

Meyer, A. and Y. Van de Peer (2005). "From 2R to 3R: evidence for a fish-specific genome duplication (FSGD)." Bioessays **27**(9): 937-945.

MMWR (2012). "Prevalence of autism spectrum disorders--Autism and Developmental Disabilities Monitoring Network, 14 sites, United States, 2008." MMWR Surveill Summ **61**(3): 1-19.

Myers, S. M., C. P. Johnson and D. American Academy of Pediatrics Council on Children With (2007). "Management of children with autism spectrum disorders." Pediatrics **120**(5): 1162-1182.

Nasevicius, a. and S. C. Ekker (2000). "Effective targeted gene 'knockdown' in zebrafish." Nature genetics **26**(2): 216-220.

O'Kane, C. J. (2011). "Drosophila as a model organism for the study of neuropsychiatric disorders." Curr Top Behav Neurosci **7**: 37-60.

Ohno, S. (1970). Evolution by gene duplication. Berlin u.a., Springer.

Panopoulou, G., S. Hennig, D. Groth, A. Krause, A. J. Poustka, R. Herwig, M. Vingron and H. Lehrach (2003). "New evidence for genome-wide duplications at the origin of vertebrates using an amphioxus gene set and completed animal genomes." Genome Res **13**(6A): 1056-1066.

Papan, C. and J. A. Camposortega (1994). "On the Formation of the Neural Keel and Neural-Tube in the Zebrafish Danio (Brachydanio) Rerio." Rouxs Archives of Developmental Biology **203**(4): 178-186.

Peça, J., C. Feliciano, J. T. Ting, W. Wang, M. F. Wells, T. N. Venkatraman, C. D. Lascola, Z. Fu and G. Feng (2011). "Shank3 mutant mice display autistic-like behaviours and striatal dysfunction." Nature **472**(7344): 437-442.

Persico, A. M. and T. Bourgeron (2006). "Searching for ways out of the autism maze: genetic, epigenetic and environmental clues." Trends Neurosci **29**(7): 349-358.

Puvabanditsin, S., M. S. Nagar, M. Joshi, G. Lambert, E. Garrow and E. Brandsma (2010). "Microdeletion of 16p11.2 associated with endocardial fibroelastosis." Am J Med Genet A **152A**(9): 2383-2386.

Quesada-Hernandez, E., L. Caneparo, S. Schneider, S. Winkler, M. Liebling, S. E. Fraser and C. P. Heisenberg (2010). "Stereotypical cell division orientation controls neural rod midline formation in zebrafish." Curr Biol **20**(21): 1966-1972.

Rao, M. and S. Sockanathan (2005). "Transmembrane protein GDE2 induces motor neuron differentiation in vivo." Science **309**(5744): 2212-2215.

Roberts, A., J. Allanson, S. K. Jadico, M. I. Kavamura, J. Noonan, J. M. Opitz, T. Young and G. Neri (2006). "The cardiofaciocutaneous syndrome." J Med Genet **43**(11): 833-842.

Roll, P., G. Rudolf, S. Pereira, B. Royer, I. E. Scheffer, A. Massacrier, M. P. Valenti, N. Roeckel-Trevisiol, S. Jamali, C. Beclin, C. Seegmuller, M. N. Metz-Lutz, A. Lemainque, M. Delepine, C. Caloustian, A. de Saint Martin, N. Bruneau, D. Depetris, M. G. Mattei, E. Flori, A. Robaglia-Schlupp, N. Levy, B. A. Neubauer, R. Ravid, C. Marescaux, S. F. Berkovic, E. Hirsch, M. Lathrop, P. Cau and P. Szepetowski (2006).

"SRPX2 mutations in disorders of language cortex and cognition." Hum Mol Genet **15**(7): 1195-1207.

Rosenfeld, J. A., J. Coppinger, B. A. Bejjani, S. Girirajan, E. E. Eichler, L. G. Shaffer and B. C. Ballif (2010). "Speech delays and behavioral problems are the predominant features in individuals with developmental delays and 16p11.2 microdeletions and microduplications." J Neurodev Disord **2**(1): 26-38.

Roxstrom-Lindquist, K. and I. Faye (2001). "The Drosophila gene Yippee reveals a novel family of putative zinc binding proteins highly conserved among eukaryotes." Insect Mol Biol **10**(1): 77-86.

Sachs, L. (2004). Angewandte Statistik Anwendung statistischer Methoden. Berlin, Springer.

Sawa, A. (2009). "Genetic animal models for schizophrenia: advantages and limitations of genetic manipulation in drosophila, zebrafish, rodents, and primates." Prog Brain Res **179**: 3-6.

Sawamoto, K., H. Wichterle, O. Gonzalez-Perez, J. A. Cholfin, M. Yamada, N. Spassky, N. S. Murcia, J. M. Garcia-Verdugo, O. Marin, J. L. Rubenstein, M. Tessier-Lavigne, H. Okano and A. Alvarez-Buylla (2006). "New neurons follow the flow of cerebrospinal fluid in the adult brain." Science **311**(5761): 629-632.

Schaaf, C. P., R. P. Goin-Kochel, K. P. Nowell, J. V. Hunter, K. A. Aleck, S. Cox, A. Patel, C. A. Bacino and M. Shinawi (2011). "Expanding the clinical spectrum of the 16p11.2 chromosomal rearrangements: three patients with syringomyelia." Eur J Hum Genet **19**(2): 152-156.

Seida, J. K., M. B. Ospina, M. Karkhaneh, L. Hartling, V. Smith and B. Clark (2009). "Systematic reviews of psychosocial interventions for autism: an umbrella review." Dev Med Child Neurol **51**(2): 95-104.

Shahwan, A., M. Farrell and N. Delanty (2005). "Progressive myoclonic epilepsies: a review of genetic and therapeutic aspects." Lancet Neurol **4**(4): 239-248.

Shen, Y., X. Chen, L. Wang, J. Guo, J. Shen, Y. An, H. Zhu, Y. Zhu, R. Xin, Y. Bao, J. F. Gusella, T. Zhang and B. L. Wu (2011). "Intra-family phenotypic heterogeneity of 16p11.2 deletion carriers in a three-generation Chinese family." Am J Med Genet B Neuropsychiatr Genet **156**(2): 225-232.

Shi, L., J. F. Liu, X. M. An and D. C. Liang (2008). "Crystal structure of glycerophosphodiester phosphodiesterase (GDPD) from Thermoanaerobacter tengcongensis, a metal ion-dependent enzyme: insight into the catalytic mechanism." Proteins **72**(1): 280-288.

Shi, L., X. Zhang, R. Golhar, F. G. Otieno, M. He, C. Hou, C. Kim, B. Keating, G. J. Lyon, K. Wang and H. Hakonarson (2013). "Whole-genome sequencing in an autism multiplex family." Mol Autism **4**(1): 8.

Shimizu-Nishikawa, K., K. Kajiwara, M. Kimura, M. Katsuki and E. Sugaya (1995). "Cloning and expression of SEZ-6, a brain-specific and seizure-related cDNA." Brain Res Mol Brain Res **28**(2): 201-210.

Shinawi, M., P. Liu, S. H. Kang, J. Shen, J. W. Belmont, D. A. Scott, F. J. Probst, W. J. Craigen, B. H. Graham, A. Pursley, G. Clark, J. Lee, M. Proud, A. Stocco, D. L. Rodriguez, B. A. Kozel, S. Sparagana, E. R. Roeder, S. G. McGrew, T. W. Kurczynski,

L. J. Allison, S. Amato, S. Savage, A. Patel, P. Stankiewicz, A. L. Beaudet, S. W. Cheung and J. R. Lupski (2010). "Recurrent reciprocal 16p11.2 rearrangements associated with global developmental delay, behavioural problems, dysmorphism, epilepsy, and abnormal head size." J Med Genet **47**(5): 332-341.

Skuse, D. H. (2000). "Imprinting, the X-chromosome, and the male brain: explaining sex differences in the liability to autism." Pediatr Res **47**(1): 9-16.

Sumiyoshi, E., A. Sugimoto and M. Yamamoto (2002). "Protein phosphatase 4 is required for centrosome maturation in mitosis and sperm meiosis in C. elegans." J Cell Sci **115**(Pt 7): 1403-1410.

Summerton, J. and D. Weller (1997). "Morpholino antisense oligomers: design, preparation, and properties." Antisense Nucleic Acid Drug Dev **7**(3): 187-195.

Sunkel, C. E., R. Gomes, P. Sampaio, J. Perdigao and C. Gonzalez (1995). "Gamma-tubulin is required for the structure and function of the microtubule organizing centre in Drosophila neuroblasts." EMBO J **14**(1): 28-36.

Thisse, C. and B. Thisse (2008). "High-resolution in situ hybridization to whole-mount zebrafish embryos." Nat Protoc **3**(1): 59-69.

Tropepe, V. and H. L. Sive (2003). "Can zebrafish be used as a model to study the neurodevelopmental causes of autism?" Genes Brain Behav **2**(5): 268-281.

Tucker, B., R. I. Richards and M. Lardelli (2006). "Contribution of mGluR and Fmr1 functional pathways to neurite morphogenesis, craniofacial development and fragile X syndrome." Hum Mol Genet **15**(23): 3446-3458.

Van Bogaert, P., R. Azizieh, J. Desir, A. Aeby, L. De Meirleir, J. F. Laes, F. Christiaens and M. J. Abramowicz (2007). "Mutation of a potassium channel-related gene in progressive myoclonic epilepsy." Ann Neurol **61**(6): 579-586.

Waga, S. and B. Stillman (1998). "The DNA replication fork in eukaryotic cells." Annu Rev Biochem **67**: 721-751.

Walters, R. G., S. Jacquemont, A. Valsesia, A. J. de Smith, D. Martinet, J. Andersson, M. Falchi, F. Chen, J. Andrieux, S. Lobbens, B. Delobel, F. Stutzmann, J. S. El-Sayed Moustafa, J. C. Chevre, C. Lecoeur, V. Vatin, S. Bouquillon, J. L. Buxton, O. Boute, M. Holder-Espinasse, J. M. Cuisset, M. P. Lemaitre, A. E. Ambresin, A. Brioschi, M. Gaillard, V. Giusti, F. Fellmann, A. Ferrarini, N. Hadjikhani, D. Campion, A. Guilmatre, A. Goldenberg, N. Calmels, J. L. Mandel, C. Le Caignec, A. David, B. Isidor, M. P. Cordier, S. Dupuis-Girod, A. Labalme, D. Sanlaville, M. Beri-Dexheimer, P. Jonveaux, B. Leheup, K. Ounap, E. G. Bochukova, E. Henning, J. Keogh, R. J. Ellis, K. D. Macdermot, M. M. van Haelst, C. Vincent-Delorme, G. Plessis, R. Touraine, A. Philippe, V. Malan, M. Mathieu-Dramard, J. Chiesa, B. Blaumeiser, R. F. Kooy, R. Caiazzo, M. Pigeyre, B. Balkau, R. Sladek, S. Bergmann, V. Mooser, D. Waterworth, A. Reymond, P. Vollenweider, G. Waeber, A. Kurg, P. Palta, T. Esko, A. Metspalu, M. Nelis, P. Elliott, A. L. Hartikainen, M. I. McCarthy, L. Peltonen, L. Carlsson, P. Jacobson, L. Sjostrom, N. Huang, M. E. Hurles, S. O'Rahilly, I. S. Farooqi, K. Mannik, M. R. Jarvelin, F. Pattou, D. Meyre, A. J. Walley, L. J. Coin, A. I. Blakemore, P. Froguel and J. S. Beckmann (2010). "A new highly penetrant form of obesity due to deletions on chromosome 16p11.2." Nature **463**(7281): 671-675.

Wang, X., P. a. McCoy, R. M. Rodriguiz, Y. Pan, H. S. Je, A. C. Roberts, C. J. Kim, J. Berrios, J. S. Colvin, D. Bousquet-Moore, I. Lorenzo, G. Wu, R. J. Weinberg, M. D.

Ehlers, B. D. Philpot, A. L. Beaudet, W. C. Wetsel and Y.-H. Jiang (2011). "Synaptic dysfunction and abnormal behaviors in mice lacking major isoforms of Shank3." Human molecular genetics **20**(15).

Weinstein, B. M., D. L. Stemple, W. Driever and M. C. Fishman (1995). "Gridlock, a localized heritable vascular patterning defect in the zebrafish." Nat Med **1**(11): 1143-1147.

Weiss, L. A., Y. Shen, J. M. Korn, D. E. Arking, D. T. Miller, R. Fossdal, E. Saemundsen, H. Stefansson, M. A. Ferreira, T. Green, O. S. Platt, D. M. Ruderfer, C. A. Walsh, D. Altshuler, A. Chakravarti, R. E. Tanzi, K. Stefansson, S. L. Santangelo, J. F. Gusella, P. Sklar, B. L. Wu, M. J. Daly and C. Autism (2008). "Association between microdeletion and microduplication at 16p11.2 and autism." N Engl J Med **358**(7): 667-675.

Westerfield, M. (2000). The zebrafish book a guide for the laboratory use of zebrafish (Danio rerio). Eugene, Institute of Neuroscience.

Willer, C. J., E. K. Speliotes, R. J. Loos, S. Li, C. M. Lindgren, I. M. Heid, S. I. Berndt, A. L. Elliott, A. U. Jackson, C. Lamina, G. Lettre, N. Lim, H. N. Lyon, S. A. McCarroll, K. Papadakis, L. Qi, J. C. Randall, R. M. Roccasecca, S. Sanna, P. Scheet, M. N. Weedon, E. Wheeler, J. H. Zhao, L. C. Jacobs, I. Prokopenko, N. Soranzo, T. Tanaka, N. J. Timpson, P. Almgren, A. Bennett, R. N. Bergman, S. A. Bingham, L. L. Bonnycastle, M. Brown, N. P. Burtt, P. Chines, L. Coin, F. S. Collins, J. M. Connell, C. Cooper, G. D. Smith, E. M. Dennison, P. Deodhar, P. Elliott, M. R. Erdos, K. Estrada, D. M. Evans, L. Gianniny, C. Gieger, C. J. Gillson, C. Guiducci, R. Hackett, D. Hadley, A. S. Hall, A. S. Havulinna, J. Hebebrand, A. Hofman, B. Isomaa, K. B. Jacobs, T. Johnson, P. Jousilahti, Z. Jovanovic, K. T. Khaw, P. Kraft, M. Kuokkanen, J. Kuusisto, J. Laitinen, E. G. Lakatta, J. Luan, R. N. Luben, M. Mangino, W. L. McArdle, T. Meitinger, A. Mulas, P. B. Munroe, N. Narisu, A. R. Ness, K. Northstone, S. O'Rahilly, C. Purmann, M. G. Rees, M. Ridderstrale, S. M. Ring, F. Rivadeneira, A. Ruokonen, M. S. Sandhu, J. Saramies, L. J. Scott, A. Scuteri, K. Silander, M. A. Sims, K. Song, J. Stephens, S. Stevens, H. M. Stringham, Y. C. Tung, T. T. Valle, C. M. Van Duijn, K. S. Vimaleswaran, P. Vollenweider, G. Waeber, C. Wallace, R. M. Watanabe, D. M. Waterworth, N. Watkins, C. Wellcome Trust Case Control, J. C. Witteman, E. Zeggini, G. Zhai, M. C. Zillikens, D. Altshuler, M. J. Caulfield, S. J. Chanock, I. S. Farooqi, L. Ferrucci, J. M. Guralnik, A. T. Hattersley, F. B. Hu, M. R. Jarvelin, M. Laakso, V. Mooser, K. K. Ong, W. H. Ouwehand, V. Salomaa, N. J. Samani, T. D. Spector, T. Tuomi, J. Tuomilehto, M. Uda, A. G. Uitterlinden, N. J. Wareham, P. Deloukas, T. M. Frayling, L. C. Groop, R. B. Hayes, D. J. Hunter, K. L. Mohlke, L. Peltonen, D. Schlessinger, D. P. Strachan, H. E. Wichmann, M. I. McCarthy, M. Boehnke, I. Barroso, G. R. Abecasis, J. N. Hirschhorn and A. T. C. Genetic Investigation of (2009). "Six new loci associated with body mass index highlight a neuronal influence on body weight regulation." Nat Genet **41**(1): 25-34.

Woolfe, A., M. Goodson, D. K. Goode, P. Snell, G. K. McEwen, T. Vavouri, S. F. Smith, P. North, H. Callaway, K. Kelly, K. Walter, I. Abnizova, W. Gilks, Y. J. Edwards, J. E. Cooke and G. Elgar (2005). "Highly conserved non-coding sequences are associated with vertebrate development." PLoS Biol **3**(1): e7.

Yan, Q. J., M. Rammal, M. Tranfaglia and R. P. Bauchwitz (2005). "Suppression of two major Fragile X Syndrome mouse model phenotypes by the mGluR5 antagonist MPEP." Neuropharmacology **49**(7): 1053-1066.

Yanaka, N. (2007). "Mammalian glycerophosphodiester phosphodiesterases." Biosci Biotechnol Biochem **71**(8): 1811-1818.

Yanaka, N., Y. Nogusa, Y. Fujioka, Y. Yamashita and N. Kato (2007). "Involvement of membrane protein GDE2 in retinoic acid-induced neurite formation in Neuro2A cells." FEBS Lett **581**(4): 712-718.

Yang, K., a. M. Sheikh, M. Malik, G. Wen, H. Zou, W. T. Brown and X. Li (2011). "Upregulation of Ras/Raf/ERK1/2 signaling and ERK5 in the brain of autistic subjects." Genes, brain, and behavior: 1-10.

Zhang, S., M. B. Feany, S. Saraswati, J. T. Littleton and N. Perrimon (2009). "Inactivation of Drosophila Huntingtin affects long-term adult functioning and the pathogenesis of a Huntington's disease model." Dis Model Mech **2**(5-6): 247-266.

Zhang, X., Y. Ozawa, H. Lee, Y. D. Wen, T. H. Tan, B. E. Wadzinski and E. Seto (2005). "Histone deacetylase 3 (HDAC3) activity is regulated by interaction with protein serine/threonine phosphatase 4." Genes Dev **19**(7): 827-839.

Zhou, G., K. A. Mihindukulasuriya, R. A. MacCorkle-Chosnek, A. Van Hooser, M. C. Hu, B. R. Brinkley and T. H. Tan (2002). "Protein phosphatase 4 is involved in tumor necrosis factor-alpha-induced activation of c-Jun N-terminal kinase." J Biol Chem **277**(8): 6391-6398.

Zou, H., Y. Yu, A. M. Sheikh, M. Malik, K. Yang, G. Wen, K. K. Chadman, W. T. Brown and X. Li (2011). "Association of upregulated Ras/Raf/ERK1/2 signaling with autism." Genes Brain Behav **10**(5): 615-624.

7 Supplementary

7.1 Detailed protocol of whole mount in situ hybridization

Re-hydration

- 75 % methanol / PBS 5 min
- 50 % methanol / PBS 5 min
- 25 % methanol / PBS 5 min
- PBST 5 min

Permeabilization and hybridization

- Proteinase K 10 µg/ml in PBST
- 4 % PFA / PBS 20 min.
- 5 min PBST / **repeat 3x**
- Wash in 50 % hyb(+)/ PBST
- Wash in 100 % hyb(+)
- Aliquote embryos into multiple tubes containing 0.5 ml hyb(+) mix and incubate at 65°C for 4 hrs.
- replace with new hyb(+) (150 µl / tube) add DIG-labeled RNA probe (1 ng/µl) incubate at 65°C overnight

Post-hybridization washes

- hyb mix (HM-), brief wash at 65°C
- 75 % HM- / 2x SSC 10 min at 65°C
- 50 % HM- / 2x SSC 10 min at 65°C
- 25 % HM- / 2x SSC 10 min at 65°C
- 2x SSC 10 min at 65°C
- 0.2x SSC 25 min at 65°C / **repeat 3x**

The following washes are performed at room temperature (RT)

- 75 % 0.2x SSC / PBST 5 min
- 50 % 0.2x SSC / PBST 5 min
- 25 % 0.2x SSC / PBST 5 min
- PBST, 5 min **repeat 2x**

Blocking

Replace PBST with blocking solution and incubate at 4°C overnight

Antibody incubation

Renew blocking solution add 1:5000 anti-DIG antibody. 4 h RT gently shaking (40 rpm)

Washing

- PBST 15 min **repeat 6x**
- AP buffer 5 min **repeat 2x**

Staining

Transfer embryos into a 24-well cell culture plate, replace AP buffer with staining solution (10 ml AP buffer, 45 µl NBT, 35 µl BCIP). The coloring is light sensitive.

- when the desired staining is reached, stop coloring by taking of as much staining solution as possible
- wash 3x with PBS
- replace PBS with 100 % glycerol (shake gently overnight, 40rpm)
- store at 4°C

Solutions

Hybridization mix (HM+) / HM- without heparin and tRNA

- 25 ml formamide (in the fridge)
- 12.5 ml 20x SSC (DEPC stock)
- 460 µl citric acid (1 M stock solution)
- 250 µl Tween (20 % stock solution)
- 250 µl tRNA (50 mg/ml stock solution in -20°C)
- 50 µl heparin (50 mg/ml stock solution in -20°C)
- add DEPC-treated water up to 50 ml

Blocking solution

PBST with 2 mg/ml BSA and 2 % sheep serum.

AP buffer

- 1 ml NaCl (5 M stock solution)
- 5 ml Tris, pH 9.5 (1 M stock solution)
- 2.5 ml $MgCl_2$ (1 M stock solution)
- 5 ml Tween (10 % stock solution)
- add sterilised water (not DEPC) up to 50 ml

7.2 Detailed protocol of whole mount RNA in situ hybridization

Day1

Deparaffinization / re-hydration

- 2 x 15 min Ultra Clear
- 2 x 10 min 100 % EtOH
- 5 min 75 % EtOH / H_2O-DEPC
- 5 min 50 % EtOH / PBS-DEPC
- 5 min 25 % EtOH / PBS-DEPC
- 2 x 5 min PBS-DEPC

Post fixing

- 15 min 4 % PFA / PBS room temperature (RT)
- Rinse in PBST-DEPC
- 2 x 5 min PBST-DEPC
- Proteinase K 15 µl (20 mg/ml) in 200 ml PBS- DEPC 10 min
- Rinse in PBST- DEPC
- 2 x 5 min PBST- DEPC
- 5 min 4 % PFA / PBS (RT), re-use PFA from before
- Rinse in PBST-DEPC
- 2 x 5 min PBST-DEPC
- Acetylation (prepare fresh 1 M stock at 4°C, keep in the dark)
  10 min 0.1 M TEA, 500 µl acetic anhydride, add to 200 ml H_2O DEPC
- Rinse in PBST-DEPC
- 2 x 5 min PBST-DEPC

Prehybridization

- put slides into a wet chamber (5x SSC/ 50 % formamide) and apply 150 µl pre-warmed hybridization buffer and add coverslip on each slide
- pehybridization for 1 - 4 h (longer prehybridization will give better results)

Hybridization

- Add 1 µl of labeled probe per 100 µl hybridization buffer and heat up to 65°C for 5 min
- Carefully lift the coverslip and apply the probe
- Incubate at 65°C overnight (seal chamber with tape)

Day 2

Post hybridization washes

- prewarm solutions
- set water bath at 37°C heat RNAse wash buffer to 37°C
- lift cover slips in 5x SSC
- 30 min 1x SSC/ 50 % Formamide 65°C
- 10 min RNAse wash buffer 37°C
- 30 min RNAse wash buffer (200 ml) + RNAse (10 mg/ml) 400 µl 37°C
- 10 min RNAse wash buffer
- 20 min 2x SSC 65°C
- 20 min 0.2x SSC 65°C
- 20 min 0.2x SSC 65°C

Antibody incubation

- wash 2x, 5 min MABT (fresh) at room temperature (RT)
- blocking in 20 % HISS/ MABT > 1 h at RT
- (Prepare during blocking) antibody preincubation 5 % HISS/ MABT antiDIG AB 1:2500 at 4°C > 2 h
- add 0.05 % Tween20 to antibody solution
- put 400 µl on each slide and cover with parafilm
- incubate 4°C overnight in wet chamber

Day 3

Antibody detection / staining

- lift cover slips in MABT
- wash 3x 5 min MABT
- 10 min ALP- buffer (fresh)
- coloring 200 ml ALP + 70 µl NBT/BCIP (each)
- place cuvette aluminium wrap on rocking platform at day RT overnight or weekend 4°C

Stop staining

- wash in ALP
- wash 2x, 5 min PBS
- 30 min 4 % PFA/PBS RT (re-use from day 1)
- wash 2x, 5 min PBS
- cover in hydro matrix, dry overnight

PBST

- 1x PBS +-0.1 % Tween20

Triethanolamine TEA

- Stock 1 M

Hybridisation buffer

- 1 ml Tris 1 M pH 7.5
- 12ml NaCL 5 M
- 200 µl EDTA 0.5 M
- 1.25 ml SDS 20 %
- 25 ml dextran sulfate 40 %
- 2 ml Denhardt's solution
- 2ml tRNA (yeast, Gibco 10 mg/ml)
- 50 ml formamid

➢ Add to 100 ml H_2O DEPC
➢ Aliquot 8ml, store at -20°C

MABT-buffer

- 100 ml maleic acid 1 M (pH7.0 ~70g NaOH pellets)
- 30 ml NaCl 5 M
- 0.05 % Tween20

➢ Add to 1000 ml H_2O bidistilled

ALP-buffer

- 16 ml NaCl 5 M
- 80 ml Tris 1 M pH 9.5
- 40 ml Mg_2Cl 1 M
- 4 ml Tween20 10 %

➢ Add to 800 ml with H_2O bidistilled

7.3 gdpd3 alignment

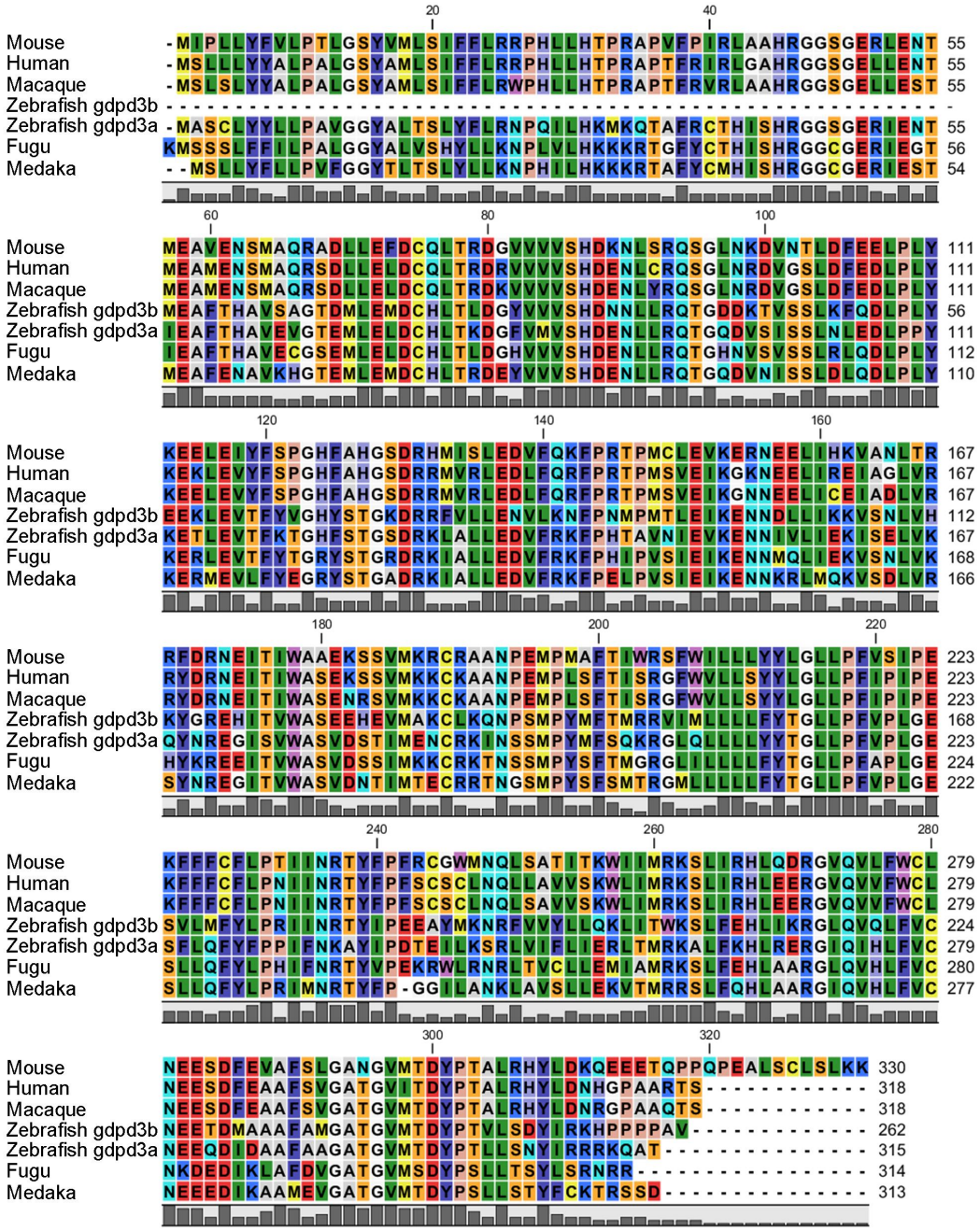

Figure 64 *gdpd3* alignment shows truncation of zebrafish *gdpd3b*
Alignment based on zebrafish *gdpd3a* GI:47085996 and *gdpd3*b GI:528495324; *gdpd3* fugu (*Takifugu rubripes*) ENSTRUG00000005467; *gdpd3* medaka (*Oryzias latipes)* ENSORLG00000011954; *gdpd3* macaque (*Macaca mulatta*) GI:302564980; *gdpd3* human (*Homo sapiens*) GI:146198639; *gdpd3* mouse (*Mus musculus*) GI:110431345

7.4 Gene IDs and Vectors

Table 29 Gene list of the 16p11.2 CNV and the orthologous zebrafish genes

Human		Zebrafish			
Gene	Ensembl ID	Gene	Ensembl ID	Chr	strand
SPN	ENSG00000197471	-			
QPRT	ENSG00000103485	-			
C16orf54	ENSG00000185905	-			
HIRIP3	ENSG00000149929	hirip3	ENSDARG00000027749	3	-
KCTD13	ENSG00000174943	*kctd13*	ENSDARG00000044769	3	-
SEZ6L2	ENSG00000174938	SEZ6L2	ENSDARG00000076052	3	-
ASPHD1	ENSG00000174939	ASPHD1	ENSDARG00000075813	3	+
DOC2A	ENSG00000149927	DOC2A	ENSDARG00000078736	3	+
MVP	ENSG00000013364	mvp	ENSDARG00000021242	3	-
FAM57B	ENSG00000149926	fam57ba	ENSDARG00000026875	3	-
CDIPT	ENSG00000103502	cdipt	ENSDARG00000070686	3	-
TAOK2	ENSG00000149930	TAOK2	ENSDARG00000074899	3	-
PPP4C	ENSG00000149923	*ppp4ca*	ENSDARG00000070570	3	+
MAPK3	ENSG00000102882	*mapk3*	ENSDARG00000070573	3	+
GDPD3	ENSG00000102886	*gdpd3*	ENSDARG00000074466	3	+
YPEL3	ENSG00000090238	ypel3	ENSDARG00000055510	3	+
CORO1A	ENSG00000102879	coro1a	ENSDARG00000054610	3	-
ALDOA	ENSG00000149925	aldoaa	ENSDARG00000011665	3	+
TBX6	ENSG00000149922	tbx6l	ENSDARG00000006939	5	+
c16orf53	ENSG00000185928	C12H16orf53	ENSDARG00000076966	12	+
FAM57B	ENSG00000149926	fam57bb	ENSDARG00000074564	12	-
MAZ	ENSG00000103495	MAZ (1of2)	ENSDARG00000063555	12	-
TAOK2	ENSG00000149930	taok2b	ENSDARG00000079261	12	-
GDPD3	ENSG00000102886	GDPD3 (2 of 2)	ENSDARG00000006944	12	-
TBX6	ENSG00000149922	tbx6	ENSDARG00000011785	12	+
PPP4C	ENSG00000149923	*ppp4cb*	ENSDARG00000076439	12	-
ALDOA	ENSG00000149925	aldoab	ENSDARG00000034470	12	-
PRRT2	ENSG00000167371	PRRT2	ENSDARG00000089367	12	-
KIF22	ENSG00000079616		ENSDARG00000077375	12	-
INO80E	ENSG00000169592	INO80E	ENSDARG00000022939	16	+
MAZ	ENSG00000103495	MAZ (2of2)	ENSDARG00000087330	21	-

Table 30 Vector used for cloning of gene fragments for RNA synthesis

gene fragment of	vector	cloned by
asphd1	pCRII	Magdalena Ciurkiewicz
gdpd3a	pCRII	Magdalena Ciurkiewicz
kctd13	pCRII	Magdalena Ciurkiewicz
mapk3	pCRII	Magdalena Ciurkiewicz
ppp4ca	pCRII	Magdalena Ciurkiewicz
ppp4cb	pCRII	Magdalena Ciurkiewicz
sez6l2	pCRII TOPO	Udo Georgi
ypel3	pCRII	Magdalena Ciurkiewicz

7.5 Zebrafish measurements

Table 31 Head size body length measurement of *asphd1* knockdown and control embryos

asphd1 5'UTR 2 dpf		*asphd1* 5'UTR 3 dpf		*asphd1* 5'UTR 4 dpf		SCMO 2 dpf		SCMO 3 dpf		SCMO 4 dpf	
head size	body length	head size	body length	head size	body length	head size	body length	head size	body length	head size	body length
415,75	2952,54	408,5	3219,3	482,21	3442,63	487,82	3179,59	498,46	3249,83	617,43	3824,93
426,7	2924,62	467,19	3223,53	572,59	3650,96	524,88	3232,39	576,35	3543,47	596,04	3864,21
432,37	2979,93	497,25	3083,37	544,15	3430,71	472,41	3056,21	556,61	3548,68	613,85	3701,94
399,25	2918,59	452,78	3172,81	520,47	3506,31	418,74	2696,14	563,45	3591,79	606,5	3716,17
400,27	2926,78	491,6	3290,41	566,2	3696,77	480,45	3058,32	576	3560,84	618,97	3830,83
405,52	2894,84	434,86	3173,19	579,78	3814,53	479,75	3155,58	532,06	3426,61	606,85	3801,05
404,94	2938,25	516,45	3322,04	558,1	3345,73	491,76	3151,55	572,85	3585,19	667,44	4013,94
413,53	2882,67	493,15	3392,84	545,85	3386,68	458,98	3097,15	551,92	3469,59	574,52	3776,59
407,91	2982,31	505,1	3343,58	588,65	3703,74	451,47	3079,47	541,13	3428,08	651,66	3833,21
369,81	2737,35	456,85	3198,73	559,49	3571,92	478,35	3094,05	575,34	3412	594,05	3832,44
428,24	2989,84	518,12	3221,54	580,97	3519,11	438,57	3131,97	531,83	3450,53	607,21	3800,56
370,63	2871,74	471,17	3270,09	590,82	3562,97	473,42	3098,01	549,58	3598,5	636,95	3903
452,99	3085,22	468,58	3114,26	571,98	3526,87	479,91	3079,3	540,59	3292,16	602,8	3802,87
411,76	2884,24	491,89	3240,12	607,662	3614,94	475,53	2986,88	534,23	3331,61	614,29	3859,05
411,43	2951,23	499,59	3110,25	511,63	3283,44	422,42	3102,02	506,51	3274,79	630,45	3598,98
397,54	2751,79	540,81	3397,41	566,59	3604,82	412,36	2912,74	552,19	3369,94	645,64	4000,95
390,95	2809,73	494,54	3219,8	585,29	3458,94	459,88	3007,98	502,06	3124,8	654,2	4074,2
440,04	2991,01	522,7	3473,68	562,68	3463,62	451,68	3058,98	554,24	3545,07	643,86	3725,35
427,2	3142,71	484,28	3211,58	582,5	3640,5	488,51	3178,76	543,67	3437,95	626,01	3647,28
431,6	3013,01	522,62	3344,08	544,15	3546,8	484,68	3135,32	518,52	3286,81	602	3718,05
406,25	3006,29	532,11	3312,8	524,25	3355,9	431,54	2669,95	563,45	3554,78	654,2	3868,89
412,89	2926,23	463,86	3111,87	523,45	3505,58	483,64	3173,53	543,62	3375,49	636,53	3889,48
431,82	3121,09	533,33	3413,38	557,72	3487,07	463,08	3052,75	545,02	3340,53	617,41	3837,24
411,81	2820,62	468,75	3224,36	545,24	3570	430,61	3077,24	542,7	3494,19	623,47	3895,2
411,9	2887,37	464,84	3365,81	557,1	3517,34	453,03	2955,93	573,96	3616,64	643,29	3719,86
423,28	2945,21	473,15	3158,58	520,59	3225,68	472,71	3095,66	508,16	3346,32	626,01	3706,22
382,89	2871,62	495,67	3266,77	561,12	3405,1	466,62	3143,26	576,85	3496,28	628,76	3792,56
423,93	3059,9	451,1	2969,45	570	3575,14	418,32	2925,35	544,21	3565,2	584,72	3671,75
419,58	2769,05	554,23	3379,46	560,64	3543,24	450,8	2983,41	556,61	3443,87	646,81	3773,99
404,94	2822,11	434,01	3122,3	523,05	3347,29	475,39	3130,47	551,42	3456,38	574,52	3753,09
407,91	2913,87	437,04	3130,26	562,06	3632,33	487,73	3058,12	544,6	3434,21	606,47	3719,11
357,89	2650,58	491,42	3257,46	527,56	3393,52	509,49	3082,66	544,55	3524,78	606,99	3768,08
419,72	3157,3	505,32	3312,4	487,4	3362,91	467,62	3116,19	576	3538		
386,03	2828,72	473,6	3185,3	558,52	3756,58	378,84	2809,01	559,8	3572,2		
393,7	2871,37	490,65	3217,51	481,8	3246,55	401,61	2872,44	543,59	3601,95		
377,18	2674,53	537,35	3308,71	488,39	3302,48	400,46	2908,21	551,43	3595,92		
404,12	2762,51	477,76	3261,96	584,72	3481,07	467,25	3142,18	543,83	3350,89		
374,23	2739,47	455,13	3164,56	601,34	3753,46	491,03	3179,63	521,34	3383,17		
388,67	2778,94	476,31	3230,07	573,36	3569,69	430,61	3081,72	541	3476,16		
438,64	2943,39	462,72	3135,51	536,53	3506,57	468,63	3184,27	530,8	3238,46		
381,5	2900,06	502,85	3034,15	543,25	3498,96	467,19	3221,81	571,27	3448,82		
405,51	2931,34	513,61	3150,18	527,65	3452,55	438,51	3080,08	563,93	3403,14		
366,37	2697,7	507,03	3295,86	584,72	3467,34	484,19	3226,38	547,59	3587,81		
415,46	2840,22	514,89	3235,78	542,22	3372,61	479,75	3172,01	571,82	3520,42		
435,44	3129,49	493,29	3195,36	568,87	3684,04	424,95	2839,96	568,04	3523,89		
454,95	2944,89	479,96	3250,24	512,21	3005,05	407,77	2952,91	555,94	3578,5		
408,27	2892,31	513,69	3217,85	541,5	3374,99	447,36	3030,32	555,71	3480,12		
451,02	3005,81	387,88	2815,98	585,29	3692	471,34	3118,56	544,36	3389,84		
402,35	2867,78	483,42	3233,82	619,29	3779,24	448,95	3087,69	517,7	3471,85		

asphd1 5'UTR 2 dpf		*asphd1* 5'UTR 3 dpf		*asphd1* 5'UTR 4 dpf		SCMO 2 dpf		SCMO 3 dpf		SCMO 4 dpf	
head size	body length	head size	body length	head size	body length	head size	body length	head size	body length	head size	body length
333,63	2825,57	488,85	3257,99	521,54	3547,84	463,08	2975,58	482,38	3331,27		
435,1	2869,39	500,83	2965,3	592,1	3605,2	427,65	2793,03	574,74	3533,57		
403,31	2827,15	501,47	3361,91	562,06	3534,97	462,28	3073,8	570,76	3437,09		
399,25	2867,78	460,03	3174,67	552,86	3371,83	438,66	3027,75	509,47	3376,99		
407,53	2874,35	442,35	3113,22	548,62	3364,78	434,87	3083,86	506,79	3310,74		
421,57	2906,54	550,12	3516,62	533,79	3370,76	476,5	3115,39	505,02	3076,05		
425,03	3013,36	449,86	3119,51	572,26	3593,15	460,19	3076,5	535,8	3399,6		
400,66	2989,92	504,86	3230,26	451,78	2885,8	454,69	3046,83	517,75	3100,62		
415,66	2920,66	473,06	3143,5	438,48	3121,28	476,11	3104,51	512,47	3442,73		
390,25	2811,23	507,03	3274,48	560,64	3423,67	474,75	3090,85	524,33	3371,61		
346,43	2633,4	512,52	3330,83	563,05	3554,85	459,05	3099,55	543,83	3484,8		
361,8	2655,85	423,53	3025,03	548,2	3409,1	462,86	2983,31	498,96	3090,07		
420,07	2995,58	488,27	3410,75	578,76	3670,74	439,18	2906,78	554,24	3441,66		
406,44	2901,67	529,89	3343,34	516,67	3308,76	442,61	2971,55	560,22	3509,92		
434,95	2949,33	523,75	3276,95	521,75	3399,86	415,6	2931,07	576,72	3356,96		
427,15	2969,2	449,26	3038,63	509,09	3331,72	446,69	3094,47	563,04	3402,95		
415,34	2922,03	402,59	3004,04	429,91	3153,9	497,89	3125,64	469,88	3226,73		
404,06	2884,48	469,95	3247	570,78	3479,08	414,63	2873,78	540,35	3505,04		
431,6	2929,46	525,02	3541,97	499,12	3240,57			528,4	3309,36		
411,31	2854,75	381,31	2996,18	548,8	3415,81						
374,51	2711	466,3	3145,54	554,18	3430,62						
434,42	2979,04	440,72	3117,7	594,48	3687,23						
457,45	3023,05	473,75	3092,97	529,59	3488,88						
413,53	2973,33	432,9	3067,17	537,38	3527,05						
		500,61	3331,06	483,14	3192,45						
		542,09	3489,82	541,19	3505,04						
		432,41	2961,97	566,95	3526,68						
		449,86	3011,64	582,95	3596,07						
		565,41	3624,2	495,28	3439,79						
		448,78	3224,8	543,54	3580,28						
		486,81	3393,67	481,01	3283,8						
		455,19	3108,04	576,76	3776,49						
		476,88	3233,64	549,79	3595,74						
		450,14	3093,43	575,94	3321,95						
		481,09	3372,93	477,34	3274,2						
		418,23	3051,72	557,51	3484,48						
		443,82	3182,24	560,11	3573,19						
		505,72	3322,36	450,88	3048						
		478,96	3337,5	507,95	3355,86						
		501,89	3358,36	499,48	3304,94						
		451,76	3027,85	576,95	3522,77						
		535,19	3446,86	511,53	3462,23						
		447,13	3201,21	571,38	3607,98						
		428,13	2913,87	528,99	3400,24						
		453,08	3019,71	527,9	3300,28						
		438,92	3190,67	495,16	3327,34						
		476,58	3225,74	543,44	3446,03						
		409,82	3167,8	503	3209,39						
		421,18	3017,45	523,86	3467,54						
		476,41	3258,48	542,43	3605,34						
		540,45	3425,13	556,52	3651,33						
		477,2	3361,81	612,46	3689,92						
		436,48	3073,31	540,06	3538,47						
		411,98	3014,26	627,89	3943,43						
		545,41	3507,88	554,27	3477,54						
		477,01	3385,34	600,13	3793,25						
		390,16	2969,54	510,44	3484,16						
		442,81	3068,49	575,59	3699,6						
		518,01	3494,05	562,95	3628,86						
		508,05	3383,51	537,9	3252,97						
		524,14	3462,79	493,33	3318,06						
		450,23	3114,11	483,86	3161,64						
		469,93	3213,01	534,11	3462,24						
		490,65	3200,92	586,72	3683,46						
		442,54	3217,46	508,99	3462,16						
		490,51	3217,97	504,45	3205,45						
		489,78	3350,59	582,8	3698						
		486,95	3277,76	506,02	3235,89						
		415,43	3090,81	550,58	3420,37						
		429,46	3161,06	438,61	3204,76						
		471,45	3105,63	483,96	3264,6						
		546,55	3360,94	500,18	3282,04						
		455,81	3131,16	446,22	3215,61						
		477,41	3117,83	498,74	3232,72						
		487,75	3198,75	518,01	3135,59						
		463,06	3210,53	492,87	3310,81						
		442,22	3116,78	492,33	3310,25						

	asphd1 5'UTR 2 dpf		*asphd1* 5'UTR 3 dpf		*asphd1* 5'UTR 4 dpf		SCMO 2 dpf		SCMO 3 dpf		SCMO 4 dpf	
	head size	body length	head size	body length	head size	body length	head size	body length	head size	body length	head size	body length
			473,57	3188,28	613,27	3709,67						
			490,4	3241,54	541,34	3338,36						
			445,67	3121,36	402,4	2926,53						
			481,38	3220,16	447,11	3110						
			466,04	3283,43	588,02	3614,03						
			566,52	3549,75	600,13	3784,69						
			468,2	3119,65	456,76	3145,51						
					563,82	3530,43						
Average	408,33	2899,68	477,90	3220,29	538,92	3452,87	456,68	3048,33	542,82	3427,14	620,62	3803,78
Standard deviation	24,77	114,01	38,22	144,85	43,30	190,39	28,41	119,04	24,89	129,35	23,49	104,94
Number of embryos	73	73	133	133	134	134	67	67	68	68	32	32

Table 32 Head size body length measurement of *kctd13* knockdown and control embryos

kctd13 5'UTR 3 dpf		*kctd13* 5'UTR 4 dpf		SCMO 3 dpf		SCMO 4 dpf	
head size	body length	head size	body length	head size	body length	head size	body length
448,89	3146,06	554,36	3506,05	545,82	3446,69	612,1	3719,45
452,95	3279,11	563,91	3509,01	541,53	3334,71	624,93	3938,76
460,7	3296,25	591,4	3519,17	520,19	3189,24	602,6	3775,22
462,67	3234,74	564,79	3526,12	538,25	3429,87	588,91	3613,04
468,34	3059,66	583,76	3537,97	503,59	3403,25	626,15	3869
470,38	3277,68	595	3540,11	492,75	3316,73	577,32	3674,45
472,2	3350,75	598,56	3546,06	549,26	3427,75	616,49	3914,87
473,24	3307,97	603,63	3546,38	532,55	3312,17	560,33	3606,46
474,16	3373,21	637,97	3548,84	514,92	3444,75	591,32	3797
477,39	3360,71	581,59	3557,39	548,65	3421,17	606,69	3806,76
477,6	3460,87	642,62	3558,3	516,63	3228,87	601,61	3709,7
478,15	3207,1	561,81	3582,34	523,71	3464,18	566,11	3696,31
478,24	3400,6	568,11	3595,4	527,46	3542,43	610,65	3827,62
481,48	3342,4	610,46	3597,45	543,81	3395,74	616,95	3763,24
482,02	3293,35	616,83	3605,04	509,9	3163,93	554,45	3647,66
484,37	3249,31	575,39	3608,46	497,3	3295,02	628,03	3770,55
484,75	3404,45	588,38	3613,05	556,05	3473,68	595,82	3765,75
485,35	3256,24	593,75	3625,04	540,21	3388,85	547,35	3698,7
485,35	3333,44	580,44	3626,06	554,9	3604,32	630,67	3733,81
485,63	3272,24	615,75	3629,81	502,38	3477,23	607,88	3582,44
488,08	3274,96	644,83	3638,04	516,58	3404,73	605,65	3807,91
490,81	3328,67	641,36	3642,44	532,55	3361,3	556,32	3607,31
491,39	3309,77	666,67	3643,49	504,04	3307,37	602,17	3722,91
491,69	3406,16	620,27	3650,92	562,5	3498,31	613,8	3763,07
491,82	3421,65	640,29	3658,36	535,69	3465,91	607,16	3800,21
494,53	3307,7	573,76	3659,13	551,74	3589,91	603,63	3725,14
495,21	3368,03	618,96	3666,85	502,64	3282,46	633,16	3989,94
495,83	3452,4	681,76	3669,6	441,99	3239,53	601,57	3646,44
496,24	3406,83	677,88	3673,12	574,92	3521,93	623,28	3882,24
498,76	3363,77	603,86	3674,15	521,31	3239,4	613,14	4000,9
498,89	3340,17	670,8	3675,03	534,69	3480,55	638,34	3858,43
502,01	3421,9	583,73	3675,21	558,37	3500,56	618,51	3810,45
502,34	3318,62	695,04	3678,99	534,82	3375,48	623,5	3749,81
502,64	3299,48	583,73	3680,14	568,15	3483,84	589,13	3809,36
502,64	3368,31	646,02	3680,19	506,34	3329,74	610,24	3788,01
503,13	3600,39	646,02	3680,19	541,35	3431,05	641,75	3987,65
503,35	3322,55	610,89	3680,85	518,97	3506,29	607,63	3881,03
508,34	3314,61	609,21	3684,48	520,99	3308,43	627,44	3819,76
510,88	3284,75	573,78	3685,39	553,59	3537,9	609,3	3883,76
511,24	3084,54	638,91	3696,96	541,35	3500,6	598,6	3633
511,92	3184,33	614,23	3697,59	559,43	3541,34	641,67	3941,23
512,63	3448,83	667,12	3697,79	553,59	3641,5	623,28	3853,78
513,32	3364,57	587,07	3698,33	509,09	3475,62	606,31	3833,45
513,81	3199,85	612,86	3699,23	539,38	3525,75	630,83	3848,72
514,92	3319,03	597,32	3718,32	506	3321,35	599,37	3787,18
514,95	3424,24	627,03	3722,98	539,65	3637,91	613,14	3822,47
515,79	3593,69	602,09	3727,38	519,52	3565,25	598,78	3857,36
516,88	3356,2	674,31	3729,67	518,06	3739,62	642,12	3855,42
520,72	3357,37	576,49	3730,12	539,65	3522,31	612,77	3762,35
522,88	3452,41	597,91	3734,69	531,02	3559,75	611,54	3733,63
522,88	3618,27	698,41	3738,02	538,06	3555,77	609,58	3747,88
523,65	3391,8	690,91	3741,07	512,48	3553,52	591,78	3787,05
524,3	3530,58	610,96	3743,41	539,65	3642,31	641,29	3728,43
525	3429,17	645,31	3745,24	558,25	3518,87	635,8	3993,37
525	3435,8	656,02	3747,08	533,51	3568,79	632,28	3794,45
525,53	3404,19	610,83	3748,59	548,05	3534,91	627,06	3812,31

kctd13 5'UTR 3 dpf		*kctd13* 5'UTR 4 dpf		SCMO 3 dpf		SCMO 4 dpf	
head size	body length	head size	body length	head size	body length	head size	body length
526,42	3527,03	664,02	3758,62	498,98	3307,85	589,98	3819,38
526,79	3450,75	633,75	3769,14	502,44	3345,43	623,5	3846,83
527,12	3403,54	598,98	3773,43	546,48	3459,27	608,37	3741,47
527,85	3562,64	593,04	3774,75	483,53	3251,77	619,66	3819,21
530,73	3351,01	718,06	3778,65	541,81	3490,71	598,6	3702,12
530,73	3466,85	670,91	3780,88	495,52	3401,01	609,28	3797,74
531,13	3553,85	619,98	3790,13	538,66	3523,13	622,23	3876,44
533,88	3556,74	634,5	3792,11	502,87	3277,52	636,67	3772,35
536,58	3476,15	656,14	3803,54	525,44	3461,27	582,44	3843,97
537,81	3337,48	680,02	3816,27	506,69	3438,57		
538,25	3437,07	602,75	3830,75				
539,47	3389,37	648,4	3840,49				
539,47	3422,4	672,84	3843,55				
539,6	3492,84	596,02	3849,86				
539,94	3408,47	699,58	3851,17				
540,6	3577,46	604,07	3865,67				
541,81	3331,18	670,91	3874,31				
541,94	3427,22	655,76	3886,25				
543,49	3449,19	623,74	3888,01				
543,81	3378,16	723,43	3890,72				
543,81	3615,07	613,43	3894,56				
545,3	3525,3	687,87	3917,09				
545,82	3539,5	658,49	3918,29				
546,18	3450,78	649,8	3933,15				
546,75	3583,84	646,18	3982,79				
548,05	3607,11	680,79	3998,23				
548,08	3446,73	630,29	4004,44				
549,17	3575,43	655,56	4005,6				
549,26	3476,5	644,92	4038,36				
549,58	3469,99	630,29	4049,57				
550,3	3457,92	643,49	4052,18				
550,68	3460,93	657,73	4143,35				
550,68	3605,35						
553,59	3558,05						
555,26	3469,45						
556,18	3480,63						
558,25	3577,4						
560,78	3534,12						
561,78	3665,66						
561,87	3530,33						
562,94	3466,1						
564,58	3428,33						
564,79	3633,91						
570,83	3601,38						
571,89	3616,04						
572,87	3523,11						
577,54	3584,27						
585,15	3704,86						
601,57	3835,5						
610,65	3815,67						
619,73	3957,28						
Average	522,61	3431,85	628,31	3736,22	**542,82**	**3427,14**	**620,62**	**3803,78**
Standard deviation	34,49	146,06	39,30	141,37	**24,89**	**129,35**	**23,49**	**104,94**
Number of embryos	107	107	88	88	**68**	**68**	**32**	**32**

Table 33 Head size body length measurement of *ppp4ca* 5'UTR morpholino knockdown and control embryos

ppp4ca 5'UTR 2 dpf		*ppp4ca* 5'UTR 3 dpf		*ppp4ca* 5'UTR 4 dpf		SCMO 2 dpf		SCMO 3 dpf		SCMO 4 dpf	
head size	body length	head size	body length	head size	body length	head size	body length	head size	body length	head size	body length
470,02	3112,93	464,57	3110,53	512,54	3478,33	424,13	2729,23	537,67	3322,86	598,03	3699,57
408,93	2976,54	429,86	2877,32	551,91	3539,62	471,93	3011,04	521,31	3331,87	587,77	3715,45
426,45	2840,69	477,55	3130,12	580,72	3496,27	450,05	2973,74	566,86	3595,3	670,65	3946,74
450,09	2970,03	494,58	3229,27	552,18	3454,34	500,74	3209,09	513,03	3367,83	628,24	3829,59
435,15	3030,89	510,12	3154,23	563,07	3586,65	482,1	3184,68	573,59	3477,24	605,74	3666,36
440,71	2864,72	513,48	3059,13	536,85	3393,53	487,76	3252,52	535,82	3222,53	634,23	3819,55
432,89	2876,44	501,3	3191,23	553,65	3449,6	494,08	3096,6	573,41	3377,07	632,28	3946,03
397,96	2734,09	465,61	2845,14	523,28	3500,01	484,46	3020,65	527,37	3492,48	609,21	3666,68
422,78	2833,02	456,77	3134,74	565,29	3239,55	470,99	3144,55	570,56	3598,39	581,24	3733,04
439,35	2834,26	490,35	3118,82	535,62	3424,87	495,02	3202,46	559,61	3662,38	624,35	3758,55
462,43	3039,59	481,3	3105,39	539,88	3550,91	436,93	3007,93	558,66	3448,59	594,13	3738,5
432,89	2817,13	472,21	3195,41	533,76	3430,1	495,02	3103,47	587,77	3515,76	653,05	3838,74
446,32	2853,68	470,48	3267,54	539,96	3418,22	465,42	3084	542,36	3420,51	667,27	3874,12
433,13	2927,7	500,2	3244,24	531,52	3385,69	457,02	2890,35	581,3	3478,67	611,54	3929,74
404,73	2822,51	454,61	2973,57	578,44	3580,47	474,71	3102,32	552,31	3506	652,69	3864,99
430,13	2970,1	467,76	3151,34	541,18	3207,47	503,49	3197,59	570,73	3563,05	606,49	3857,5

ppp4ca 5'UTR 2 dpf		*ppp4ca* 5'UTR 3 dpf		*ppp4ca* 5'UTR 4 dpf		SCMO 2 dpf		SCMO 3 dpf		SCMO 4 dpf	
head size	body length	head size	body length	head size	body length	head size	body length	head size	body length	head size	body length
410,89	2891,94	510,87	3288,77	598,87	3647,6	482,1	3123,82	584,44	3569,75	631,62	3702,35
446,72	3054,13	462,75	2970,66	579,96	3554,87	485,26	3124,4	585,06	3654,97	618,51	3841,8
427,98	2924,79	491,36	3299,66	594,52	3605,57	478,18	3189,73	545,5	3535,82	627,18	3638,94
437,31	3005,12	473,4	3182,86	585,24	3635,77	452,8	3115,69	529,62	3339,16	621,13	3965,24
437,75	2969,98	494,85	2951,44	533,69	3353,09	483,29	3190,52	581,53	3600,88	620,27	3847,24
455	2981,33	499,82	3409,85	521,69	3501,57	477,29	3066,8	588,7	3580,91	620,27	3628,25
454,6	2996,11	466,56	3006,54	560,43	3333,04	475,66	3030,98	571,62	3501,83	607,16	3809,5
386,59	2762,32	539,62	3305,03	499,66	3388,8	507,79	3130,37	526,79	3556,22	660,66	3946,12
445,69	2796,13	459,52	2953,28	531,7	3185,53			528,53	3329,74	602,12	3737,06
450,43	2925,93	444,29	3157,8	582,27	3520,85			576,77	3633,28	603,35	3692,49
345,35	2863,9	436,04	3105,07	542,91	3257,78			592,26	3556,37	596,02	3909,73
401,7	2947,59	481,3	3163,45	552,71	3560,71			511,39	3556,42	621,9	3823,92
438,08	2855,44	470,83	3030,66	533,68	3456,89			575,17	3521,93	644,12	3865,58
437,65	2683,81	459,82	2994,46	531,35	3450,29			500,3	3153,52	605,64	3780,52
465,5	2984,26	504,84	3301,72	588,36	3668,46			516,88	3479,46	573,58	3705,24
432,66	2827,21	426,5	3114,89	576,33	3644,82			568,64	3554,36	598,52	3782,74
440,23	2809,84	499	3422,55	498,35	3464,78			580,45	3530,03	552,2	3740,81
401,37	2843,9	440,63	3070,16	478,53	2826,05					619,93	3804,87
370,03	2673,16	450,33	3132,52	539,8	3056,78					612,93	3815,65
442,11	2938,02	475,87	3175,51	491,57	2929,88					579,29	3727,23
398,24	2699,14	477,23	3297,41	553,65	3579,08					634,9	3803,74
448,99	3061,49	489,73	3035,33	556,1	3451,97					640,57	3908,95
418,92	2765,75	487,22	3087,47	587,77	3611					611,49	3711,95
440,23	2903,8	494,7	3064,41	531,9	3629,92					631,05	3866,34
447,31	2943,15	469,94	3247,08	454,16	2977,07						
438,93	3057,2	474,55	2951,92	555,54	3325,1						
413,33	2703,69	457,74	3204,56	540,16	3293,67						
446,01	2946,44	478,4	2982,98	531,84	3301,15						
442,19	2757,58	452,14	2941,23	559,66	3450,8						
423,7	2726,53	490,53	3021,96	520,51	3410,77						
462,62	3003,97	496,39	3149,33	560,91	3378,77						
468,59	2921,54	474,55	3075,44	585,23	3605,39						
394,44	2824,35	503,96	3038,61	568,2	3567,64						
475,19	2970,67	499,8	2963,48	506,54	3360,6						
465,95	3008,24	500,2	3282,61	527,7	3419,69						
417,98	2843,3	531,62	3383,44	498,85	3348,77						
440,1	2628,03	496,01	2979,2	571,78	3426,78						
451,77	2919,89			549,86	3283,21						
444,39	2851,12			518,74	3341,46						
457,02	2992,1			525,15	3180,87						
458,87	2921,27			558,84	3424						
441,23	2910,02			540,16	2714,99						
399	2982,85										
434,5	2876,82										
386,39	2679,06										
437,11	2936,3										
434,5	2784,57										
422,7	2914,67										
452,94	3103,76										
456,2	2934,59										
459,63	2959,11										
414,78	2871,91										
432,47	2919,52										
Average	476,51	3090,94	555,64	3485,91	617,28	3798,54	463,60	3015,43	571,17	3561,69	612,99	3825,00
Standard deviation	20,64	115,56	26,90	121,95	25,37	92,14	26,75	126,93	21,44	58,20	28,28	114,01
Number of embryos	24	24	33	33	40	40	23	23	27	27	46	46

Table 34 Head size body length measurement of *ppp4ca* splice site morpholino knockdown and control embryos

ppp4ca splice site 2 dpf		*ppp4ca* splice site 3 dpf		*ppp4ca* splice site 4 dpf		SCMO 2 dpf		SCMO 3 dpf		SCMO 4 dpf	
head size	body length	head size	body length	head size	body length	head size	body length	head size	body length	head size	body length
390,01	2878,27	514,46	3434,62	547,5	3544,25	482,69	3155,58	596,49	3551,97	658,17	3906,38
419,72	2736,36	467,54	3099,86	553,2	3384,11	478,1	3084,59	547,35	3523,93	656,11	3844,47
479,98	3158,97	529,08	3366,59	523,71	3254,86	436,53	2878,05	570,73	3578,65	610,24	3769,44
413,76	2866,86	541,52	3232,63	549,64	3059,52	460,41	2911,01	606,71	3680,11	625,32	3772,57
419,56	2804,35	540,97	3643,1	568,14	3637,48	500,73	3181,35	562,99	3451,39	650,71	3768,34
419,83	2699,26	485,44	3116,11	514,35	3068,39	445,8	2989,07	580,8	3641,06	630,3	3877,82
452,15	2944,74	505,28	3054,13	531,5	3219,18	454	3083,01	604,48	3603,16	616,83	3961,84
441,42	2881,01	527,89	3372,27	555,77	3278,71	460,75	2980,29	592,48	3589,28	582,93	3741,74
456,58	2775,08	518,12	3256,69	528,03	3235,27	481,52	3060,08	592,57	3529,33	648,01	3946,82
421,04	2776,99	451,66	2924,2	596,13	3758,97	497,58	3152,95	559,45	3635,5	614,26	3837,58
452,04	2855,33	443,29	2863,53	603,07	3558,26	467,24	2923,76	548,84	3584,07	609,37	3815,97
418,72	2748,65	505,79	3179,69	534,6	3314,47	487,6	3169,38	579,3	3547,51	602,6	3795,72
428,7	2941,07	466,03	3050,7	552,69	3333,29	498,38	3069,49	576,06	3606,37	575,17	3661,85
403,91	2696,8	472,77	3205,14	509,94	3407,95	441,05	3029,58	551,59	3526,42	614,79	3771,59

ppp4ca splice site 2 dpf		*ppp4ca* splice site 3 dpf		*ppp4ca* splice site 4 dpf		SCMO 2 dpf		SCMO 3 dpf		SCMO 4 dpf	
head size	body length	head size	body length	head size	body length	head size	body length	head size	body length	head size	body length
412,74	2746,1	492,08	3132,19	590,7	3578,51	461,98	3114,93	568,06	3495,86	559,34	3695,17
394,24	2721,98	514,39	3248,94	569,91	3583,58	434,33	2787,03	591,02	3683,46	632,35	4015,9
452,82	2857,93	495,22	3026,48	552,23	3629,4	463,44	3056,49	507,4	3485,77	623,95	3917,39
383,27	2772,29	520,97	3204,96	534,18	3452,63	487,09	3070,86	551,24	3500,8	554,14	3750,01
430,06	2870,32	482,64	3090,7	582,77	3700,88	481,35	3101,22	560,31	3477,93	594,86	3831,03
427,41	2892,65	482,15	2868,87	561,93	3515,52	436,93	2902,96	562,6	3555,99	604,77	3833,83
435,28	2763,54	462,37	3059,24	499,7	3366,85	392,32	2768,31	555,51	3556,97	620,39	3922,78
413,38	2792,85	455,35	2912,91	526,03	3504,71	481,27	3102,99	598,4	3566,033	646,25	3975,9
437,64	2708,69	511,73	3149,06	528,95	2976,79	431,76	2781,94	580,69	3566,1	606,31	3782,88
450,73	2942,47	506,76	3221,87	550,61	3496,04			571,37	3551,44	625,45	3874,22
392,77	2928,32	470,28	3051,87	561,4	3166,93			564,58	3501,21	635,11	4080,83
442,96	2846,02	479,57	3230,55	567,27	3674,06			568,97	3588,64	609,71	3691,88
430,84	2685,28	506,25	3205,15	567,24	3271,48			571,62	3586,8	548,82	3581,28
459,42	2799,98	529,63	3271,67	589,69	3568,26					598,78	3915,71
429,46	2634,14	466,33	3010,59	608,34	3687,5					600,09	3897,48
431,44	2808,32	512,25	3235,77	578,4	3229,85					567,17	3518,78
378,93	2639,2	473,3	3193,84	545,73	3380,75					614,51	3832,85
408,03	2768,06	439,15	2875,12	591,2	3610,92					585,58	3725,12
440,55	2906,62	496,94	2785,23	520,12	3341,41					601,66	3740,13
400,12	2858,12	456,27	2982,1	501,57	2883,52					640,18	3800,68
386,39	2791,8	508,09	3178,77	543,09	3507,98					599,8	3918,87
425,45	2813,1	448,49	3071,55	520,66	3264,94					605,87	3862,79
403,16	2804,01	463,25	3162,08	564,54	3418,46					632,35	3891,69
418,43	2778,25	532,86	3382,72	541,83	3555,97					650,89	3673,15
446,36	2844,99	486,22	2936,01	532,73	3506,37					560,31	3675,44
477,23	2901,26	524,26	3242,62	576,03	3094,64					647,28	3959,67
417,37	2887,78	505,68	3037,5	518,83	3085,21					588,71	3886,8
412,23	2760,27	450,17	2931,3	515,3	3302,55					630,58	3976,43
381,13	2816,73	481,01	3029,5	536,4	3134,09					650,75	3865,4
444,76	3009,19	546,37	3298,64	553,81	3422,24					642,5	3787,64
407,99	2680,96	479,76	3175,35	561,19	3470,16					615,75	3714,96
432,55	2981,16	511,7	3166,5	564,04	3367,5					608,66	3881,05
415,51	2786,88	510,01	3121,69	526,03	3182,96						
		504,85	3224,05	562,07	3451,58						
		508,36	3158,55	523,28	3462,8						
		478,81	3090,9	519,72	3142,58						
		482,28	3196,83	579,01	3564,8						
		445,59	2976,64	539,35	3533,23						
		511,6	3095,2	538,75	3229,04						
		463,61	3208,57	527,01	3166,78						
		457,15	3050,11	536,76	3560,32						
		489,26	3343,9								
		508,03	3178,58								
		557,88	3652,98								
		508,53	3307,96								
		511,39	3262,51								
		579,62	3502,89								
		482,38	3076,56								
		536	3180,1								
		481,01	3048,09								
		507,75	3316,76								
		495,09	2954,4								
		498,33	2946,68								
		525,35	3033,32								
		449,51	3097,91								
		562,41	3422,2								
		527,17	3149,45								
		524,66	3247,08								
		479,57	3086,81								
		516,46	3277,14								
		529,35	3515,92								
		466,93	3070,82								
		505,79	3022,92								
		529,35	2975,2								
		463,13	2978,15								
		514,67	3138,67								
		511,72	3015,22								
		536	3153,4								
		528,83	3426,32								
		523,49	3204,06								
Average	424,21	2820,49	498,49	3153,30	548,67	3383,61	463,60	3015,43	571,17	3561,69	612,99	3825,00
Standard deviation	23,99	101,08	30,29	168,67	26,32	201,62	26,75	126,93	21,44	58,20	28,28	114,01
Number of embryos	47	47	84	84	55	55	23	23	27	27	46	46

Table 35 Head size body length measurement of *ppp4cb* knockdown and control embryos

ppp4cb 5'UTR 2 dpf		*ppp4cb* 5'UTR 3 dpf		*ppp4cb* 5'UTR 4 dpf		SCMO 2 dpf		SCMO 3 dpf		SCMO 4 dpf	
head size	body length	head size	body length	head size	body length	head size	body length	head size	body length	head size	body length
403,97	2902,42	472,6	2835,53	526,15	3143,97	484,88	3137,4	532,55	3607,35	598,03	3699,57
409,55	2910,45	485,09	2964,63	545,08	3564,26	477,92	3087,38	531,13	3512,55	587,77	3715,45
411,61	2927,63	520,32	3024,11	577,95	3894,58	484,4	3165,65	565,83	3463,61	670,65	3946,74
390,8	2788,28	429,31	2828,2	525,86	3439,9	488,55	3311,01	526,01	3500,1	628,24	3829,59
413,04	2873,63	490,11	3126,5	495,05	2607,56	506,1	3156,57	556,15	3577,26	605,74	3666,36
452,48	3004,14	444,26	2850,13	544,08	3325,79	527,9	3186,7	543,49	3421,7	634,23	3819,55
365,57	2616,17	395,47	2675,64	578,09	3425,47	508,67	3228,85	529,79	3584,94	632,28	3946,03
487,79	3115,79	466,35	3192,46	528,27	3137,71	466,54	3177,19	516,63	3314,66	609,21	3666,68
377,05	2751,62	459,71	3379,44	493,59	3352,66	424,13	2729,23	540,26	3454,88	617,43	3824,93
437,92	2601,08	534,69	3529,32	541,94	3839,45	471,93	3011,04	587,79	3641,38	596,04	3864,21
421,41	3060,23	573,27	3541,19	465,02	2804,87	450,05	2973,74	573,96	3579,72	613,85	3701,94
447,86	3019,07	480,55	3226,5	520,2	3494,11	500,74	3209,09	592,2	3599,23	606,5	3716,17
431,09	3012,38	470,11	2917,35	479,91	2791,2	482,1	3184,68	560,22	3655,2	618,97	3830,83
428,7	2754,78	495,27	3285,12	556,03	3591,69	487,76	3252,52	577,25	3555,56	606,85	3801,05
436,04	3002,29	429,31	2666,47	539,15	3537,12	494,08	3096,6	570,3	3532,8	667,44	4013,94
392,83	2632,44	491,63	2976,14	561,2	3882,12	484,46	3020,65	524,33	3585	574,52	3776,59
		538,65	3375,66	443,98	2903,21	470,99	3144,55	547,43	3568,87	651,66	3833,21
		480,12	2749,73	524,52	3292,83	495,02	3202,46	579,56	3552,81	594,05	3832,44
		495,85	3409,54	540,55	3865,85	436,93	3007,93	530,65	3475,29	607,21	3800,56
		541,14	3544,85	567,47	3974,09	495,02	3103,47	570,3	3630,17	636,95	3903
		520,94	3517,44	577,65	3636,48	465,42	3084	575,94	3578,9	602,8	3802,87
		434,2	2629,23	573,33	3561,31	457,02	2890,35	559,57	3592,84	614,29	3859,05
		517,65	3158,64	503,76	3406,27	474,71	3102,32	563,15	3631,34	630,45	3598,98
		461,27	2901,29	524,7	3303,56	503,49	3197,59	549,58	3604,79	645,64	4000,95
		464,56	2906,19	576,47	3774,24	482,1	3123,82	577,25	3477,07	654,2	4074,2
		464,59	3406,45	458,01	3046,96	485,26	3124,4	563,33	3669,82	643,86	3725,35
		444,4	2936,72	528,91	3495,68	478,18	3189,73	536,7	3354,9	626,01	3647,28
		505,5	3090,8	656,27	3825,36	452,8	3115,69	566,54	3514,96	602	3718,05
		519,86	3422,48	581,93	3708,02	483,29	3190,52	553,48	3329,83	654,2	3868,89
		425,22	2772,52	569,25	3757,38	477,29	3066,8	569,7	3658,54	636,53	3889,48
		562,67	3440,08	532,25	3451,49	475,66	3030,98	550,06	3459,2	617,41	3837,24
		591,9	3726,65	514,08	3443,62	507,79	3130,37	508,65	3369,42	623,47	3895,2
		585,84	3609,24	525,38	3437,51	482,69	3155,58	544,75	3469,77	643,29	3719,86
		623,23	3720,25	570,52	3641,12	478,1	3084,59	568,68	3532,61	626,01	3706,22
		533,67	3118,76	552,51	3551,96	436,53	2878,05	572,45	3699,18	628,76	3792,56
		542,86	3014,56	507,32	3335,31	460,41	2911,01	558,93	3563,09	584,72	3671,75
		503,9	2910,81	513,78	3396,54	500,73	3181,35	553,48	3496,64	646,81	3773,99
		433,58	2801,92	471,27	3133,93	445,8	2989,07	537,2	3481,61	574,52	3753,09
		517,74	3328,79	529,58	3481,78	454	3083,01	562,68	3465,67	606,47	3719,11
		578,05	3790,54	575,59	3627,09	460,75	2980,29	556,54	3515,58	606,99	3768,08
		574,21	3656,34	574,43	3523	481,52	3060,08	541,39	3446,56		
		591,64	3723,91	560,38	3522,73	497,58	3152,95	586,36	3472,06		
		570,07	3805,62	520,87	3926,98	467,24	2923,76	596,38	3544,28		
		494,54	3055,81	571,01	3687,39	487,6	3169,38	554,24	3475,9		
		458,37	2846,53			498,38	3069,49	606,03	3580,52		
		594,33	3800,5			441,05	3029,58	589,42	3508,51		
		567,65	3428,76			461,98	3114,93	579,5	3656,77		
		586,66	3265,75			434,33	2787,03	543,66	3523,69		
		565,47	3811,87			463,44	3056,49	580,27	3605,33		
		559,12	3615,8			487,09	3070,86	593	3597,32		
		561,05	3151,12			481,35	3101,22	576,13	3625,35		
		558,69	3445,5			436,93	2902,96	578,68	3562,86		
		545,04	3158,13			392,32	2768,31	557,29	3629,56		
		590,13	3741,3			481,27	3102,99	547,98	3440,51		
		565,53	3936,02			431,76	2781,94	546,82	3386,43		
Average	419,23	2873,28	514,69	3249,91	536,89	3466,91	470,19	3053,99	562,98	3539,41	620,62	3803,78
Standard deviation	30,64	164,84	55,41	358,49	40,05	314,24	24,45	125,85	20,22	87,36	23,49	104,94
Number of embryos	16	16	55	55	44	44	47	47	47	47	32	32

Table 36 Head size body length measurement of *sez6l2* knockdown and control embryos

sez6l2 5'UTR 2 dpf		*sez6l2* 5'UTR 3 dpf		*sez6l2* 5'UTR 4 dpf		SCMO 2 dpf		SCMO 3 dpf		SCMO 4 dpf	
head size	body length	head size	body length	head size	body length	head size	body length	head size	body length	head size	body length
471,12	3011,86	524,61	3377,53	576,52	3716,66	484,88	3137,4	532,55	3607,35	598,03	3699,57
428,91	2789,02	495,96	3292,06	589,13	3799,01	477,92	3087,38	531,13	3512,55	587,77	3715,45
386,03	2903,36	532,33	3515,36	566,2	3593,46	484,4	3165,65	565,83	3463,61	670,65	3946,74
446,97	3036,23	493,86	3297,16	609,99	3668,67	488,55	3311,01	526,01	3500,1	628,24	3829,59
463,06	2968,03	486,71	3266,48	556,86	3770,22	506,1	3156,57	556,15	3577,26	605,74	3666,36
462,16	3016,91	529,27	3491,41	587,45	3639,4	527,9	3186,7	543,49	3421,7	634,23	3819,55
427,15	2966,95	525,99	3446,06	561,27	3351,29	508,67	3228,85	529,79	3584,94	632,28	3946,03
425,79	2988,3	554,4	3593,33	580,36	3586,29	466,54	3177,19	516,63	3314,66	609,21	3666,68
394,38	2832,07	544,3	3402,78	579,78	3713,14	426,16	3034,1	555,95	3437,34	581,24	3733,04
413,62	2977,93	464,48	3135,81	558,1	3582,28	484,38	3221,73	520,69	3354,1	624,35	3758,55
429,62	2799,42	510,55	3451,41	543,84	3609,28	447,79	3110,5	522,62	3443	594,13	3738,5

sez6l2 5'UTR 2 dpf		*sez6l2* 5'UTR 3 dpf		*sez6l2* 5'UTR 4 dpf	
head size	body length	head size	body length	head size	body length
425,39	2827,17	514,96	3368,65	561,29	3576,25
425,03	2955,86	518,15	3371,42	561,27	3708,27
442,46	2945,85	496,08	3295,35	582,5	3643,67
420,86	3016,58	562,94	3510,23	602,71	3953,7
381,44	2695,25	479,67	3335,25	577,41	3667,75
431,41	2823,29	481,66	3380,5	562,68	3674,06
389,58	2961,09	519,8	3518,79	546,46	3746,2
377,28	2791,1	497,33	3253,61	629,58	3797,33
441,52	2987,4	516,35	3489,22	609,95	3783,11
451,71	3122,22	508,12	3458,7	578,31	3795,74
406,44	2561,48	510,73	3284,14	558,98	3724,62
410,5	3025,09	534,2	3428,23	558,19	3589,51
438,94	2889,99	530,02	3323,29	517	3607,13
387,45	2799,71	544,89	3494,61	593,66	3642,37
402,85	2796,15	565,16	3546,64	572,26	3584,97
423,35	3011,25	534,2	3439,06	597,37	3806,21
444,54	2968,31	502,9	3261,83	580,36	3689,27
434,01	2993,06	516,73	3356,71	572,59	3807,88
408,05	2877,01	512,51	3333,7	586,44	3753,24
411,76	2824,45	538,17	3498,31	607,28	3762,25
465,15	3008,93	501,45	3343,03	555,33	3591,83
373,73	2642,61	530,7	3339,02	540,93	3551,25
443,12	2935,33	520,5	3371,06	601,32	3786,42
449,1	2938,87	551,81	3410,22	546,94	3577,33
450,93	2961,03	510,73	3226,12	583,7	3754,94
454,65	3000,99	529,44	3385,27	552,12	3697,01
462,16	2924,8	548,23	3404,6	566,59	3772,18
391,69	2864,62	538,78	3504,63	551,9	3478,96
370,71	2740,94	544,86	3437,74	578,76	3685,15
377,13	2943,93	511,81	3480,27	616,75	3827,39
451,14	3046,38	518,12	3436,58	612,54	3783,37
427,15	3030,59	509,43	3343,09	600,17	3801,63
455,39	3039,95	495,69	3272,13	588,38	3770,75
427,89	2911,2	466,23	3383,34	614,35	3882,7
449,84	3003,06	459,75	3289,81	576,52	3742,22
419,88	2980,91	522,93	3429,55	592,16	3652,57
427,15	2973,23	522,93	3410,92	531,47	3586,67
443,34	3007,44	527,82	3406,07	607,61	3862,26
404,5	2867,37	505,59	3397,09	586,19	3796,23
398,6	2924,93	505,1	3314,78	563,93	3719,5
446,44	2982,64	504,62	3353,88	555,33	3572,39
431,13	3017,4	510,72	3310,12	532,61	3661,67
442,94	2959,91	504,78	3474,05	563,47	3665,55
457,93	2993,88	520,7	3217,63	521,75	3456,79
365,58	2724,9	494,05	3432,08	566,59	3603,06
385,9	2685,47	507,03	3352,83	585,9	3731,58
463,7	2961,68	533,18	3468,5	583,26	3859,47
469,47	3090	518,14	3239,61	572,59	3616,4
386,49	2815,81	473,41	3208,39	541,77	3432,64
434,71	2880,13	511,51	3426,69	586,63	3815,6
457,98	2977,93	464,14	3131,35	591,41	3844,73
421,2	2938,62	549,65	3482,7	550,53	3512,19
427,41	2978,79	494,57	3239,84	563,62	3533,95
382,89	2944,55	492,1	3414,21	523,96	3575,47
423,28	2848,96	487,27	3359,4	534,26	3804,79
408,54	2958,23	485,31	3387,54	568,14	3643,77
403,31	2850,25	520,6	3430,6	569,47	3635,25
450,24	3030,11	489,8	3526,09	559,18	3606,85
391,86	2887,8	501,86	3509,85	572,33	3678,33
439,37	2860,11	513,59	3524,8	547,77	3483
394,38	2711,2	514,17	3364,25	534,26	3707,26
402,44	2995,81	546,62	3572,46	561,43	3480,33
428,25	2977,08	491,04	3487,96	576,62	3602,71
419	3033,46	499,59	3373,73	592,83	3831,9
434,67	2838,8	534,45	3575,19	552,29	3791,95
404,79	3011,64	491,51	3380,31	545,41	3493,37
416,31	3004,69	515,61	3402,97	544,94	3711,14
431,09	2934,56	449,51	3208,13	504,03	3585,94
369,29	2585,66	494,56	3317,37	521,6	3580,48
380,99	2666,92	475,76	3328,76	542,42	3737,98
417,99	3036,15	521,62	3467,1	592,04	3808,8
437,53	3024,91	429,1	3364,27	601,25	3613,11
419,35	2942,44	474,77	3477,5	589,46	3785,11
438,94	3186,95	528,29	3466,34	574,95	3809,06
436,04	3089,17	536,91	3492,73	598,27	3569,17
434,17	2995,25	524,31	3343,03	545,19	3735,94
438,58	3112,88	544,04	3561,91	577,81	3732,82

SCMO 2 dpf		SCMO 3 dpf		SCMO 4 dpf	
head size	body length	head size	body length	head size	body length
484,38	3031,51	526,31	3513,24	653,05	3838,74
481,84	3114,33	534,5	3350,93	667,27	3874,12
481,26	3116,12	545,37	3467,25	611,54	3929,74
457,39	3093,74	566,63	3402,5	652,69	3864,99
461,31	3074,07	524,49	3513,59	606,49	3857,5
520,97	3231,14	546,24	3519,91	631,62	3702,35
518,42	3262,39	527,13	3306,13	618,51	3841,8
469,61	3134,53	509,35	3458,66	627,18	3638,94
538,76	3345,09	566,63	3664,21	621,13	3965,24
474,54	3182,51	579,95	3485,76	620,27	3847,24
509,87	3214,69	512,44	3515,03	620,27	3628,25
452,71	3083,52	537,96	3379	607,16	3809,5
485,67	3100,19	491,96	3345,23	660,66	3946,12
474,82	3066,85	523,65	3551,51	602,12	3737,06
453,65	3133	524,77	3464,08	603,35	3692,49
465,57	3079,58	512,13	3417,59	596,02	3909,73
534,66	3279,96	531,15	3558,67	621,9	3823,92
534,66	3279,96	506,09	3334,91	644,12	3865,58
473,57	3253,5	526,81	3563,35	605,64	3780,52
455,72	3075,5	507,4	3298,83	573,58	3705,24
518,25	3334,9	504,14	3487,65	598,52	3782,74
505,26	3213,84	557,41	3470,12	552,2	3740,81
499,01	3269,06	541,76	3511,18	619,93	3804,87
491,6	3185,05	496,79	3476,22	612,93	3815,65
437,22	2943,18	551,59	3501,99	579,29	3727,23
478,11	3104,06	556,05	3526,68	634,9	3803,74
543,21	3348,22	570,48	3492,24	640,57	3908,95
506,33	3248,7	502,87	3372,75	611,49	3711,95
493,43	3208,4	575,74	3525,31	631,05	3866,34
464,31	3176,83	549,71	3591,61	658,17	3906,38
517,77	3133,76	558,25	3562,66	656,11	3844,47
492,02	3247,34	558,79	3638,06	610,24	3769,44
529,88	3326,2	522,62	3304,25	625,32	3772,57
454,8	3111,05	534,44	3540,67	650,71	3768,34
506,38	3236,62	518,34	3444,33	630,3	3877,82
428,92	3113,51	565,29	3587,66	616,83	3961,84
421,07	2945,61	494,33	3259,77	582,93	3741,74
505,35	3166,07	545,12	3555,82	648,01	3946,82
474,13	3100,6	506,9	3453,29	614,26	3837,58
496,43	3197,81	568,97	3580,71	609,37	3815,97
493,65	3225,08	523,9	3388,71	602,6	3795,72
503,15	3228,28	548,74	3462,55	575,17	3661,85
476,91	3240,68	545,28	3516,48	614,79	3771,59
472,52	3198,35	562,99	3652,58		
479,32	3229,08	522,53	3478,97		
470,72	3089,34	520,25	3373,83		
461,44	3054,2	570,06	3651,89		
		516,88	3499,44		
		532,06	3522,01		
		530,34	3425,62		
		556,4	3438,93		
		524	3498,75		
		534,44	3670,77		
		517,18	3304,49		
		533,26	3558,4		
		551,24	3551,88		
		514,51	3353,85		
		564,02	3497,53		
		591,22	3420,96		
		579,42	3584,23		
		535,59	3463,4		

sez6l2 5'UTR 2 dpf		*sez6l2* 5'UTR 3 dpf		*sez6l2* 5'UTR 4 dpf		SCMO 2 dpf		SCMO 3 dpf		SCMO 4 dpf	
head size	body length	head size	body length	head size	body length	head size	body length	head size	body length	head size	body length
413,76	3025,88	536,13	3343,91	580,07	3626,87						
405,38	3025	485,09	3416,6	613,96	3878,29						
458,15	3208,16	459,46	3472,94	571,36	3622,36						
363,62	2727,74	495,61	3522,18	586,39	3776,2						
400,21	2927,51	515,64	3493,35	580,89	3693,17						
431,44	3023,92	431,85	3343,22	580,8	3614,86						
430,85	2980,68	505,63	3589,56	588,29	3728,75						
426,42	3012,19	475,76	3059,47	557,37	3585,87						
381,51	2859,28	501,23	3337,95	563,52	3746,28						
439,34	2919,85	532,13	3486,28	539,46	3379,83						
448,93	2997,44	495,22	3389,79	586,69	3781,76						
416,16	3072,02	519,86	3409,12	571,36	3649,27						
409,79	2923,99	543,08	3526,97	558,6	3776,92						
393,35	2968,41	479,9	3451,87	562,49	3803,41						
419,44	2846,4	497,82	3415,59	568,44	3521						
469,43	3144,94	520,94	3400,95	571,36	3742,07						
434,67	3156,96	480,12	3512,31	539,34	3304,95						
427,82	3058,25	543,08	3515,37	527,27	3282,25						
431,66	2879,35	504,03	3270,57	551,89	3726,6						
436,72	2959,96	519,95	3580,32	541,08	3638,82						
404,79	2826,13			568,44	3655,55						
431,04	2855,02			521,6	3470,7						
433,71	2969,62			552,76	3545,15						
431,25	3062,32			580,18	3703,34						
396,82	2974,01			568,62	3597,7						
427,74	3034,39			517,36	3739,86						
401,23	3050,4			580,04	3556,75						
430,85	2875,57			604,21	3789,15						
442,36	3042,91			557,74	3583,76						
401,89	2988			583,64	3477,78						
428,15	2988,53			569,82	3871,65						
432,55	3125,1			576,12	3636,38						
403,66	2917,07			605,41	3610,59						
419,44	3007,24			523,08	3444,46						
				556,01	3713,16						
Average	422,66	2941,63	509,82	3398,29	568,98	3668,70	485,41	3169,74	536,88	3479,52	618,26	3803,95
Standard deviation	25,25	117,37	26,35	104,75	24,83	126,00	28,52	92,19	22,88	96,18	25,26	89,56
Number of embryos	122	122	108	108	123	123	58	58	72	72	54	54

8 Selbstständigkeitserklärung

Hiermit erkläre ich, dass ich die vorliegende Arbeit selbständig und unter Verwendung keiner anderen als der von mir angegebenen Quellen und Hilfsmittel verfasst habe. Ferner erkläre ich, dass ich bisher weder an der Freien Universität Berlin noch anderweitig versucht habe, eine Dissertation einzureichen oder mich einer Doktorprüfung zu unterziehen.

Berlin, den 10.02.2014 Udo Georgi